NUREG/CR-5649
ANL-90/33
Vol. 1

COMMIX-1C: A Three-Dimensional Transient Single-Phase Computer Program for Thermal-Hydraulic Analysis of Single-Component and Multicomponent Engineering Systems

Equations and Numerics

Prepared by
H. M. Domanus, Y. S. Cha, T. H. Chien, R. C. Schmitt, W. T. Sha

Argonne National Laboratory

Prepared for
U.S. Nuclear Regulatory Commission

AVAILABILITY NOTICE

Availability of Reference Materials Cited in NRC Publications

Most documents cited in NRC publications will be available from one of the following sources:

1. The NRC Public Document Room, 2120 L Street, NW, Lower Level, Washington, DC 20555

2. The Superintendent of Documents, U.S. Government Printing Office, P.O. Box 37082, Washington, DC 20013-7082

3. The National Technical Information Service, Springfield, VA 22161

Although the listing that follows represents the majority of documents cited in NRC publications, it is not intended to be exhaustive.

Referenced documents available for inspection and copying for a fee from the NRC Public Document Room include NRC correspondence and internal NRC memoranda; NRC Office of Inspection and Enforcement bulletins, circulars, information notices, inspection and investigation notices; Licensee Event Reports; vendor reports and correspondence; Commission papers; and applicant and licensee documents and correspondence.

The following documents in the NUREG series are available for purchase from the GPO Sales Program: formal NRC staff and contractor reports, NRC-sponsored conference proceedings, and NRC booklets and brochures. Also available are Regulatory Guides, NRC regulations in the *Code of Federal Regulations*, and *Nuclear Regulatory Commission Issuances*.

Documents available from the National Technical Information Service include NUREG series reports and technical reports prepared by other federal agencies and reports prepared by the Atomic Energy Commission, forerunner agency to the Nuclear Regulatory Commission.

Documents available from public and special technical libraries include all open literature items, such as books, journal and periodical articles, and transactions. *Federal Register* notices, federal and state legislation, and congressional reports can usually be obtained from these libraries.

Documents such as theses, dissertations, foreign reports and translations, and non-NRC conference proceedings are available for purchase from the organization sponsoring the publication cited.

Single copies of NRC draft reports are available free, to the extent of supply, upon written request to the Office of Information Resources Management, Distribution Section, U.S. Nuclear Regulatory Commission, Washington, DC 20555.

Copies of industry codes and standards used in a substantive manner in the NRC regulatory process are maintained at the NRC Library, 7920 Norfolk Avenue, Bethesda, Maryland, and are available there for reference use by the public. Codes and standards are usually copyrighted and may be purchased from the originating organization or, if they are American National Standards, from the American National Standards Institute, 1430 Broadway, New York, NY 10018.

DISCLAIMER NOTICE

NUREG/CR-5649
ANL-90/33
Vol. 1
R7

COMMIX-1C: A Three-Dimensional Transient Single-Phase Computer Program for Thermal-Hydraulic Analysis of Single-Component and Multicomponent Engineering Systems

Equations and Numerics

Manuscript Completed: July 1990
Date Published: November 1990

Prepared by
H. M. Domanus, Y. S. Cha, T. H. Chien, R. C. Schmitt, W. T. Sha

Argonne National Laboratory
9700 South Cass Avenue
Argonne, IL 60439

Prepared for
Division of Systems Research
Office of Nuclear Regulatory Research
U.S. Nuclear Regulatory Commission
Washington, DC 20555
NRC FIN A22550

List of Contributors

At the request of and under sponsorship from the U.S. Nuclear Regulatory Commission, the COMMIX-1C computer code was constructed by re[illegible]lected features from previous COMMIX versions and adding innovations. The task of making COMMIX-1C available and useful was a team effort, and the participants are listed below according to their activities.

Documentation:	Y. S. Cha, R. C. Schmitt, W. T. Sha, and H. M. Domanus
Previous COMMIX versions:	H. M. Domanus, R. C. Schmitt, and W. T. Sha
Software Design, Models, and Methods:	H. M. Domanus and R. C. Schmitt
Code Programming and Development:	H. M. Domanus, R. C. Schmitt, and T. H. Chien
Validation:	H. M. Domanus, T. H. Chien, Y. S. Cha, and W. T. Sha
Overall Project Direction and Management:	W. T. Sha

COMMIX-1C: A Three-Dimensional Transient Single-Phase Computer Program for Thermal-Hydraulic Analysis of Single- and Multicomponent Engineering Systems

Volume I: Equations and Numerics

Abstract

The COMMIX-1C computer program is an extended and improved version of previous COMMIX codes with four major additions or modifications: (1) a new finite-volume formulation for the mass, momentum, and energy equations to extend the applications to subsonic compressible flows and to make the calculations more robust; (2) a flow-modulated skew-upwind discretization scheme to reduce numerical diffusion; (3) two new matrix solvers for the discretized equations to increase the flexibility and efficiency of numerical computation; and (4) a k-ε two-equation turbulence model that is more robust and better validated than those in previous COMMIX codes. In addition, there are numerous smaller modifications that improve overall operation greatly.

COMMIX-1C solves the conservation equations of mass, momentum, and energy, as well as the transport equations of turbulence parameters. It is designed to perform steady-state/transient, single-phase, three-dimensional analysis of fluid flow with heat transfer in a single-component or a multicomponent engineering system. The program was developed for the analysis of heat transfer and fluid flow processes in a nuclear reactor system. However, it is designed in a generalized fashion so that, with little or no modification, it can be used to analyze processes in any engineering equipment or in any system.

The following are unique features of the COMMIX-1C code:

- *Porous-Medium Formulation*: COMMIX-1C uses a new porous-medium formulation with the parameters of volume porosity, directional surface porosity, distributed resistance, and distributed heat source or sink. With this formulation, the COMMIX code has the capability to model an anisotropic flow domain with stationary structures, and it can be used to treat irregular geometries. The porous-medium formulation with the additional parameter of directional surface porosity represents a unified approach to thermal-hydraulic analysis. Because of this feature, it is now possible to perform a multidimensional thermal-hydraulic simulation of either a single component, such as a rod bundle, reactor plenum, piping system, or heat exchanger, or of a multicomponent system that is a combination of such components.

- *Three Matrix Solvers*: In COMMIX-1C, three matrix solvers, the successive overrelaxation method, the Yale Sparse Matrix Package, and the preconditioned conjugate gradient method for symmetric matrix, are available to solve the pressure equation and scalar transport equations. Depending on the size of the computational domain, the user can choose the solver that is best suited

for a given problem. These three matrix solvers greatly increase the flexibility and efficiency of numerical computation for COMMIX-1C compared to previous COMMIX codes.

- *Geometrical Package:* A special geometrical package has been developed and implemented to permit modeling of any complex geometry in the most storage-efficient way.

- *Skew-Upwind Discretization Scheme:* A new flow-modulated skew-upwind discretization scheme has been developed and implemented to reduce the numerical diffusion observed in simulations of flow inclined to grid lines. The scheme also eliminates temperature over/undershoots that occur when simulations are performed with other skew-upwind differencing schemes.

Volume I (Equations and Numerics) of this report describes in detail the basic equations, formulations, solution procedures, and models for auxiliary phenomena. Volume II (User's Guide and Manual) contains the input instruction, sample problems, flow charts, and description of available options and boundary conditions.

CONTENTS

FIGURES

TABLES

Executive Summary

The COMMIX (*Com*ponent *Mix*ing) codes are designed for analyzing heat transfer and fluid flow. The COMMIX-1C computer program—an extended version of previous COMMIX codes—is designed to analyze steady-state/transient, single-phase, three-dimensional flow with heat transfer in a reactor component/multicomponent system.

The four major improvements that have been implemented in previous COMMIX codes (including COMMIX-1B) to develop COMMIX-1C are

- New finite-volume formulation for the mass, momentum, and energy equations to extend application to subsonic compressible flows. The new momentum formulation employs the concept of a volume-averaged velocity. It makes the numerical calculation more robust than in previous COMMIX versions. It also makes the location of pressure change coincide with that of density change for one-dimensional flows. In addition, the new discretized momentum equations also satisfy the one-dimensional Bernoulli equation.

- Addition of a new flow-modulated skew-upwind discretization scheme in the energy equation to reduce numerical diffusion. This new scheme is considered better than the previous volume-flow-weighted skew-upwind difference scheme in COMMIX-1B because it not only reduces numerical diffusion but also has a theoretical basis for not producing overshoots and undershoots that are physically unrealistic.

- Addition of two matrix solvers, the Yale Sparse Matrix Package and the preconditioned conjugate gradient method, for the solution of discretized equations. These two new matrix solvers, plus the existing solver using the successive overrelaxation method, greatly enhance the flexibility and efficiency of COMMIX-1C in dealing with various engineering problems.

- An improved k-ε two-equation turbulence model that is more robust and better validated than that in previous COMMIX codes.

In addition to these major improvements, there are numerous minor modifications that significantly improve the overall operation.

One of the major unique features of COMMIX is its porous-medium formulation, which has been rigorously derived through local volume averaging. In the new formulation, we use volume porosity, directional surface porosity (directional because surface porosity is an anisotropic vector quantity), distributed resistance, and distributed heat source or sink. *The concept of adding the parameter of directional surface porosity is relatively new.* In the conventional porous-medium formulation, only the volume porosity, distributed resistance, and distributed heat source are used. Volume porosity is the ratio of the volume occupied by fluid in a control volume to the total control volume. Surface porosity is similarly defined as the ratio of fluid flow area through a control surface to the total control surface area. The porous-medium formulation has the capability of modeling both the anisotropic flow domain and irregular geometry.

In any numerical analysis of an engineering system, modeling must include distributed resistance (friction factor) because, in general, it is not a precisely known quantity. Thus, with the conventional porous-medium formulation, the flow distribution that we obtain depends completely on how accurately we model the distributed resistance. However, in the case of the present porous-medium formulation, due to the introduction of directional surface porosity (a geometrical quantity that can be prescribed accurately), the dependence of the velocity field on resistance modeling is reduced. Hence, we obtain improved resolution and accuracy in the modeling of velocity and temperature fields. The present porous-medium formulation thus represents the first *unified approach* to thermal-hydraulic analysis. The conventional porous-medium formulation can be considered a subset of this present porous-medium formulation.

The COMMIX code provides detailed local velocity and temperature fields for the problems under consideration. The conservation equations of mass, momentum, and energy and the transport equations of turbulence parameters are solved as a boundary-value problem in space and an initial-value problem in time. The discretization equations are obtained by integrating the conservation equations over a control volume.

The code has a wide range of applicability. It is capable of solving thermal-hydraulic problems involving either a single component, such as a rod bundle, reactor plenum, piping system, heat exchanger, etc., or a multicomponent system that is a combination of these components.

COMMIX has two alternative solution schemes. One is semi-implicit and is a modification of the ICE technique. The other, a fully implicit scheme called SIMPLEST-ANL, is a modification of the numerical procedure known as SIMPLER.

The code has a modular structure and permits analysis with either Cartesian or cylindrical coordinate systems. It has four thermal-hydraulic property packages: water vapor, sodium vapor, liquid sodium, and liquid water. Besides these four packages, an option is available for users to input simplified thermal-physical property correlations that are valid in the desired range of applications.

Another unique feature of the COMMIX code is its geometrical package. The basic concept is to use computational cells (either in Cartesian or cylindrical coordinates) as building blocks that are stacked to approximate the shape of the physical systems under consideration. Then volume porosity and directional surface porosity are used to account for the differences between the geometry used in computation and the actual configuration. This feature permits the COMMIX code to model any irregular and complex geometry encountered in a real engineering system. Furthermore, the computer storage requirement of the COMMIX code is optimized; only the computational cells used in calculations are counted.

Volume I (Equations and Numerics) of this report describes in detail the basic equations, formulation, flow-modulated skew-upwind discretization scheme, and solution procedures. It also describes models used for the following phenomena:

- Momentum interaction between fluid and stationary solid structures.
- Thermal interaction between fluid and stationary solid structures.

- k-ε two-equation turbulence model.

In Volume II (User's Guide and Manual), we provide flow charts, descriptions of subroutines, geometry modeling, initialization procedures, input descriptions, etc. Two sample problems are also included so that readers who plan to use COMMIX-1C can become familiar with the input/output structures of the code.

1 Introduction

COMMIX (for *Com*ponent *Mix*ing) is a computer code for heat transfer and fluid flow analysis. Since the development of COMMIX-1 in 1976, many features have been added and refined to augment the code's capability and applicability. Consequently, COMMIX has become a very general-purpose computer code with a very wide range of applications. Although developed for nuclear reactor applications, with no or minimal modifications COMMIX can be used to analyze various processes in engineering systems.

Many industries and organizations involved in the design or analysis of nuclear reactors are already using COMMIX. However, due to the code's generality of formulation and its wide range of applications, people from other disciplines have also found COMMIX a very useful tool. We therefore expect the number of COMMIX users to increase in the future. Prospective users of COMMIX can benefit from a comprehensive description of the code. The purpose of the present report is to meet this need.

In describing COMMIX-1C, we have two distinct aims. One is to convey to the reader the capabilities of COMMIX, the equations that are solved, and how they are solved; that is the subject of this volume (Volume I: Equations and Numerics). The second aim is to present a step-by-step procedure on the use of COMMIX. To achieve this, we must describe the procedure in sufficient detail that a reader has little or no difficulty in beginning to use COMMIX. This complex task is the subject of the second volume (Volume II: User's Guide and Manual).

This volume (I) describes the basic equations, formulations of discretization equations, auxiliary models, solution procedures, etc. Volume II describes all the information needed by the user, e.g., input description, flow chart, sample problems, and user options.

1.1 Overview of COMMIX-1C

The COMMIX-1C code is a generalized computer code for heat transfer and fluid flow analysis. Although designed specifically for reactor component/multicomponent applications, it has been developed in a way that makes it applicable to many other complex engineering system. Its capability includes steady-state/transient, three-dimensional, and single-phase analysis of nuclear reactor systems under normal and off-normal operating conditions.

In general, a computer code developed for numerical simulation of an engineering process can be classified as either a system code or a component code.

- A system code generally deals with many interlinking components; it accounts for component interactions to provide an overall analysis of a whole system without detailed analysis of all the components of a system.

- A component code, in contrast, deals with only one component of interest and provides a detailed numerical simulation of a single component.

COMMIX-1C can be described as both a system code and a component code because it is capable of providing detailed information about a single component or of analyzing a multi-component system in sufficient detail. Because of this broad capability, COMMIX-1C can also provide detailed information about component interactions.

COMMIX-1C is an extended and upgraded version of the previous COMMIX codes, including COMMIX,[1] COMMIX-1A,[2] and COMMIX-1B,[3] which were released in 1981, 1983, and 1985, respectively. COMMIX-1C has retained all the flexibilities and generalities of its predecessors, but now contains some additional and improved features:

- A new finite-volume formulation of the mass, momentum, and energy equations to extend the applications to subsonic compressible flows. The new momentum formulation employs the concept of a volume-averaged velocity, which makes the computation more robust than in previous COMMIX versions. The new formulation makes the location of pressure change coincide with that of density change in one-dimensional flows. The new discretized momentum equations also satisfy the one-dimensional Bernoulli equation.

- A new flow-modulated skew-upwind discretization (FMSUD) scheme to reduce numerical diffusion for flows inclined to grid lines. The FMSUD scheme is considered better than the volume-weighted skew-upwind difference scheme in COMMIX-1B because the FMSUD scheme in COMMIX-1C not only reduces numerical diffusion, but also does not produce overshoots and undershoots that are physically unrealistic.

- A modified k-ε two-equation turbulence model that is more robust and better validated than the k-ε two-equation turbulence model in COMMIX-1B.

- Three matrix solvers, i.e., the successive overrelaxation (SOR) method, the Yale Sparse Matrix Package (YSMP), and the preconditioned conjugate gradient (PCG) method, are now available in COMMIX-1C. These matrix solvers are implemented in modular fashion, which provides the user with greater flexibility in choosing a solution method better suited to a given problem.

COMMIX-1C solves the conservation equations of mass, momentum, and energy, as well as transport equations of turbulence parameters, as a boundary-value problem in space and an initial-value problem in time. The staggered grid system is used, which considers the field variables as located at the center of a cell and flow variables as located at the surface of a cell.

The COMMIX series of codes are well tested. Already, many computations for complex situations have been performed.[4-39] A number of simulations using COMMIX-1C have been

performed since 1985.[40-41] The structure of the code is modular. It has many important features that are described in the following section.

1.2 Major Features of COMMIX-1C

1.2.1 Porous-Medium Formulation

As do all the codes in the COMMIX series, COMMIX-1C employs conservation equations of mass, momentum, and energy that are based on a new porous-medium formulation utilizing local volume averaging.[42-48] The formulation uses four parameters—volume porosity, directional surface porosity, distributed resistance, and distributed heat source (sink)— to model the effects of internal solid structures. In the conventional porous-medium formulation, only three parameters—volume porosity, distributed resistance, and distributed heat source—are used. The addition of a fourth parameter, directional surface porosity,[42-51] is a relatively new concept.*

The volume porosity parameter is defined as the ratio of the volume occupied by fluid in a control volume to the total control volume. Directional surface porosity is similarly defined as the ratio of area allowed for fluid flow through a control surface to the total control surface area. We use the adjective "directional" because surface porosity is an anisotropic quantity.

Introducing the fourth parameter, directional surface porosity, has several advantages. In any thermal-hydraulic analysis, flow resistance due to internal structures and/or irregular geometry (the friction factor) generally is not precisely known for most engineering applications and must be modeled as a distributed resistance. In the conventional porous-medium formulation, the accuracy of numerical prediction therefore depends primarily on how well the resistance is modeled. In the case of the new porous-medium formulation, two parameters (distributed resistance and directional surface porosity) are available for modeling of velocity and temperature fields in anisotropic media. Incidentally, directional surface porosity is a geometrical parameter and can be calculated precisely. By the introduction of directional surface porosity in the new porous-medium formulation, we reduce the dependence of numerical prediction on the modeling of distributed resistance (an empirical parameter not precisely known). Thus, the concept of adding directional surface porosity greatly facilitates the modeling of velocity and temperature fields in anisotropic media and, in general, improves resolution and accuracy. Another unique feature of the porous-medium formulation is that it can be used to model irregular geometry.

If we set directional surface porosity equal to one, the new formulation reduces to the conventional porous-medium formulation. We can therefore consider the conventional porous-medium formulation as a subset of the new porous-medium formulation. Furthermore, if we set the volume porosity equal to one and the distributed resistance and heat source to zero, the porous-medium formulation reduces to a continuum-medium

*Recently, the new porous-medium formulations have been further refined via time-volume averaging.

formulation. Thus, the new porous-medium formulation can be considered a most general and unified approach to thermal-hydraulic analysis.

1.2.2 Two Solution Algorithms

In COMMIX-1C, there are two solution algorithms as user options:

- A semi-implicit algorithm derived from the Los Alamos ICE Technique.[52-54] This algorithm is ideally suited for analyzing fast transients, where we are interested in details at small time intervals (on the order of Courant time-step size).
- A fully implicit algorithm named SIMPLEST-ANL. This algorithm is a modification of the Patankar-Spalding numerical procedure[55] known as SIMPLE/SIMPLER. It is particularly suitable for analyzing steady-state systems, as well as slow and moderate transients.

1.2.3 Three Matrix Solvers

The form of all the discretized equations in COMMIX-1C can be expressed as

$$a_0^{\phi}\phi_0 - \sum_{\ell=1}^{6} a_\ell^{\phi}\phi_\ell - b_0^{\phi} = 0 ,$$

where ϕ is a dependent variable and the subscript ℓ stands for the indices of neighboring points. This general form of the discretization equation leads itself to various solution schemes. In COMMIX-1C, three matrix solvers (SOR, YSMP, and PCG) are available and the user can choose any one of the methods to solve the discretized equations. The combination of two solution algorithms and three matrix solvers greatly increases the flexibility for the user to select the solution algorithm and the matrix solvers best suited for a given problem.

1.2.4 Flow-Modulated Skew-Upwind Discretization (FMSUD) Scheme

In engineering applications, frequently the local velocity is not parallel to the grid lines. This may introduce the so-called numerical diffusion, which is nonphysical and thus reduces the accuracy of the numerical results. In COMMIX-1C, a flow-modulated skew-upwind discretization scheme is implemented in the energy equation to reduce numerical diffusion. The FMSUD scheme does not produce physically unrealistic overshoots and undershoots and is, therefore, considered better than the volume-weighted and mass-flow-weighted skew-upwind difference schemes in other COMMIX versions.

1.2.5 Geometry Package

The geometry package developed and implemented in previous COMMIX versions is also retained in COMMIX-1C. This package is capable of approximating any irregular geometry. It uses basic computational cells as building blocks to model the geometry under

consideration. Then both volume porosities and directional surface porosities are used to account for the differences between the approximated and actual configuration.

To save computer storage, a computational cell is defined by a number rather than by its conventional (i, j, k) location, where i, j, and k are the computational cell indices in the three principal axes (e.g., x, y, and z in the Cartesian coordinate system). With this approach, the storage requirement depends only on the total number of computational cells and not on the value of the product IMAX*JMAX*KMAX, where IMAX, JMAX, and KMAX denote the maximum values of computational cell indices in the three corresponding principal axes.

A normal three-dimensional computational cell has six surfaces. But to facilitate true and proper modeling of a complex irregular geometry (most geometries in engineering systems are complex and irregular), we have provided flexibility so that a user can specify an additional seventh surface, called an irregular surface, to a computational cell.

1.3 Other Features of COMMIX-1C

- Two options are provided to give COMMIX-1C a wide range of applications in dealing with turbulent flows:
  - Constant turbulent diffusivity model.
  - Two-equation k-ε turbulence model.
- The discretization equations are formulated by integrating the conservation equations and transport equations over a control volume surrounding a grid point. Thus, the derivation process and resulting equations have direct physical meaning, and the consequent solution satisfies conservation principles.
- The program has a decoupled-transient-simulation option that permits solution of
  - mass-momentum equations only, or
  - energy equation only, or
  - coupled mass-momentum and energy equations,

  at any given time step.
- The code has an option that allows use of either Cartesian or cylindrical coordinates.
- The COMMIX-1C code has a modular structure that permits rapid implementation of the latest available drag models, heat-transfer models, etc.
- COMMIX-1C has built-in properties for liquid sodium and water, and sodium vapor and water vapor, with an option permitting use of simplified property correlations for any fluids and solid structures.
- The code also contains
  - A generalized resistance model to permit specification of resistance due to internal structures (fuel rods, wire wrap, baffles, grid spacers, etc.)

- A generalized thermal structure formulation to model thermal interaction between structures (fuel rods, wire wraps, duct wall, baffles, etc.) and surrounding fluid.

- Heat source/sink and boundary conditions can be functions of time.

- The COMMIX-1C code is structured to permit solution of 1-D, 2-D, or 3-D calculations.

1.4 Organization of the Report

This volume describes the formulations of the governing equations for three-dimensional, single-phase, steady-state/transient flow with heat transfer. The description starts with differential equations and deals with numerical methods incorporated into the COMMIX-1C program. Section 2 is devoted to the general form of governing conservation equations for a quasicontinuum domain. This generalization facilitates unified development of the numerical method and the construction of the computer program.

The quasicontinuum domain is defined as a medium that contains finite, dispersed, stationary heat-generating (or absorbing) solid structures. The effects of solid structures in a medium are accounted for by introducing volume porosity, directional surface porosity, distributed resistance, and distributed heat sources.

Section 3 describes the staggered grid arrangement and the conventions used in COMMIX-1C to define the location of a control volume. Section 4 assembles the finite-volume equations. The finite-volume formulation of the general equation is presented in Sec. 4.5. Because a staggered grid system is used, the control volumes for momentum equations are different and require special consideration. The special features of the finite-volume equations for momentum are discussed in Sec. 4.6.

The pressure appearing in the momentum equation must be such that the velocity distribution obtained satisfies the continuity equation. The derivation of the pressure equation (derived by combining the momentum and continuity equations) is presented in Sec. 5.

Currently, two options are available to account for turbulence effects:

- *Constant Turbulent Diffusivity*: This model is very simple; the turbulent viscosity and turbulent thermal conductivity are assumed constant. No transport equation is solved. This option is suitable only for scoping analysis because it does not provide detailed information on turbulence.

- *The k-ε Two-Equation Turbulence Model*: The transport equations of turbulence kinetic energy k and dissipation rate of turbulence kinetic energy ε are solved to evaluate turbulence quantities. This is more general than the Prandtl mixing length hypothesis and the one-equation turbulence model and is computationally more economical than the complex multiequation models of turbulence that are still in the development stage.

These models are described in Sec. 6.

General practice in the formulation of convective terms is to use pure-upwind differencing rather than central differencing. This is because the pure-upwind scheme prevents instability at high Peclet numbers. However, it has been found that with pure-upwind differencing, the false (numerical) diffusion can be large if the flow is inclined to grid lines. To reduce the numerical diffusion, we have implemented a new flow-modulated skew-upwind discretization (FMSUD) scheme. Derivations of the two-dimensional and three-dimensional FMSUD schemes and numerical examples are presented in Sec. 7.

Section 8 describes several models that have been maintained in COMMIX-1C; these include a generalized-force model and a generalized thermal-structure model. The force model computes distributed resistance to account for the friction between fluid and submerged solids. The thermal-structure model is designed for computing the distributed heat source (fluid and submerged solids) and the thermal inertia of submerged solids.

In COMMIX-1C, there are several boundary condition options for momentum, energy, and continuity equations. These options are described in Sec. 9.

In COMMIX-1C, two alternative formulations leading to two alternative solution procedures are available—the semi-implicit modified ICE-type solution scheme and the fully implicit solution scheme SIMPLEST-ANL, an extension of the numerical procedures known as SIMPLE/SIMPLER. These two solution procedures are described in Sec. 10. There are three matrix solvers (the successive over-relaxation method, the Yale Sparse Matrix Package, and the preconditioned conjugate gradient method) available in COMMIX-1C to solve the discretized scalar transport equations and the pressure equation. These matrix solvers are also described in Sec. 10.

Volume II of this report is written specifically for COMMIX-1C users. It describes steady-state and transient calculation and various procedures in the preparation of load modules, input data, reading and writing of restart files, etc. Two sample problems, along with their description, input, and output, are presented to provide a sound introduction to the capabilities of COMMIX-1C. The code input description is also included in Volume II.

2 General Form of Conservation Equations

The conservation equations of mass, momentum, and energy possess a common form. If we denote the general dependent variable as ϕ, the corresponding conservation equations have the following form in the Cartesian coordinate system:

In continuum domain:

$$\underbrace{\frac{\partial}{\partial t}(\rho\phi)}_{\text{Unsteady}} + \underbrace{\frac{\partial}{\partial x}(\rho u\phi) + \frac{\partial}{\partial y}(\rho v\phi) + \frac{\partial}{\partial z}(\rho w\phi)}_{\text{Convection}} = \underbrace{\frac{\partial}{\partial x}\left(\Gamma_\phi \frac{\partial\phi}{\partial x}\right) + \frac{\partial}{\partial y}\left(\Gamma_\phi \frac{\partial\phi}{\partial y}\right) + \frac{\partial}{\partial z}\left(\Gamma_\phi \frac{\partial\phi}{\partial z}\right)}_{\text{Diffusion}} + \underbrace{S_\phi}_{\text{Source}} \tag{2.1a}$$

In quasicontinuum domain:[45]

$$\underbrace{\frac{\partial}{\partial t}(\gamma_v \rho\phi)}_{\text{Unsteady}} + \underbrace{\frac{\Delta(\gamma_x \rho u\phi)}{\Delta x} + \frac{\Delta(\gamma_y \rho v\phi)}{\Delta y} + \frac{\Delta(\gamma_z \rho w\phi)}{\Delta z}}_{\text{Convection}}$$

$$= \underbrace{\frac{\Delta\left(\gamma_x \Gamma_\phi \frac{\partial\phi}{\partial x}\right)}{\Delta x} + \frac{\Delta\left(\gamma_y \Gamma_\phi \frac{\partial\phi}{\partial y}\right)}{\Delta y} + \frac{\Delta\left(\gamma_z \Gamma_\phi \frac{\partial\phi}{\partial z}\right)}{\Delta z}}_{\text{Diffusion}} + \underbrace{\gamma_v S_\phi}_{\text{Source}} \qquad (2.1b)$$

Here, u, v, and w are the velocities in the x, y, and z directions, respectively; γ_v is the volume porosity (fraction of the volume occupied by the fluid) and γ_x, γ_y, and γ_z are the directional surface porosities (fraction of the surface area that is unobstructed to fluid flow) in the x, y, and z directions, respectively. The convective and diffusive terms $\Delta(\varphi)/\Delta x_i$ in Eq. 2.1b are defined as

$$\frac{\Delta(\varphi)}{\Delta x_i} = \frac{\varphi\left(x_i + \Delta x_i/2\right) - \varphi\left(x_i - \Delta x_i/2\right)}{\Delta x_i} \qquad (2.2)$$

In which x_i stands for the x, y, or z coordinate. The diffusion coefficient Γ_ϕ and the source term S_ϕ are specific to each meaning of ϕ. The sources for all conservation equations are given in Tables 1 and 2.

The conservation equations in the cylindrical coordinate system also have the same general form (Eq. 2.1) when we place the centrifugal and Coriolis force terms in the source term S_ϕ. We can, therefore, apply all formulations for the Cartesian coordinates to cylindrical coordinates with the simple transformations shown in Table 3.

Equation 2.1b can be considered very general, because it reduces to the conservation equation for a continuum (Eq. 2.1a) when we make volume porosities and directional surface porosities = 1 ($\gamma_v = \gamma_x = \gamma_y = \gamma_z = 1.0$), distributed resistances $R_x = R_y = R_z = 0$ (or $R_r = R_\theta = R_z = 0$ in a cylindrical coordinate system), and heat source $\dot{Q}_{sb} = 0$.

For turbulent flow, all quantities in Eq. 2.1 are considered time-averaged values, and the diffusion coefficient Γ is interpreted as the effective (laminar and turbulent) diffusion coefficient, i.e.,

$$\Gamma_\phi = \Gamma_{\phi,\text{laminar}} + \Gamma_{\phi,\text{turbulent}}. \qquad (2.3)$$

We can also express the effective diffusion coefficient in terms of the corresponding turbulent Prandtl number, i.e.,

$$\Gamma_\phi = \mu_{\text{laminar}} + \frac{\mu_{\text{turbulent}}}{\sigma_\phi}. \qquad (2.4)$$

Here, σ_ϕ is the turbulent Prandtl number based on the diffusivity of variable ϕ.

Table 1. Source terms in Cartesian coordinate system[a]

Equation	Variable (ϕ)	Direction	Diffusion Coefficient (Γ_ϕ)	Source Term (S_ϕ)
Continuity	1	Scalar	0	0
Momentum				
(i)	u	x	μ	$\rho g_x + V_x - R_x - \left(\frac{\partial p}{\partial x}\right)$
(ii)	v	y	μ	$\rho g_y + V_y - R_y - \left(\frac{\partial p}{\partial y}\right)$
(iii)	w	z	μ	$\rho g_z + V_z - R_z - \left(\frac{\partial p}{\partial z}\right)$
Energy	h	Scalar	λ	$\frac{dp}{dt} + \dot{Q}_{rb} + \dot{Q} + \Phi$

[a] V_x, V_y, V_z Balance of the viscous diffusion terms
R_x, R_y, R_z Distributed resistances due to solid structures in a momentum control volume
$\dot{Q}_{rb}$ Rate of heat liberated from solid structures per unit fluid volume
$\dot{Q}$ Rate of internal heat generation per unit fluid volume
Φ Dissipation function

Table 2. Source terms in cylindrical coordinate system[a]

Equation	Variable (ϕ)	Direction	Diffusion Coefficient (Γ_ϕ)	Source Term (S_ϕ)
Continuity	1	Scalar	0	0
Momentum				
(i)	v_r	r	μ	$\rho\frac{v_\theta^{2*}}{r} \rho g_r + V_r - R_r - \frac{1}{r}\frac{\partial}{\partial r}(rp)$
(ii)	v_θ	θ	μ	$-\frac{\rho v_r v_\theta}{r} + \rho g_\theta + V_\theta - R_\theta - \frac{1}{r}\frac{\partial}{\partial \theta}(P)$
(iii)	v_z	z	μ	$\rho g_z + V_z - R_z - \frac{\partial}{\partial z}(p)$
Energy	h	Scalar	λ	$\frac{dp}{dt} + \dot{Q}_{rb} + \dot{Q} + \Phi$

[a] * Centrifugal force term
** Coriolis force term
V_r, V_θ, V_z Balance of the viscous diffusion terms
R_x, R_θ, R_z Distributed resistances due to solid structures in a momentum control volume
$\dot{Q}_{rb}$ Rate of heat liberated from solid structures per unit fluid volume
$\dot{Q}$ Rate of internal heat generation per unit fluid volume
Φ Dissipation function

Table 3. Transformations for Cartesian and cylindrical coordinate systems

Cartesian Coordinates	Cylindrical Coordinates
x	r
y	θ
z	z
Δx	Δr
Δy	rΔθ
Δz	Δz
u	v_r
v	v_θ
w	v_z

The transport equations of turbulence parameters k and ε for computation of the turbulent diffusion coefficient also have the same general form as Eq. 2.1; however, for clarity of presentation, they are included in Sec. 6.

3 Control Volume

3.1 Construction of a Computational Cell

The computational cells around a grid point can be defined in a number of ways. In COMMIX-1C, the computational cell is defined by the locations of cell volume faces, and a grid point is placed in the geometrical center of each cell volume. Cell sizes can be nonuniform. This type of construction is shown in Fig. 1. The convention used in COMMIX-1C for defining the neighboring cells and cell faces is given in Table 4.

3.2 Control Volume for Field Variables

In COMMIX, we use the staggered grid system, in which all dependent field variables (pressure, temperature, density, enthalpy, turbulent kinetic energy, physical properties, etc.) are calculated at a cell center and all flow variables (velocity components) are calculated at the surfaces of a cell.

For a field variable, we consider the control volume to be as shown in Fig. 2. It is constructed around a grid point 0, which has grid points 1 (i-1), and 2 (i+1) as its west and east neighbors; grid point 3 (j-1) and 4 (j+1) as its bottom and top neighbors; and grid points 5 (k-1) and 6 (k+1) as its south and north neighbors. We integrate each term of the conservation equation, step by step, over the control volume to derive the finite-volume equation.

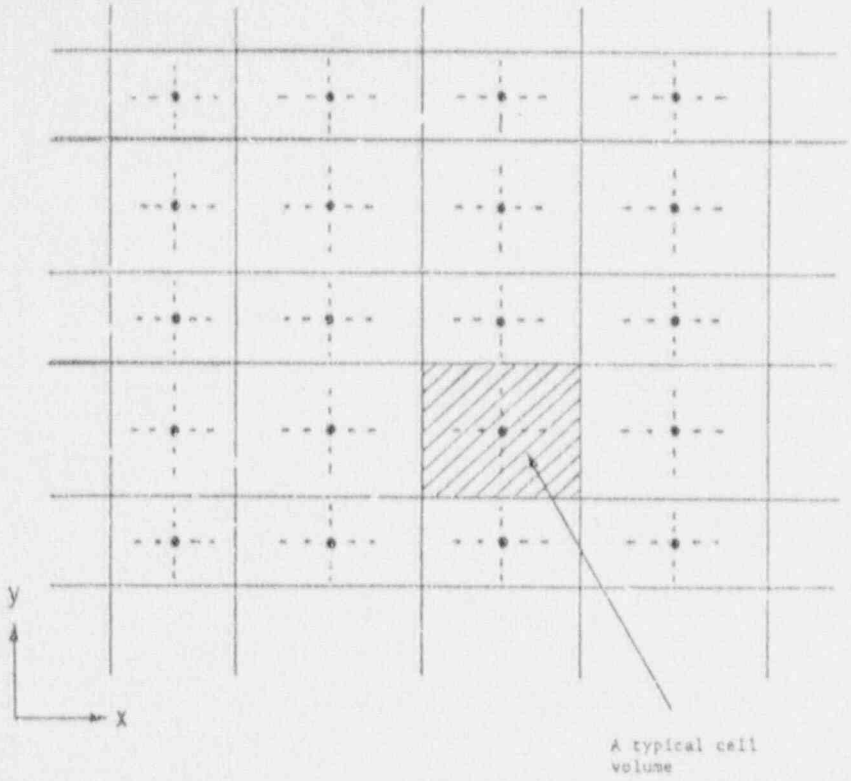

Fig. 1. Construction of cell volumes

Table 4. Convention used in COMMIX-1C to define neighboring-cell control volumes

Subscript	Cell Centers			Cell-Face Center		
	x	y	z	x	y	z
0	i,	j,	k			
1	i-1,	j,	k	i-1/2	j,	k
2	i+1,	j,	k	i+1/2,	j,	k
3	i,	j-1,	k	i,	j-1/2,	k
4	i,	j+1,	k	i,	j+1/2	k
5	i,	j,	k-1	i,	j,	k-1/2
6	i,	j,	k+1	i,	j,	k+1/2

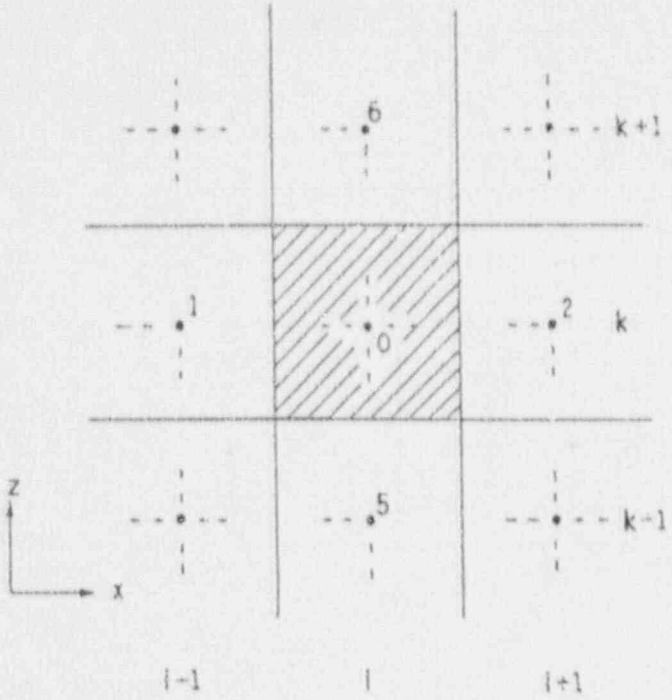

Fig. 2. Cell volume around point 0 in i,j,k notation

3.3 Control Volume for Flow Variables

Although most dependent variables are calculated for a grid point, the velocity components u, v, and w are exceptions. They are calculated for displaced or "staggered" locations, not at the grid point. The displaced locations of the velocity components are such that they are placed on the faces of a control volume. Thus, the k-direction velocity w is calculated at the faces normal to the k direction.

Figure 3 shows the locations of u and w by short arrows on a two-dimensional grid; the three-dimensional counterpart can be easily imagined. With respect to a grid point, the u location is displaced only in the i direction, the w location only in the k direction, and so on. The location for w thus lies in the k direction link, joining two adjacent grid points. It is the pressure difference between these grid points that will be used to drive the velocity w located between them. This is the main consequence of the staggered grid.

A direct consequence of the staggered grid is that the control volumes to be used for the conservation of momentum must also be staggered. The control volumes shown in Figs. 1 and 2 will now be referred to as the main control volumes. The control volumes for momentum will be staggered in the direction of the momentum such that the faces normal to that direction pass through the grid points (see Fig. 4). Thus, the pressures at these grid points can be directly used for calculating the pressure force on the momentum control volume. Table 5 shows the convention used for the subscripts, and Fig. 4 shows the momentum control volumes for the x and z directions.

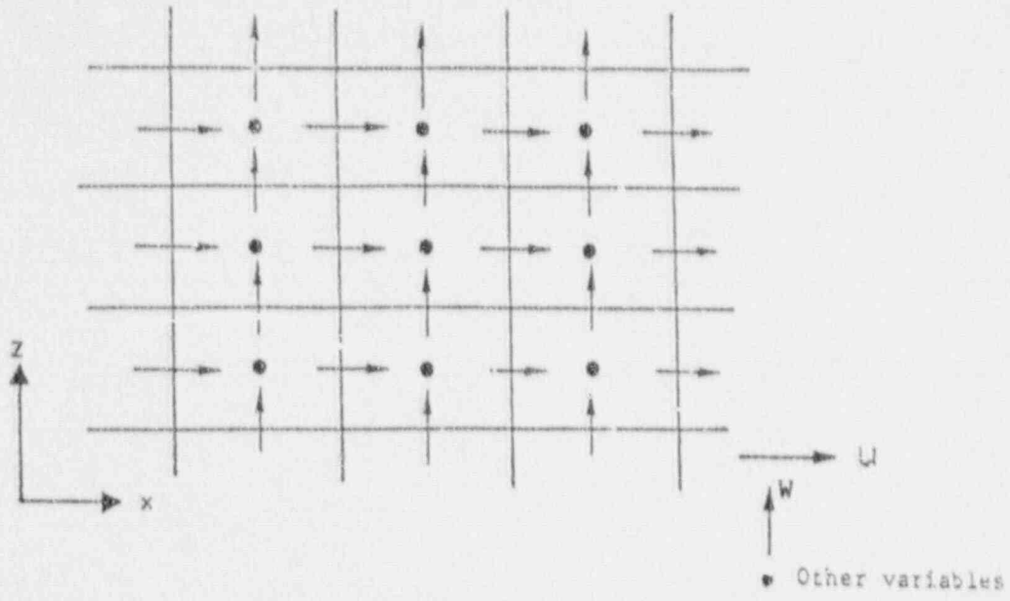

Fig. 3. Staggered grid

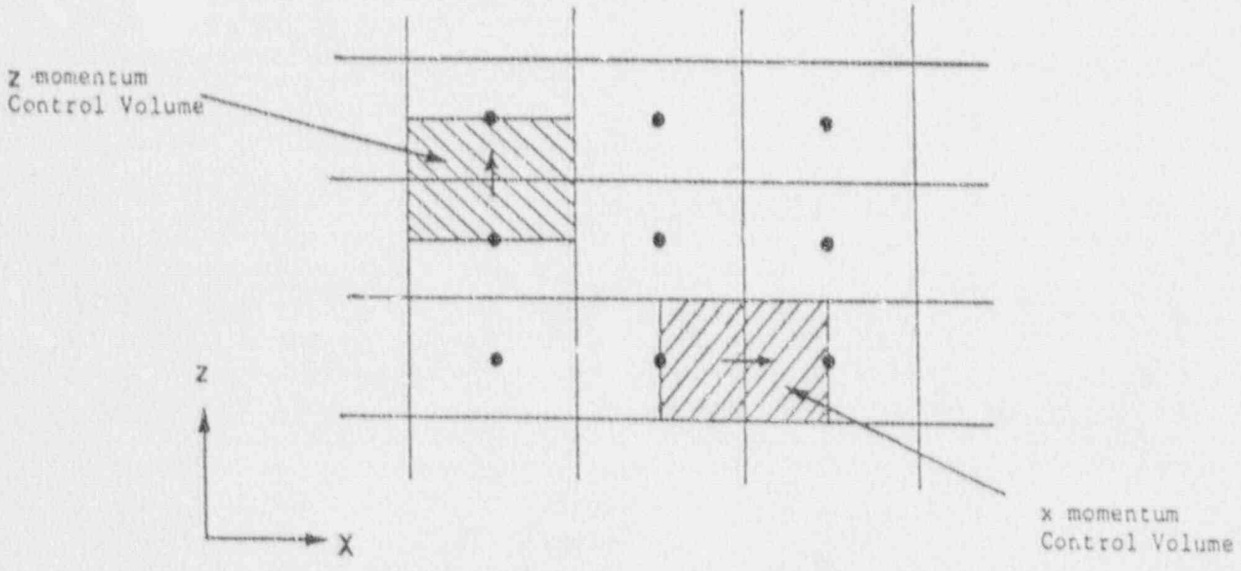

Fig. 4. Momentum control volumes

Table 5. Convention used in COMMIX-1C to define neighboring control volumes for z-direction momentum equations

Subscript	Momentum Control Volume Centers			Momentum Control Volume Face Centers		
	x	y	z	x	y	z
0	i,	j,	k+1/2			
1	i-1,	j,	k+1/2	i-1/2,	j,	k+1/2
2	i+1,	j,	k+1/2	i+1/2,	j,	k+1/2
3	i,	j-1,	k+1/2	i,	j-1/2,	k+1/2
4	i,	j+1,	k+1/2	i,	j+1/2	k+1/2
5	i,	j,	k-1/2	i,	j,	k
6	i,	j,	k+3/2	i,	j,	k+1

4 Finite-Volume Formulation

Although the finite-volume formulation is applied to a grid in both the Cartesian and cylindrical coordinate systems, only a Cartesian coordinate grid system is used here to demonstrate the formulation of the finite-volume equations. Similarly, we have used only the z-momentum equation to illustrate the formulation of the momentum equation. Extension of the derivation to the x and y momentum equations is straightforward. It should be noted that the main control volume is applicable to both the energy and the continuity equations, and the momentum control volume is applicable to the momentum equations.

The finite-volume equations are derived by integrating the governing equation (Eq. 2.1) over a control volume. We integrate each term separately.

4.1 Convection Term

4.1.1 Main Control Volume

The integration of the convection terms over the control volume gives

$$\int\left[\frac{\Delta(\gamma_x \rho u\phi)}{\Delta x}+\frac{\Delta(\gamma_y \rho v\phi)}{\Delta y}+\frac{\Delta(\gamma_z \rho w\phi)}{\Delta z}\right]dx\,dy\,dz$$

$$= F_2\langle\phi\rangle_2^0 - F_1\langle\phi\rangle_0^1 + F_4\langle\phi\rangle_4^0 - F_3\langle\phi\rangle_0^3 + F_6\langle\phi\rangle_6^0 - F_5\langle\phi\rangle_0^5 . \qquad (4.1)$$

Here, F (= density x velocity x flow area) is the mass flow across the surface of the control volume, and subscripts 1–6 stand for the west, east, top, bottom, south, and north surfaces, respectively (see Fig. 5). For example,

$$F_2 = F_{i+1/2} = \langle\rho\rangle_2^0\left(\gamma_x u\Delta y\Delta z\right)_2 = \langle\rho\rangle_2^0\left(uA_x\right)_2 = \langle\rho\rangle_{i+1}^1\left(uA_x\right)_{i+1/2} \tag{4.2}$$

is the mass flux at the east surface, as shown in Fig. 5. $\langle\phi\rangle_2^0$ is the value of ϕ associated with surface "2," which is convected by the mass flow F_2. Since only the values of ϕ associated with cell volumes are available for the main control volume, a relationship must be assumed between the associated surface and volume values. The upwind difference scheme provides one such relation as

$$\langle\phi\rangle_2^0 = \langle\phi\rangle_{i+1}^1 = \phi_0 = \phi_i \quad (\text{if } F_2 \text{ is } +\text{ve}), \tag{4.3a}$$

$$= \phi_2 = \phi_{i+1} \quad (\text{if } F_2 \text{ is } -\text{ve}) \tag{4.3b}$$

The superscript location value is to be used for positive velocity, and the subscript location is to be used for negative velocity. Each term on the right side of Eq. 4.1 can also be written as, for example,

$$F_2\langle\phi\rangle_2^0 = \left|0,F_2\right|\phi_0 - \left|0,-F_2\right|\phi_2 . \tag{4.4}$$

The operator $|\ |$ is defined as equal to the greater of two arguments, i.e.,

$$\begin{aligned} |A,B| &= A \quad \text{if } A > B, \\ &= B \quad \text{if } B > A. \end{aligned} \tag{4.5}$$

In accordance with the above convention and after some simplification, we rewrite Eq. 4.1 as

$$\int\left[\frac{\Delta\left(\gamma_x\rho u\phi\right)}{\Delta x}+\frac{\Delta\left(\gamma_y\rho v\phi\right)}{\Delta y}+\frac{\Delta\left(\gamma_z\rho w\phi\right)}{\Delta z}\right]dx\,dy\,dz$$

$$= \left[\left|0,F_2\right|+\left|0,F_4\right|+\left|0,F_6\right|+\left|0,-F_1\right|+\left|0,-F_3\right|+\left|0,-F_5\right|\right]\tilde{\phi}_0$$

$$-\left[\left|0,-F_2\right|\tilde{\phi}_2+\left|0,-F_4\right|\tilde{\phi}_4+\left|0,-F_6\right|\tilde{\phi}_6+\left|0,F_1\right|\tilde{\phi}_1+\left|0,F_3\right|\tilde{\phi}_3+\left|0,F_5\right|\tilde{\phi}_5\right]. \tag{4.6}$$

Note that we have introduced a curly bar over the dependent variable ϕ in Eq. 4.6. We define

$$\alpha\phi^{n+1}+(1-\alpha)\phi^n, \tag{4.7}$$

where α is an implicitness parameter. The introduction of the implicitness parameter α makes the convective flux formulation, Eq. 4.6, very general, i.e., from the semi-implicit formulation where some variables are at old-time values ($\alpha = 0$) to a fully implicit formulation where all variables are at new-time values ($\alpha = 1$).

All six convective fluxes for the main control volume are listed in Table 6.

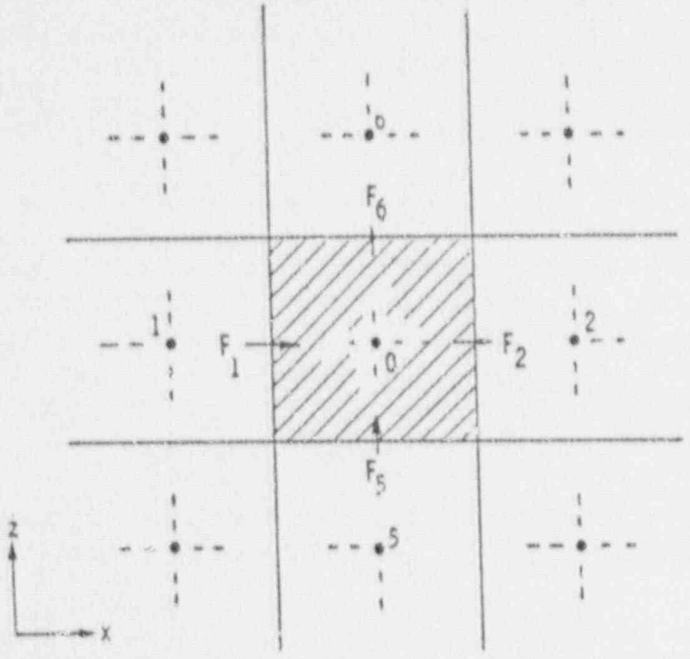

Fig. 5. Convective fluxes for main control volume

Table 6. Convective fluxes for main control volume

$F_1 = (A_x u)_{i-1/2} \langle\rho\rangle_0^1$
$F_2 = (A_x u)_{i+1/2} \langle\rho\rangle_2^0$
$F_3 = (A_y v)_{j-1/2} \langle\rho\rangle_0^3$
$F_4 = (A_y v)_{j+1/2} \langle\rho\rangle_4^0$
$F_5 = (A_z w)_{k-1/2} \langle\rho\rangle_0^5$
$F_6 = (A_z w)_{k+1/2} \langle\rho\rangle_6^0$

4.1.2 Momentum Control Volume

Figure 6 shows the staggered mesh for the z-momentum control volume. The various mass flows shown in the figure are as follows:

$$F_{z0} = \langle\rho\rangle_{\theta}^{0} A_{z0} W_0 \tag{4.8a}$$

$$F_{z1} = \langle\rho\rangle_{\theta 1}^{1} A_{z1} W_1 \tag{4.8b}$$

$$F_{z2} = \langle\rho\rangle_{\theta 2}^{2} A_{z2} W_2 \tag{4.8c}$$

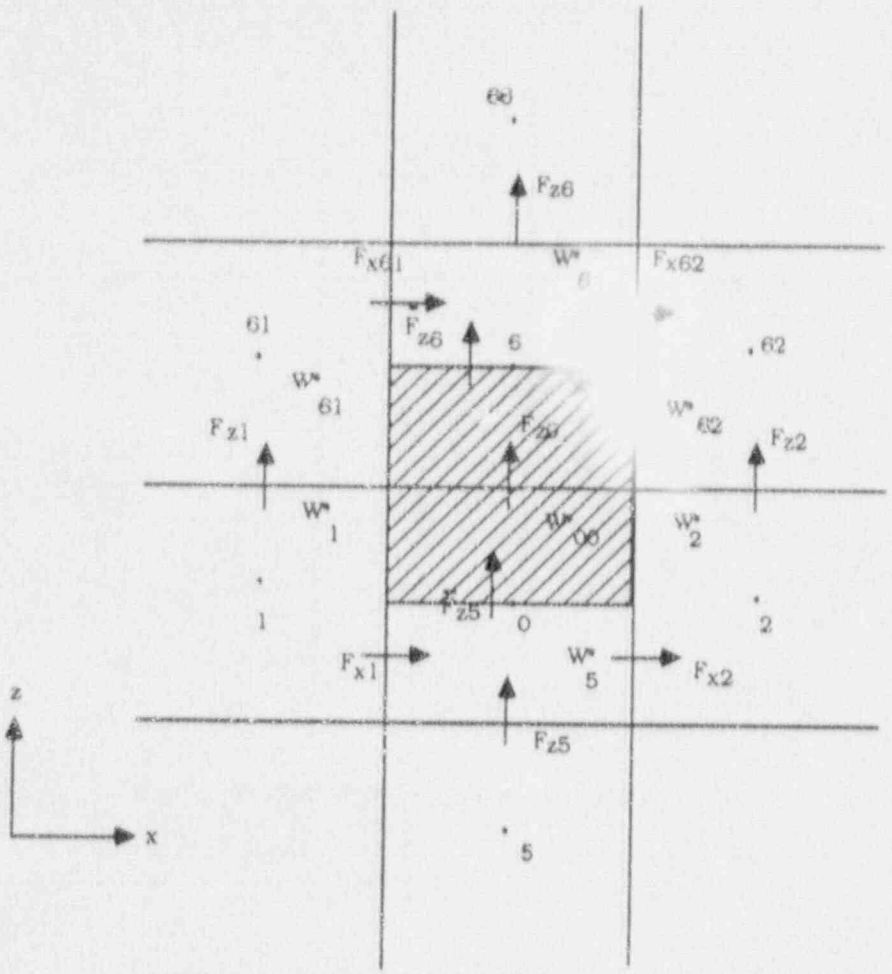

Fig. 6. Convective fluxes and average velocities for z-momentum control volume

$$F_{z5} = \langle \rho \rangle_{0}^{5} A_{z5} W_5 \tag{4.8d}$$

$$F_{z6} = \langle \rho \rangle_{z6}^{6} A_{z6} W_6 \tag{4.8e}$$

$$F_{x1} = \langle \rho \rangle_{0}^{1} A_{x1} u_1 \tag{4.8f}$$

$$F_{x2} = \langle \rho \rangle_{2}^{0} A_{x2} u_2 \tag{4.8g}$$

$$F_{x61} = \langle \rho \rangle_{6}^{61} A_{x61} u_{61} \tag{4.8h}$$

$$F_{x62} = \langle \rho \rangle_{62}^{6} A_{x62} u_{62} \tag{4.8i}$$

where the velocities w and u are defined at the cell faces as shown in Fig. 3. The mass flow rates on the north and south faces of the staggered mesh ($\bar{F}_{z5}$ and $\bar{F}_{z6}$) are not directly available. In COMMIX-1C, it is assumed that

$$\bar{F}_{z5} = (F_{z0} + F_{z5})/2 \tag{4.8j}$$

$$\bar{F}_{z6} = (F_{z0} + F_{z6})/2 . \tag{4.8k}$$

In previous COMMIX versions, the velocity, w, is assumed to be transported by the convective fluxes. In COMMIX-1C, however, we assume that the transported quantity is a momentum per unit mass associated with a certain volume instead of the facial velocity w. Referring to Fig. 6, the z momentum (M_z) associated with the lower half of the staggered mesh is

$$(M_z)_{V_0/2} = \int_{V_0/2} \gamma_v \rho w dx dy dz . \tag{4.9a}$$

If a volume-averaged velocity W^*_{00} is defined as

$$\rho_0 \frac{V_0}{2} W^*_{00} = (M_z)_{V_0/2} , \tag{4.9b}$$

then

$$W^*_{00} = \frac{2(M_z)_{V_0/2}}{V_0 \rho_0} = \frac{2\int_{V_0/2} \gamma_v \rho w dx dy dz}{\rho_0 V_0} , \tag{4.9c}$$

or

$$W^*_{00} = \frac{2\int_{\Delta z_0/2} \left[\int_{A_z} (\gamma_s \rho w) dx dy\right] dz}{\rho_0 V_0} . \tag{4.9d}$$

The integral inside the bracket of Eq. 4.9d is the mass flow rate through any cross-sectional area Az inside the volume $V_0/2$. In COMMIX-1C, this mass flow rate is assumed to be equal to F_{z0} and Eq. 4.9d becomes

$$W^*_{00} = \frac{\Delta z_0 F_{z0}}{\rho_0 V_0} . \tag{4.9e}$$

W^*_{00} represents the momentum per unit mass of the fluid in the volume $V_0/2$ and is the quantity assumed to be transported. W^*_{00} has the dimension of velocity and can also be considered as a volume-averaged velocity defined by Eq. 4.9c.

Similarly, a volume-averaged velocity can be defined for the upper half of the staggered mesh in Fig. 6:

$$\frac{V_6}{2} \rho_6 W^*_{06} = (M_z)_{V_6/2} = \int_{V_6/2} \gamma_v \rho w dx dy dz \tag{4.9f}$$

and

$$W^*_{06} = \frac{\Delta z_0 F_{z0}}{\rho_6 V_6} . \tag{4.9g}$$

The volume-averaged velocities (w^*) associated with their respective volumes are also shown in Fig. 6 and are defined by the following equations:

$$W^*_{00} = \frac{F_{z0}\Delta z_0}{\rho_0 V_0} = \frac{\langle\rho\rangle^0_6 A_{z0}\Delta z_0}{\rho_0 V_0}\cdot W_0 \tag{4.10a}$$

$$W^*_{06} = \frac{F_{z0}\Delta z_6}{\rho_6 V_6} = \frac{\langle\rho\rangle^0_6 A_{z0}\Delta z_6}{\rho_6 V_6}\cdot W_0 \tag{4.10b}$$

$$W^*_1 = \frac{F_{z1}\Delta z_0}{\rho_1 V_1} = \frac{\langle\rho\rangle^1_{61} A_{z1}\Delta z_0}{\rho_1 V_1}\cdot W_1 \tag{4.10c}$$

$$W^*_2 = \frac{F_{z2}\Delta z_0}{\rho_2 V_2} = \frac{\langle\rho\rangle^2_{62} A_{z2}\Delta z_0}{\rho_2 V_2}\cdot W_2 \tag{4.10d}$$

$$W^*_5 = \frac{F_{z5}\Delta z_0}{\rho_0 V_0} = \frac{\langle\rho\rangle^5_{0} A_{z5}\Delta z_0}{\rho_0 V_0}\cdot W_5 \tag{4.10e}$$

$$W^*_6 = \frac{F_{z6}\Delta z_6}{\rho_6 V_6} = \frac{\langle\rho\rangle^6_{66} A_{z6}\Delta z_6}{\rho_6 V_6}\cdot W_6 \tag{4.10f}$$

$$W^*_{61} = \frac{F_{z1}\Delta z_6}{\rho_{61} V_{61}} = \frac{\langle\rho\rangle^1_{61} A_{z1}\Delta z_6}{\rho_{61} V_{61}}\cdot W_1 \tag{4.10g}$$

$$W^*_{62} = \frac{F_{z2}\Delta z_6}{\rho_{62} V_{62}} = \frac{\langle\rho\rangle^2_{62} A_{z2}\Delta z_6}{\rho_{62} V_{62}}\cdot W_2 \tag{4.10h}$$

where $V = \gamma_v \Delta x\Delta y\Delta z$ is the volume of the fluid at that location. Equation 4.10 can be considered as the closure relations (and assumptions) that link the volume-averaged velocities to the facial velocities. These assumptions are necessary because the volume averaged velocities are not directly available quantities. The derivation described here is somewhat more complicated than those in previous COMMIX versions. But the calculations using the present formulation are found to be more robust than those in previous COMMIX versions in some applications. In addition, as we shall demonstrate later, the previous hypothesized closure relations will reduce to a formulation that ensures that the pressure drop occurs at the same location as the density gradient in one-dimensional steady state flows. As shown by Padilla and Rowe,[56] using the so-called donor flow formulation, this effect can be important when significant density gradients occur in a system. Furthermore, as we shall demonstrate later, the closure relations described here, used in the momentum equations, satisfy the one-dimensional steady-state Bernoulli equation.

Now we can write the finite-volume expressions for the convective terms in the z momentum equation (Fig. 6).

$$\int \frac{\Delta(\gamma_z \rho w w)}{\Delta z}\, dx\, dy\, dz$$

$$= \left|0,\overline{F}_{x6}\right| W^*_{06} - \left|0,-\overline{F}_{x6}\right| W^*_6 - \left|0,\overline{F}_{x5}\right| W^*_5 + \left|0,-\overline{F}_{x5}\right| W^*_{00}\ , \tag{4.11a}$$

$$\int \frac{\Delta(\gamma_x \rho w u)}{\Delta x}\, dx\, dy\, dz$$

$$= \frac{1}{2}\left|0, F_{x2}\right| W_{00}^{*} - \frac{1}{2}\left|0, -F_{x2}\right| W_{2}^{*} + \frac{1}{2}\left|0, F_{x62}\right| W_{06}^{*} - \frac{1}{2}\left|0, -F_{x62}\right| W_{62}^{*}$$

$$- \frac{1}{2}\left|0, F_{x1}\right| W_{1}^{*} + \frac{1}{2}\left|0, -F_{x1}\right| W_{00}^{*} - \frac{1}{2}\left|0, F_{x61}\right| W_{61}^{*} + \frac{1}{2}\left|0, -F_{x61}\right| W_{06}^{*} \qquad (4.11b)$$

The third convective term (ρwv) in Eq. 2.1b can be written similarly as Eq. 4.11b. By adding all three convective terms and by using Eqs. 4.8 and 4.10 we obtain the finite-volume expression for z momentum control volume in the following form:

$$\int \left[\frac{\Delta(\gamma_z \rho w w)}{\Delta z} + \frac{\Delta(\gamma_x \rho w u)}{\Delta x} + \frac{\Delta(\gamma_y \rho w v)}{\Delta y}\right] dx\, dy\, dz$$

$$= a_0^{wc} w_0 - a_1^{wc} w_1 - a_2^{wc} w_2 - a_3^{wc} w_3 - a_4^{wc} w_4 - a_5^{wc} w_5 - a_6^{wc} w_6 \qquad (4.12)$$

where the coefficients are defined by the following equations:

$$a_0^{wc} = \frac{\langle\rho\rangle_6^0 A_{z0} \Delta z_6}{\rho_6 V_6}\left(\left|0, \overline{F}_{z6}\right| + \frac{1}{2}\left|0, -F_{x62}\right| + \frac{1}{2}\left|0, -F_{x61}\right| + \frac{1}{2}\left|0, -F_{y64}\right| + \frac{1}{2}\left|0, -F_{y63}\right|\right)$$

$$+ \frac{\langle\rho\rangle_6^0 A_{z0} \Delta z_0}{\rho_0 V_0}\left(\left|0, -\overline{F}_{z5}\right| + \frac{1}{2}\left|0, F_{x2}\right| + \frac{1}{2}\left|0, -F_{x1}\right| + \frac{1}{2}\left|0, F_{y4}\right| + \frac{1}{2}\left|0, -F_{y3}\right|\right) \qquad (4.13a)$$

$$a_1^{wc} = \frac{1}{2}\left[\left|0, F_{x1}\right| \Delta z_0 \langle\rho\rangle_{61}^{1} A_{z1}/\rho_1 V_1 + \left|0, F_{x61}\right| \Delta z_6 \langle\rho\rangle_{61}^{1} A_{z1}/\rho_{61} V_{61}\right] \qquad (4.13b)$$

$$a_2^{wc} = \frac{1}{2}\left[\left|0, -F_{x2}\right| \Delta z_0 \langle\rho\rangle_{62}^{2} A z_2/\rho_2 V_2 + \left|0, -F_{x62}\right| \Delta z_6 \langle\rho\rangle_{62}^{2} A z_2/\rho_{62} V_{62}\right] \qquad (4.13c)$$

$$a_3^{wc} = \frac{1}{2}\left[\left|0, F_{y3}\right| \Delta z_0 \langle\rho\rangle_{63}^{3} A z_3/\rho_3 V_3 + \left|0, F_{y63}\right| \Delta z_6 \langle\rho\rangle_{63}^{3} A z_3/\rho_{63} V_{63}\right] \qquad (4.13d)$$

$$a_4^{wc} = \frac{1}{2}\left[\left|0, -F_{y4}\right| \Delta z_0 \langle\rho\rangle_{64}^{4} A z_4/\rho_4 V_4 + \left|0, -F_{y64}\right| \Delta z_6 \langle\rho\rangle_{64}^{4} A z_4/\rho_{64} V_{64}\right] \qquad (4.13e)$$

$$a_5^{wc} = \left|0, \overline{F}_{z5}\right| \Delta z_0 \langle\rho\rangle_0^5 A z_5/\rho_0 V_0 \qquad (4.13f)$$

$$a_6^{wc} = \left|0, -\overline{F}_{z6}\right| \Delta z_6 \langle\rho\rangle_{66}^{6} A z_6/\rho_6 V_6 \qquad (4.13g)$$

Here the superscript "w" indicates the w-momentum equation and "c" indicates convection. The various convective fluxes for the z-momentum control volume are listed in Table 7.

Similar finite-volume expressions can be derived for the x and y momentum control volumes. We can rewrite Eq. 4.12 in a more general form

$$\int \left[\frac{\Delta(\gamma_z \rho w \phi)}{\Delta z} + \frac{\Delta(\gamma_y \rho v \phi)}{\Delta y} + \frac{\Delta(\gamma_x \rho u \phi)}{\Delta x}\right] dx\, dy\, dz$$

Table 7. Convective fluxes for z-momentum control volume

$$\bar{F}_{z5} = \frac{1}{2}(F_{z5} + F_{z0}) = \frac{1}{2}\left[\langle\rho\rangle_6^0 Az_0\ w_0 + \langle\rho\rangle_0^5 Az_5\ w_5\right]$$

$$\bar{F}_{z6} = \frac{1}{2}(F_{z6} + F_{z0}) = \frac{1}{2}\left[\langle\rho\rangle_{66}^6 Az_6\ w_6 + \langle\rho\rangle_6^0 Az_0\ w_0\right]$$

$$F_{z0} = \langle\rho\rangle_{k+1}^{k}(Az\ w)_{k+1/2} = \langle\rho\rangle_6^0 Az_0\ w_0$$

$$F_{z1} = \langle\rho\rangle_{i-1,k+1}^{i-1,k}(Az\ w)_{i-1,k+1/2} = \langle\rho\rangle_{61}^{1} Az_1\ w_1$$

$$F_{z2} = \langle\rho\rangle_{i+1,k+1}^{i+1,k}(Az\ w)_{i+1,k+1/2} = \langle\rho\rangle_{62}^{2} Az_2\ w_2$$

$$F_{z3} = \langle\rho\rangle_{j-1,k+1}^{j-1,k}(Az\ w)_{j-1,k+1/2} = \langle\rho\rangle_{63}^{3} Az_{63}\ w_3$$

$$F_{z4} = \langle\rho\rangle_{j+1,k+1}^{j+1,k}(Az\ w)_{j+1,k+1/2} = \langle\rho\rangle_{64}^{4} Az_{64}\ w_4$$

$$F_{z5} = \langle\rho\rangle_{k}^{k-1}(Az\ w)_{k-1/2} = \langle\rho\rangle_0^5 Az_5\ w_5$$

$$F_{z6} = \langle\rho\rangle_{k+2}^{k+1}(Az\ w)_{k+3/2} = \langle\rho\rangle_{66}^{6} Az_6\ w_6$$

$$F_{x2} = \langle\rho\rangle_{i+1}^{i}(Ax\ u)_{i+1/2} = \langle\rho\rangle_2^0 Ax_2\ u_2$$

$$F_{x1} = \langle\rho\rangle_{i}^{i-1}(Ax\ u)_{i-1/2} = \langle\rho\rangle_0^1 Ax_1\ u_1$$

$$F_{x62} = \langle\rho\rangle_{i+1,k+1}^{i,k+1}(Ax\ u)_{i+1/2,k+1} = \langle\rho\rangle_{62}^{6} Ax_{62}\ u_{62}$$

$$F_{x61} = \langle\rho\rangle_{i+1,k+1}^{i-1,k+1}(Ax\ u)_{i-1/2,k+1} = \langle\rho\rangle_{61}^{61} Ax_{61}\ u_{61}$$

$$F_{y4} = \langle\rho\rangle_{j+1}^{j}(Ay\ v)_{j+1/2} = \langle\rho\rangle_4^0 Ay_4\ v_4$$

$$F_{y3} = \langle\rho\rangle_{j}^{j-1}(Ay\ v)_{j-1/2} = \langle\rho\rangle_0^3 Ay_3\ v_3$$

$$F_{y64} = \langle\rho\rangle_{j+1,k+1}^{j,k+1}(Ay\ v)_{j+1/2,k+1} = \langle\rho\rangle_{64}^{6} Ay_{64}\ v_{64}$$

$$F_{y63} = \langle\rho\rangle_{j,k+1}^{j-1,k+1}(Ay\ v)_{j-1/2,k+1} = \langle\rho\rangle_6^{63} Ay_{63}\ v_{63}$$

$$= a_0^{\phi c}\tilde{\phi}_0 - a_1^{\phi c}\tilde{\phi}_1 - a_2^{\phi c}\tilde{\phi}_2 - a_3^{\phi c}\tilde{\phi}_3 - a_4^{\phi c}\tilde{\phi}_4 - a_5^{\phi c}\tilde{\phi}_5 - a_6^{\phi c}\tilde{\phi}_6 . \tag{4.14}$$

Here again, we have employed the general variable ϕ, which can represent either u, v, or w because we are dealing with momentum control volumes. Also, we have introduced a curly bar over the dependent variable ϕ. As defined in Eq. 4.7, $\tilde{\phi}$ represents a combination of old and new time values.

To demonstrate that the pressure drop occurs at the same location where the density change occurs, we consider a steady-state one-dimensional flow with constant flow area. Assuming that convection is dominating, Eq. 2.1b for the z direction becomes

$$\frac{\Delta(\gamma_z \rho w w)}{\Delta z} = -\gamma_v \frac{\partial p}{\partial z} . \tag{4.15}$$

Integrating over the z momentum control volume (Fig. 6) and assuming that w is positive, we obtain from Eq. 4.11a

$$\bar{F}_{z6}\, w'_{06} - \bar{F}_{z5}\, w'_5 = -(P_6 - P_0)\,Az , \tag{4.16}$$

where Az is the flow area in the z direction. Substituting Eqs. 4.8 and 4.10 into Eq. 4.16,

$$(F_{z0} + F_{z6})F_{z0} / 2\rho_6\, Az_6 - (F_{z0} + F_{z5})F_{z5} / 2\rho_0\, Az_0 = -(P_6 - P_0)\,Az \tag{4.17}$$

For one-dimensional flow with constant flow area

$$Az_0 = Az_5 = Az_6 = Az ,$$

$$F_{z0} = \rho_0\, Az_0\, W_0 = \rho\, Az\, W ,$$

$$F_{z5} = \rho_5\, Az_5\, W_5 = \rho\, Az\, W ,$$

$$F_{z6} = \rho_6\, Az_6\, W_6 = \rho\, Az\, W ,$$

and Eq. 4.17 reduces to

$$(\rho W)^2 \left(\frac{1}{\rho_6} - \frac{1}{\rho_0}\right) = -(P_6 - P_0) , \tag{4.18}$$

which indicates that the pressure drop occurs at the same location where the density change occurs. In a similar manner, it can be demonstrated that the same relation holds if W is negative.

4.2 Diffusion Term

4.2.1 Main Control Volume

The integration of diffusion terms over a main control volume (Fig. 7) gives

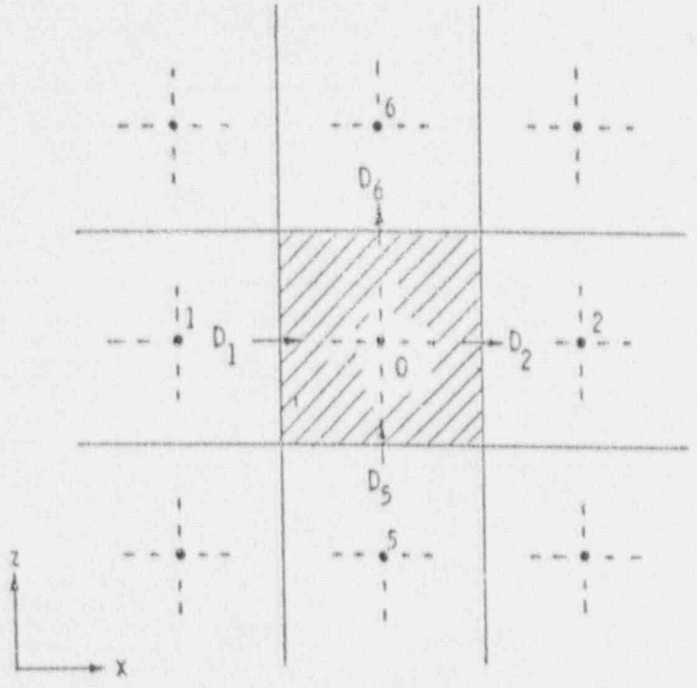

Fig. 7. Diffusion fluxes for main control volume

Table 8. Diffusion strengths for main control volume

$D_1 = (A_x)_{i-1/2}(\Gamma_0 + \Gamma_1)/(\Delta x_0 + \Delta x_1)$
$D_2 = (A_x)_{i+1/2}(\Gamma_0 + \Gamma_2)/(\Delta x_0 + \Delta x_2)$
$D_3 = (A_y)_{j-1/2}(\Gamma_0 + \Gamma_3)/(\Delta y_0 + \Delta y_3)$
$D_4 = (A_y)_{j+1/2}(\Gamma_0 + \Gamma_4)/(\Delta y_0 + \Delta y_4)$
$D_5 = (A_z)_{k-1/2}(\Gamma_0 + \Gamma_5)/(\Delta z_0 + \Delta z_5)$
$D_6 = (A_z)_{k+1/2}(\Gamma_0 + \Gamma_6)/(\Delta z_0 + \Delta z_6)$

$$\int\left[\frac{\Delta\left(\gamma_x\Gamma_\phi\frac{\partial\phi}{\partial x}\right)}{\Delta x}+\frac{\Delta\left(\gamma_Y\Gamma_\phi\frac{\partial\phi}{\partial y}\right)}{\Delta y}+\frac{\Delta\left(\gamma_z\Gamma_\phi\frac{\partial\phi}{\partial z}\right)}{\Delta z}\right]dx\,dy\,dz$$

$$=D_2(\tilde{\phi}_2-\tilde{\phi}_0)-D_1(\tilde{\phi}_0-\tilde{\phi}_1)+D_4(\tilde{\phi}_4-\tilde{\phi}_0)-D_3(\tilde{\phi}_0-\tilde{\phi}_3)+D_6(\tilde{\phi}_6-\tilde{\phi}_0)-D_5(\tilde{\phi}_0-\tilde{\phi}_5),$$

$$=D_1\tilde{\phi}_1+D_2\tilde{\phi}_2+D_3\tilde{\phi}_3+D_4\tilde{\phi}_4+D_5\tilde{\phi}_5+D_6\tilde{\phi}_6$$

$$-(D_1+D_2+D_3+D_4+D_5+D_6)\tilde{\phi}_0\,. \qquad (4.19)$$

Here, D (= effective diffusivity x flow area/distance between the centers of two control volumes) is the diffusion strength across the surface of the control volume, $\tilde{\phi}$ (Eq. 4.7), represents the sum of the contributions of old and new time values, and Γ_ϕ is the effective diffusivity for the variable ϕ.

To determine the value of D at a surface, we assume the diffusivity, Γ, varies continuously from one main control volume to the next and use the following average diffusion strength, e.g.,

$$D_2=(Ax)_{i+1/2}(\Gamma_0+\Gamma_2)/(\Delta x_0+\Delta x_2) \qquad (4.20)$$

The values of diffusion strength for main control volume are listed in Table 8.

4.2.2 Momentum Control Volume

The integration of the diffusion terms over z-momentum control volume (Fig. 8) also results in an expression similar to Eq. 4.19:

$$\int\left[\frac{\Delta\left(\gamma_x\Gamma_\phi\frac{\partial\phi}{\partial x}\right)}{\Delta x}+\frac{\Delta\left(\gamma_y\Gamma_\phi\frac{\partial\phi}{\partial y}\right)}{\Delta y}+\frac{\Delta\left(\gamma_z\Gamma_\phi\frac{\partial\phi}{\partial z}\right)}{\Delta z}\right]dx\,dy\,dz$$

$$=\overline{D}_1\tilde{\phi}_1+\overline{D}_2\tilde{\phi}_2+\overline{D}_3\tilde{\phi}_3+\overline{D}_4\tilde{\phi}_4+\overline{D}_5\tilde{\phi}_5+\overline{D}_6\tilde{\phi}_6$$

$$-(\overline{D}_1+\overline{D}_2+\overline{D}_3+\overline{D}_4+\overline{D}_5+\overline{D}_6)\tilde{\phi}_0\,. \qquad (4.21)$$

The only difference is that we now use the momentum control volume diffusion strength $\overline{D}$, instead of the main control volume diffusion strength D, e.g.,

$$\overline{D}_6=\frac{1}{2}\left[(Az)_k+(Az)_{k+1}\right]\left(\frac{\Gamma}{\Delta z}\right)_6\,. \qquad (4.22)$$

The values of the diffusion strengths $\overline{D}$ for the z momentum control volume are listed in Table 9.

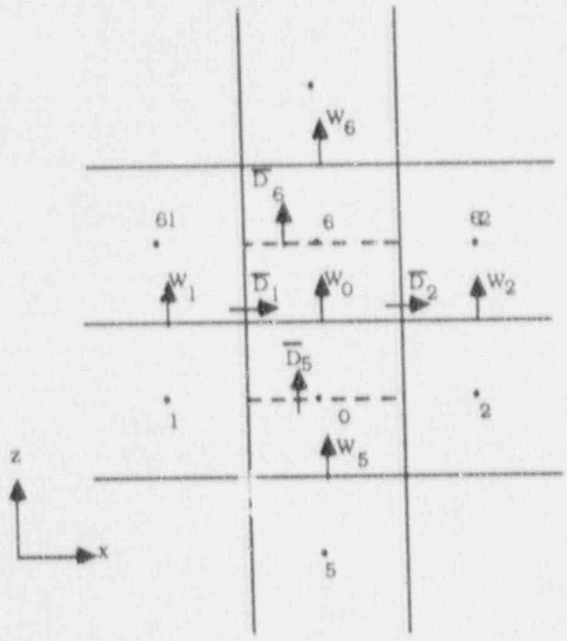

Fig. 8. Diffusion fluxes for z-momentum control volume

Table 9. Diffusion strengths for z-momentum control volume

$$\bar{D}_1 = \frac{1}{4}\left[(Ax)_{i-1/2,k} + (Ax)_{i-1/2,k+1}\right]\left[\frac{(\Gamma_0 + \Gamma_1)}{(\Delta x_0 + \Delta x_1)}, \frac{(\Gamma_6 + \Gamma_{61})}{(\Delta x_6 + \Delta x_{61})}\right]$$

$$\bar{D}_2 = \frac{1}{4}\left[(Ax)_{i+1/2,k+1} + (Ax)_{i+1/2,k}\right]\left[\frac{(\Gamma_0 + \Gamma_2)}{(\Delta x_0 + \Delta x_1)} + \frac{(\Gamma_6 + \Gamma_{62})}{(\Delta x_6 + \Delta x_{62})}\right]$$

$$\bar{D}_3 = \frac{1}{4}\left[(Ay)_{j-1/2,k} + (Ay)_{j-1/2,k+1}\right]\left[\frac{(\Gamma_0 + \Gamma_3)}{(\Delta y_0 + \Delta y_3)} + \frac{(\Gamma_6 + \Gamma_{63})}{(\Delta y_6 + \Delta y_{63})}\right]$$

$$\bar{D}_4 = \frac{1}{4}\left[(Ay)_{j+1/2,k} + (Ay)_{j+1/2,k+1}\right]\left[\frac{(\Gamma_0 + \Gamma_4)}{(\Delta y_0 + \Delta y_4)} + \frac{(\Gamma_6 + \Gamma_{64})}{(\Delta y_6 + \Delta y_{64})}\right]$$

$$\bar{D}_5 = \frac{1}{2}\left[(Az)_k + (Az)_{k-1}\right]\left(\frac{\Gamma}{\Delta z}\right)_0$$

$$\bar{D}_6 = \frac{1}{2}\left[(Az)_k + (Az)_{k+1}\right]\left(\frac{\Gamma}{\Delta z}\right)_6$$

4.3 Unsteady Term

4.3.1 Main Control Volume

Representation of the term $\partial(\gamma_v\rho\phi)/\partial t$ is obtained assuming that the values ρ_0 and ϕ_0 prevail over the control volume surrounding point 0 (see Fig. 9). Integration of the unsteady terms over the control volume then gives

$$\int \frac{\partial}{\partial t}(\gamma_v\rho\phi)\,dx\,dy\,dz = \frac{(\rho\phi)_0 - (\rho\phi)_0^n}{\Delta t} V_0 \ , \tag{4.23}$$

where $V_0 = \gamma_v\,\Delta x\,\Delta y\,\Delta z$ is the volume of the fluid; the superscript n refers to known old time-step values, and the superscript n+1 for new time-step values is omitted for simplicity.

4.3.2 Momentum Control Volume

Referring to the z momentum control volume shown in Fig. 6, and recalling that the momentum of the staggered mesh consists of two parts, i.e.,

$$\begin{aligned} M_s &= (M_s)_{V_s/2} + (M_s)_{V_s/2} \\ &= \int_{V_s/2}\gamma_v\rho w\,dx\,dy\,dz + \int_{V_s/2}\gamma_v\rho w\,dx\,dy\,dz, \end{aligned} \tag{4.24}$$

Integrating the unsteady term over the control volume gives

$$\begin{aligned} \int \frac{\partial}{\partial t}(\gamma_v\rho w)\,dx\,dy\,dz &= \int_{V_0/2}\frac{\partial}{\partial t}(\gamma_v\rho w)\,dx\,dy\,dz + \int_{V_\delta/2}\frac{\partial}{\partial t}(\gamma_v\rho w)\,dx\,dy\,dz \\ &= \frac{\partial}{\partial t}(M_s)_{V_s/2} + \frac{\partial}{\partial t}(M_s)_{V_s/2} \\ &= \frac{\partial}{\partial t}\left(\frac{V_0\rho_0 W_{00}^*}{2}\right) + \frac{\partial}{\partial t}\left(\frac{V_\delta\rho_\delta W_{0\delta}^*}{2}\right) \\ &= \frac{1}{\Delta t}\left[\frac{V_0}{2}\left(\rho_0 W_{00}^* - \rho_0^n W_{00}^{*n}\right) + \frac{V_\delta}{2}\left(\rho_\delta W_{0\delta}^* - \rho_\delta^n W_{0\delta}^{*n}\right)\right]. \end{aligned} \tag{4.25a}$$

In the derivation of Eq. 4.25a, we have employed Eqs. 4.9b and 4.9f, which were introduced previously to define the volume averaged velocity w^*. Again, the superscript n refers to the old time-step values, and the superscript n+1 for new time-step values is omitted for simplicity.

Substituting Eq. 4.10 into Eq. 4.25a, and after rearranging, we obtain

$$\int \frac{\partial}{\partial t}(\gamma_v\rho w)\,dx\,dy\,dz$$

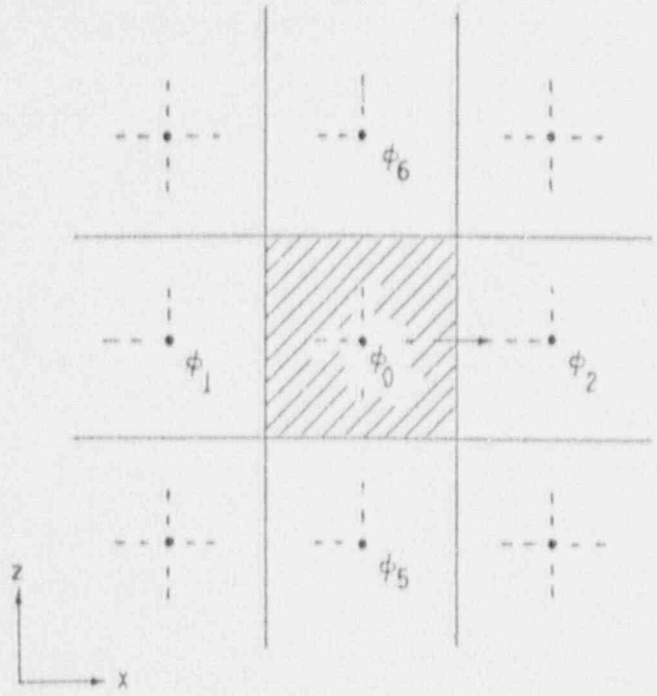

Fig. 9. Control volume for field variables

$$= \frac{\Delta z_0 \langle \rho \rangle_6^0 \left(\Delta z_0 + \Delta z_6 \right)}{2\Delta t} w_0 - \frac{\Delta z_0 \left[\langle \rho \rangle_6^0 \right]^n \left(\Delta z_0 + \Delta z_6 \right)}{2\Delta t} w_0^n \qquad (4.25b)$$

In Eq. 4.25b, we have again employed the closure relations (Eq. 4.10) described in Section 4.1.2.

Note that Eq. 4.25b has two potential limitations: (a) if there is a large density change in the control volume, the approximation may be less accurate; (b) if the volume porosity is substantially different than the surface porosity in the momentum control volume, this may also lead to less accuracy. An alternative formulation of the unsteady term as shown in Eq. 4.23 is provided as a user's option in which both volume-weighted average porosity and volume-weighted average density are used.

4.4 Source Term

The finite-difference representation of the source term S in Eq. 2.1 is expressed as

$$S_\phi = S_{c\phi} + S_{p\phi} \phi_0 \ , \qquad (4.26)$$

where $S_{c\phi}$, $S_{p\phi}$, and ϕ_0 are assumed to prevail over the control volume surrounding point 0. This "linearization" of the source term is an effective device for stability and convergence. The exact expressions for the source term coefficients $S_{c\phi}$ and $S_{p\phi}$ depend on the actual form of the source S_ϕ. The coefficient $S_{p\phi}$ is always less than or equal to zero; otherwise instability, divergence, or physically unrealistic solutions would result.

Integration of the source term over the main control volume gives

$$\int S_\phi \, dx\, dy\, dz = S_{c\phi} V_0 + S_{p\phi} V_0 \tilde{\phi}_0 \ , \tag{4.27}$$

where $V_0 = \gamma_V \Delta x \, \Delta y \, \Delta z$ is the fluid volume.

Integration of the source term over the z momentum control volume gives

$$\int S_\phi \, dx\, dy\, dz = S_{c\phi} \bar{V}_0 + S_{p\phi} \bar{V}_0 \tilde{\phi}_0 \ , \tag{4.28}$$

where

$$\bar{V}_0 = \left(\Delta z_0 + \Delta z_\delta\right) \Big/ \left(\frac{\Delta z_0}{V_0} + \frac{\Delta z_\delta}{V_\delta} \right) . \tag{4.29}$$

$\bar{V}_0$ is the characteristic volume used in the finite-volume integration. It will become clear later why we have employed Eq. 4.29 as the characteristic volume for the integration of the z momentum control volume.

4.5 General Finite-Volume Equation for Main Control Volume

Having looked at each term of the general equation separately, we now assemble all terms of Eqs. 4.6, 4.19, 4.23, and 4.27 for the main control volume to obtain the general finite-volume equation.

$$\int \left[(\text{Unsteady}) + (\text{Convection}) - (\text{Diffusion}) - (\text{Source}) \right] dx\, dy\, dz$$

$$= \underbrace{\frac{(\rho\phi)_0 - (\rho\phi)_0^n}{\Delta t} V_0}_{\text{(Unsteady)}} + \underbrace{\left(|0, -F_1| + |0, F_2| + \cdots \right) \tilde{\phi}_0}_{\text{(Convection)}}$$

$$\underbrace{- \left(|0, F_1| \tilde{\phi}_1 + |0, -F_2| \tilde{\phi}_2 + \cdots \right)}_{\text{(Convection)}} + \underbrace{\left(D_1 + D_2 + \cdots \right) \tilde{\phi}_0}_{\text{(Diffusion)}}$$

$$\underbrace{- \left(D_1 \tilde{\phi}_1 + D_2 \tilde{\phi}_2 + \cdots \right)}_{\text{(Diffusion)}} \underbrace{- S_{c\phi} V_0 - S_{p\phi} \tilde{\phi}_0 V_0}_{\text{(Source)}} = 0 \ , \tag{4.30}$$

We now rearrange Eq. 4.30 so that only the terms containing ϕ_0 are on the left side of the equation, noting that

$$\tilde{\phi} = \alpha\phi + (1 - \alpha)\phi^n \ . \tag{4.31}$$

After some algebra and rearrangement, we obtain

$$\phi_0 \left\{ \frac{\rho_0 V_0}{\Delta t} + \alpha \left[\left(|0, -F_1| + \cdots + |0, F_6| \right) + \left(D_1 + \cdots + D_6 \right) - S_{p\phi} V_0 \right] \right\}$$

$$= \left[\left(|0,F_1| + D_1\right)\phi_1 + \cdots + \left(|0,-F_6| + D_6\right)\phi_6\right]\alpha$$

$$+ \left[\left(|0,F_1| + D_1\right)\phi_1^n + \cdots + \left(|0,-F_6| + D_6\right)\phi_6^n\right](1-\alpha)$$

$$- \phi_6^n(1-\alpha)\left[\left(|0,-F_1| + \cdots |0,F_6|\right) + \left(D_1 + \cdots D_6\right) - S_{p\phi}V_0\right]$$

$$+ \left(\frac{\rho_0^n \phi_0^n}{\Delta t} V_0 + S_{c\phi} V_0\right). \tag{4.32}$$

or

$$\boxed{a_0^\phi \phi_0 = \left(a_1^\phi \phi_1 + a_2^\phi \phi_2 + a_3^\phi \phi_3 + a_4^\phi \phi_4 + a_5^\phi \phi_5 + a_6^\phi \phi_6\right)\alpha + b_0^\phi .} \tag{4.33}$$

where

$$b_0^\phi = b1_0^\phi + b2_0^\phi + b3_0^\phi . \tag{4.34}$$

For ease in reading, the coefficients of Eqs. 4.33 and 4.34 for the main control volumes are given in Table 10. Because we have combined the extreme semi-implicit and fully implicit formulations in one general form, the coefficients of Table 10 may appear somewhat confusing. We have therefore also included Tables 11 and 12, which give the coefficients for extreme semi-implicit ($\alpha = 0$) formulation and fully implicit ($\alpha = 1$) formulation.

It may be noted from Table 10 that we have expressed the coefficient a_0^ϕ in two forms. The first form, $a_0^\phi(1)$, is obtained by assembling all the terms of Eqs. 4.6, 4.19, 4.23, and 4.27. The second form, $a_0(2)$, is obtained by subtracting the continuity equation from the first form, $a_0(1)$; that is,

$$a_0(1) - (\text{continuity equation}) = a_0(2). \tag{4.35}$$

The use of the second form, $a_0(2)$, is preferred; this is the form implemented in COMMIX-1C. The reason is that this form is independent of the continuity equation that may or may not be satisfied during the solution of the energy equation. The second form is also referred to as the transport form.

In deriving the transport form of the coefficient a_0 for the main control volume, we have made use of the continuity equation as described below (if the reader is not interested in details, the rest of this section can be skipped).

If we substitute $\phi = 1$, $S_\phi = 0$, and $\Gamma_\phi = 0$ in the general equation (Eq. 2.1) for the main control volume, we have the continuity equation. Therefore, all formulations derived so far also are applicable to the continuity equation.

To derive the continuity equation, we substitute $\phi = 1$ in Eq. 4.32, remembering that $D = 0$ and $S = 0$ for the continuity equation. After simplification, we have the following:

Table 10. General finite-volume equation for main control volume (Eqs. 4.33 and 4.34) and its coefficients

$$a_0^\phi \phi_0 = \alpha\left(a_1^\phi \phi_1 + \cdots + a_6^\phi \phi_6\right) + \left(b1_0^\phi + b2_0^\phi + b3_0^\phi\right)$$

$$a_1^\phi = \left(|0, F_1| + D_1\right) \qquad a_2^\phi = \left(|0, -F_2| + D_2\right)$$

$$a_3^\phi = \left(|0, F_3| + D_3\right) \qquad a_4^\phi = \left(|0, -F_4| + D_4\right)$$

$$a_5^\phi = \left(|0, F_5| + D_5\right) \qquad a_6^\phi = \left(|0, -F_6| + D_6\right)$$

$$b1_0^\phi = (1-\alpha)\left(a_1^\phi \phi_1^n + a_2^\phi \phi_2^n + a_3^\phi \phi_3^n + a_4^\phi \phi_4^n + a_5^\phi \phi_5^n + a_6^\phi \phi_6^n\right)$$

$$b2_0^\phi = -(1-\alpha)\left[\left(|0, -F_1| + \cdots + |0, F_6|\right) + \left(D_1 + \cdots + D_6\right) - S_{p\phi} V_0\right]\phi_0^n$$

$$b3_0^\phi = \left(\frac{\rho^n \phi^n}{\Delta t} + S_{c\phi}\right)_0 V_0$$

$$a_0^\phi(1) = \frac{\rho_0 V_0}{\Delta t} + \alpha\left[\left(|0, -F_1| + \cdots + |0, F_6|\right) + \left(D_1 + D_2 \cdots + D_6\right) - S_{p\phi} V_0\right]$$

(1st form)

$$a_0^\phi(2) = \alpha\left(a_1^\phi + a_2^\phi + \cdots a_6^\phi\right) + \left(\frac{\rho_0^n}{\Delta t} - S_{p\phi}\right) V_0 + (1-\alpha)\left(F_1 - F_2 + F_3 - F_4 + F_5 - F_6\right)$$

(2nd form)

Continuity Equation in the Discretized Form

$$\frac{\rho_0 V_0}{\Delta t} + \alpha\left(|0, -F_1| + \cdots + |0, F_6|\right) - \alpha\left(|0, F_1| + \cdots + |0, -F_6|\right)$$

$$- (1-\alpha)\left(|0, F_1| + \cdots + |0, -F_6|\right) + (1-\alpha)\left(|0, -F_1| + \cdots + |0, F_6|\right) - \frac{\rho_0^n V_0}{\Delta t} = 0. \qquad (4.36)$$

Please note that the first density term in the continuity equation (Eq. 4.36) is at the new time, while the second density term is at the old time. The subtraction of Eq. 4.36 from $a_0(1)$, after some algebra, results in the second form, $a_0(2)$:

$$a_0^\phi(2) = a_0^\phi(1) - \text{Continuity Equation 4.36}$$

$$= \alpha\left[\left(D_1 + \cdots + D_6\right) - S_{p\phi} V_0\right] + \alpha\left(|0, F_1| + \cdots + |0, -F_6|\right)$$

$$+ (1-\alpha)\left(|0, F_1| + \cdots + |0, -F_6|\right) - (1-\alpha)\left(|0, -F_1| + \cdots + |0, F_6|\right) + \frac{\rho_0^n V_0}{\Delta t}$$

Table 11. Extreme semi-implicit ($\alpha = 0$) finite-volume equation for main control volume (Eqs. 4.33 and 4.34) and its coefficients $a_0^\phi \phi_0 = \left(b1_0^\phi + b2_0^\phi + b3_0^\phi\right)$

$$b1_0^\phi = \left(a_1^\phi \phi_1^n + a_2^\phi \phi_2^n + a_3^\phi \phi_3^n + a_4^\phi \phi_4^n + a_5^\phi \phi_5^n + a_6^\phi \phi_6^n\right)$$

$$b2_0^\phi = -\left[\left(|0,-F_1| + \cdots + |0,F_6|\right) + \left(D_1 + \cdots + D_6\right) - S_{p\phi} V_0\right]$$

$$b3_0^\phi = \left(\frac{\rho^n \phi^n}{\Delta t} + S_{c\phi}\right)_0 V_0$$

$$a_0^\phi(1) = \frac{\rho_0 V_0}{\Delta t}$$

(1st form)

$$a_0^\phi(2) = \left(\frac{\rho_0^n}{\Delta t} + S_{p\phi}\right) V_0 + \left(F_1 - F_2 + F_3 - F_4 + F_5 - F_6\right)$$

(2nd form)

Table 12. Fully implicit ($\alpha = 1$) finite-volume equation for main control volume (Eqs. 4.33 and 4.34) and its coefficients $a_0^\phi \phi_0 = \left(a_1^\phi \phi_1 + \cdots + a_6^\phi \phi_6 + b3_0^\phi\right)$

$$a_1^\phi = \left(|0,F_1| + D_1\right) \qquad a_2^\phi = \left(|0,-F_2| + D_2\right)$$

$$a_3^\phi = \left(|0,F_3| + D_3\right) \qquad a_4^\phi = \left(|0,-F_4| + D_4\right)$$

$$a_5^\phi = \left(|0,F_5| + D_5\right) \qquad a_6^\phi = \left(|0,-F_6| + D_6\right)$$

$$b3_0^\phi = \left(\frac{\rho^n \phi^n}{\Delta t} + S_{c\phi}\right)_0 V_0$$

$$a_0^\phi(1) = \frac{\rho_0 V_0}{\Delta t} + \left[\left(|0,-F_1| + \cdots + |0,F_6|\right) + \left(D_1 + D_2 \cdots + D_6\right) - S_{p\phi} V_0\right]$$

(1st form)

$$a_0^\phi(2) = \left(a_1^\phi + a_2^\phi + \cdots a_6^\phi\right) + \left(\frac{\rho_0^n}{\Delta t} - S_{p\phi}\right) V_0$$

(2nd form)

$$= \alpha\left[\left(|0,-F_1| + D_1\right) + \cdots + \left(|0,-F_6| + D_6\right)\right] + \left(\frac{\rho_0^n}{\Delta t} - \alpha S_{p\phi}\right)V_0$$

$$+ (1-\alpha)\left[\left(|0,F_1| - |0,-F_1|\right) + \cdots + \left(|0,-F_6| - |0,F_6|\right)\right]$$

$$= \alpha\left(a_1^\phi + a_2^\phi + a_3^\phi + a_4^\phi + a_5^\phi + a_6^\phi\right) + \left(\frac{\rho_0^n}{\Delta t} - \alpha S_{p\phi}\right)V_0$$

$$+ (1-\alpha)(F_1 - F_2 + F_3 - F_4 + F_5 - F_6) \qquad (4.37)$$

because

$$|0,F_1| - |0,-F_1| = F_1$$

and

$$|0,-F_2| - |0,F_2| = -F_2 .$$

Finally, it should be noted that the general variable ϕ for the main control volume can represent any transported variable such as enthalpy, turbulence kinetic energy, or rate of dissipation of the turbulence kinetic energy.

4.6 General Finite-Volume Equation for z-Momentum Control Volume

We can derive the finite-volume equation for z momentum by following the same procedure as for the finite-volume equation of the main control volume, with one exception. We see that the pressure gradient term appears in the momentum equation, but the pressure field is neither known beforehand nor directly obtainable from some sort of "conservation equation for pressure." Therefore, we consider pressure as unknown and determine it indirectly from the constraint that the velocity field satisfies the continuity equation. For this reason, we display the pressure-containing term in the finite-volume form of the momentum equation separately and do not include it in the source term.

From these considerations, the discretized equation for the z-momentum control volume shown in Fig. 6 is written as

$$a_0^w w_0 = a_1^w w_1 + a_2^w w_2 + a_3^w w_3 + a_4^w w_4 + a_5^w w_5 + a_6^w w_6 + b_0^w - d_w(P_6 - P_0) \qquad (4.38)$$

where

$$d_w = \overline{V}_0 \Big/ \left[\frac{1}{2}(\Delta z_0 + \Delta z_6)\right], \qquad (4.39)$$

and $\overline{V}_0$ is the characteristic volume for the momentum control volume defined by Eq. 4.29. The reason that Eq. 4.39 is employed here is that we want the discretized momentum equation to satisfy the one-dimensional steady-state Bernoulli's equation (with constant density and neglecting gravity effect), which can be written as (Fig. 6)

$$\rho\left(\overline{w}_6^2 - \overline{w}_0^2\right)/2 = -(P_6 - P_0), \qquad (4.40)$$

where $\bar{w}_6$ and $\bar{w}_0$ are the average velocities associated with the control volume centered at grid points 6 and 0, respectively. From continuity, we have

$$\rho \bar{w}_6 \frac{V_6}{\Delta z_6} = \rho \bar{w}_0 \frac{V_0}{\Delta z_0} = F_{z0} = \rho A z_0 w_0. \tag{4.41}$$

Substituting Eq. 4.41 into Eq. 4.40, we obtain the following equation, which must be satisfied by the discretized, one-dimensional z-momentum equation

$$\frac{F_{z0}^2}{2\rho}\left[\left(\frac{\Delta z_6}{V_6}\right)^2 - \left(\frac{\Delta z_0}{V_0}\right)^2\right] = -(P_6 - P_0). \tag{4.42}$$

The one-dimensional momentum equation in the z direction is

$$\frac{\Delta(\gamma_z \rho w w)}{\Delta z} = -\gamma_v \frac{\partial P}{\partial z} \tag{4.43}$$

Integrating over the z-momentum control volume (Fig. 6), and assuming that w is positive and

$$\int_{V_0} \gamma_v \frac{\partial P}{\partial z}\, dv = \frac{P_6 - P_0}{\frac{1}{2}(\Delta z_0 + \Delta z_6)} \bar{V}_0,$$

we obtain

$$\bar{F}_{z6} W_{06}^* - \bar{F}_{z5} W_5^* = -(P_6 - P_0)\bar{V}_0 / \left[\frac{1}{2}(\Delta z_0 + \Delta z_6)\right], \tag{4.44}$$

where $\bar{V}_0$ is the characteristic volume to be determined. Substituting Eqs. 4.8 and 4.10 into Eq. 4.44,

$$\frac{(F_{z0} + F_{z6})F_{z0}\Delta z_6}{2\rho_6 V_6} - \frac{(F_{z0} + F_{z5})F_{z5}\Delta z_0}{2\rho_0 V_0} = -\frac{(P_6 - P_0)\bar{V}_0}{\frac{1}{2}(\Delta z_0 + \Delta z_6)}. \tag{4.45}$$

For one-dimensional flow with constant density,

$$F_{z0} = F_{z5} = F_{z6},$$

$$\rho_0 = \rho_6 = \rho.$$

Therefore, Eq. 4.45 reduces to

$$\frac{F_{z0}^2}{2\rho}\left[\frac{\Delta z_6}{V_6} - \frac{\Delta z_0}{V_0}\right](\Delta z_6 + \Delta z_0) = -(P_6 - P_0)\bar{V}_0. \tag{4.46}$$

Dividing Eq. 4.46 by Eq. 4.42, we obtain

$$\bar{V}_0 = \frac{\Delta z_6 + \Delta z_0}{\frac{\Delta z_6}{V_6} + \frac{\Delta z_0}{V_0}}. \tag{4.47}$$

Equation 4.47 is identical to Eq. 4.29. Thus, the characteristic volume $\bar{V}_0$ employed in Eq. 4.39 is the proper volume for integration over the z-momentum control volume, and the resulting finite-volume equation satisfies the one-dimensional Bernoulli equation.

The coefficients $a_0^v \cdots a_6^v$ and $b_0^v = b1_0^v + b2_0^v + b3_0^v$ are assembled from Eqs. 4.12, 4.21, 4.25, and 4.28. The resulting equation has the same form as Eq. 4.33, except that the contributions of the source that enter a_0^v and b_0^v do not contain the pressure gradient. The effect of the pressure gradient is expressed by the last term in Eq. 4.38. The coefficients for the z-momentum control volume are presented in Tables 13–15. We have again replaced the velocity w by the general variable ϕ in Tables 13–15. This is only to indicate that the x- and y-momentum equations can be derived in a similar manner as the z-momentum equation. In Tables 13–15, we have provided two different forms of the coefficient a_0^ϕ. The first form, $a_0^\phi(1)$, is obtained from the momentum equation only and is referred to as the conservative form because conservation of momentum is satisfied over the control volume. The second form, $a_0^\phi(2)$, is derived by employing both the momentum and the continuity equations even though the latter may not be satisfied during an iteration. Experience indicates that using the continuity equation often helps to speed up the convergence during iterations. The second form of the coefficient is referred to as the transport form of the momentum equation and is implemented in COMMIX-1C. To derive the transport form of the z-momentum equation, we begin with the discretized continuity equation for cell 0 and cell 6, which can be written as

$$\left(\rho_0 - \rho_0^n\right)V_0 / \Delta t + F_{z0} - F_{z5} + F_{x2} - F_{x1} + Fy_4 - Fy_3 = 0 \tag{4.48}$$

for cell 0, and

$$\left(\rho_6 - \rho_6^n\right)V_6 / \Delta t + F_{z6} - F_{z0} + F_{x62} - F_{x61} + Fy_{64} - Fy_{63} = 0 \tag{4.49}$$

for cell 6. The transport form of the z-momentum equation is obtained as follows:

$$\begin{array}{l}\text{transport form of z-momentum equation}\end{array} = \begin{array}{l}\text{conservative form of z-momentum equation}\end{array} - \frac{\dot{w}_{00}}{2} \times \text{Eq. 4.48} - \frac{\dot{w}_{06}}{2} \times \text{Eq. 4.49.} \tag{4.50}$$

It can be observed that Eqs. 4.48 and 4.49 contain only the time-dependent terms and the convective fluxes. The diffusion terms and the source terms remain the same in the transport form as compared to conservative form of the z-momentum equation. Thus, all the coefficients are the same in the conservative and transport forms of the z-momentum equation, with the exception of the coefficient a_0^ϕ. Equation 4.50 can be reduced to

$$a_0^\phi(2) = a_0^\phi(1) - \frac{\dot{w}_{00}}{2} \times \text{Eq. 4.48} - \frac{\dot{w}_{06}}{2} \times \text{Eq. 4.49.} \tag{4.51}$$

After some manipulation and rearrangement, the final forms of $a_0^\phi(2)$ turn out to be identical to those given in Tables 13–15.

Table 13. Coefficients of general finite-volume equation for z-momentum control volume

$$a_0^{\phi}\phi_0 = \alpha\left(a_1^{\phi}\phi_1 + \cdots + a_6^{\phi}\phi_6\right) + \left(b1_0^{\phi} + b2_0^{\phi} + b3_0^{\phi}\right)$$

$$a_1^{\phi} = \frac{\langle\rho\rangle_{61}^{1} Az_1}{2}\left(|0,F_{x1}|\Delta z_0 / \rho_1 V_1 + |0,F_{x61}|\Delta z_6 / \rho_{61} V_{61}\right) + \overline{D}_1$$

$$a_2^{\phi} = \frac{\langle\rho\rangle_{62}^{2} Az_2}{2}\left(|0,-F_{x2}|\Delta z_0 / \rho_2 V_2 + |0,-F_{x62}|\Delta z_6 / \rho_{62} V_{62}\right) + \overline{D}_2$$

$$a_3^{\phi} = \frac{\langle\rho\rangle_{63}^{3} Az_3}{2}\left(|0,F_{y3}|\Delta z_0 / \rho_3 V_3 + |0,F_{y63}|\Delta z_6 / \rho_{63} V_{63}\right) + \overline{D}_3$$

$$a_4^{\phi} = \frac{\langle\rho\rangle_{64}^{4} Az_4}{2}\left(|0,-F_{y4}|\Delta z_0 / \rho_4 V_4 + |0,-F_{y64}|\Delta z_6 / \rho_{64} V_{64}\right) + \overline{D}_4$$

$$a_5^{\phi} = \frac{\langle\rho\rangle_{0}^{5} Az_5 \Delta z_0}{\rho_0 V_0}|0,\overline{F}_{z5}| + \overline{D}_5$$

$$a_6^{\phi} = \frac{\langle\rho\rangle_{66}^{6} Az_6 \Delta z_6}{\rho_6 V_6}|0,-\overline{F}_{z6}| + \overline{D}_6$$

$$b1_0^{\phi} = (1-\alpha)\left(a_1^{\phi}\phi_1^n + a_2^{\phi}\phi_2^n + \cdots + a_6^{\phi}\phi_6^n\right)$$

$$b2_0^{\phi} = -(1-\alpha)\left[\frac{1}{2}\left(|0,F_{x1}|\frac{\langle\rho\rangle_{61}^{6} Az_1 \Delta z_0}{\rho_1 V_1} + \cdots + |0,-F_{y64}|\frac{\langle\rho\rangle_{64}^{4} Az_4 \Delta z_6}{\rho_{64} V_{64}}\right)\right.$$
$$\left. + |0,\overline{F}_{z5}|\frac{\langle\rho\rangle_{0}^{5} Az_5 \Delta z_0}{\rho_0 V_0} + |0,-\overline{F}_{z6}|\frac{\langle\rho\rangle_{66}^{6} Az_6 \Delta z_6}{\rho_6 V_6} + \overline{D}_1 + \cdots + \overline{D}_6 - S_{p\phi}\overline{V}_0\right]\phi_0^n$$

$$b3_0^{\phi} = Az_0\left[\langle\rho\rangle_{6}^{0}\right]^n(\Delta z_0 + \Delta z_6)\phi_0^n / 2\Delta t + S_{c\phi}\overline{V}_0$$

$$a_0^{\phi}(1) = Az_0\langle\rho\rangle_{6}^{0}(\Delta z_0 + \Delta z_6) / 2\Delta t$$
$$+ \alpha\frac{\langle\rho\rangle_{6}^{0} Az_0 \Delta z_6}{\rho_6 V_6}\left(|0,\overline{F}_{z6}| + \frac{1}{2}|0,F_{x6_1}| + \frac{1}{2}|0,-F_{x61}| + \frac{1}{2}|0,F_{y64}| + \frac{1}{2}|0,-F_{y63}|\right)$$
$$+ \alpha\frac{\langle\rho\rangle_{6}^{0} Az_0 \Delta z_0}{\rho_0 V_0}\left(|0,-\overline{F}_{z5}| + \frac{1}{2}|0,F_{x2}| + \frac{1}{2}|0,-F_{x1}| + \frac{1}{2}|0,F_{y4}| + \frac{1}{2}|0,-F_{y3}|\right)$$
$$+\left(\overline{D}_1 + \cdots + \overline{D}_6 - S_{p\phi}\overline{V}_0\right)\alpha$$

$$a_0^{\phi}(2) = \frac{\langle\rho\rangle_{6}^{0} Az_0}{2\Delta t}\left[\left(\frac{\rho_0^n}{\rho_0}\right)\Delta z_0 + \left(\frac{\rho_6^n}{\rho_6}\right)\Delta z_6\right]$$
$$+ \alpha\frac{\langle\rho\rangle_{6}^{0} Az_0 \Delta z_6}{\rho_6 V_6}\left(|0,-\overline{F}_{z6}| + \frac{1}{2}|0,-F_{x62}| + \frac{1}{2}|0,F_{x61}| + \frac{1}{2}|0,-F_{y64}| + \frac{1}{2}|0,F_{y63}| + F_{z0}\right)$$
$$+ \alpha\frac{\langle\rho\rangle_{6}^{0} Az_0 \Delta z_0}{\rho_0 V_0}\left(|0,\overline{F}_{z5}| + \frac{1}{2}|0,-F_{x2}| + \frac{1}{2}|0,F_{x1}| + \frac{1}{2}|0,-F_{y4}| + \frac{1}{2}|0,F_{y3}| - F_{z0}\right)$$
$$+\left(\overline{D}_1 + \cdots + \overline{D}_6 - S_{p\phi}\overline{V}_0\right)\alpha$$

Table 14. Coefficients of extreme semi-implicit ($\alpha = 0$) finite-volume equation for z-momentum control volume
$a_0^{\phi}\phi_0 = b1_0^{\phi} + b2_0^{\phi} + b3_0^{\phi}$

$$b1_0^{\phi} = a_1^{\phi}\phi_1^n + a_2^{\phi}\phi_2^n + \cdots + a_6^{\phi}\phi_6^n$$

$$b2_0^{\phi} = -\left[\frac{1}{2}\left(|0,F_{x1}|\frac{\Delta z_0\langle\rho\rangle_{61}^{1}Az_1}{\rho_1 V_1} + \cdots + |0,-F_{y64}|\frac{\Delta z_6\langle\rho\rangle_{64}^{4}Az_4}{\rho_{64}V_{64}}\right)\right.$$
$$\left. + |0,\bar{F}_{z5}|\frac{\Delta z_0\langle\rho\rangle_0^5 Az_5}{\rho_0 V_0} + |0,-\bar{F}_{z6}|\frac{\Delta z_6\langle\rho\rangle_{66}^{6}Az_6}{\rho_6 V_6} + \bar{D}_1 + \cdots + \bar{D}_6 - S_{p\phi}\bar{V}_0\right]\phi_0^n$$

$$b3_0^{\phi} = Az_0\left[\langle\rho\rangle_6^0\right]^n(\Delta z_0 + \Delta z_6)\phi_0^n / 2\Delta t + S_{c\phi}\bar{V}_0$$

$$a_0^{\phi}(1) = Az_0\langle\rho\rangle_6^0(\Delta z_0 + \Delta z_6) / 2\Delta t$$

$$a_0^{\phi}(2) = \frac{\langle\rho\rangle_6^0 Az_0}{2\Delta t}\left[\left(\frac{\rho_0^n}{\rho_0}\right)\Delta z_0 + \left(\frac{\rho_6^n}{\rho_6}\right)\Delta z_6\right]$$

Table 15. Coefficients of fully implicit ($\alpha = 1$) finite-volume equation for z-momentum control volume
$a_0^{\phi}\phi_0 = \left(a_1^{\phi}\phi_1 + \cdots + a_6^{\phi}\phi_6 + b3_0^{\phi}\right)$

$$a_1^{\phi} = \frac{\langle\rho\rangle_{61}^{1} Az_1}{2}\left(|0,F_{x1}|\Delta z_0 / \rho_1 V_1 + |0,F_{x61}|\Delta z_6 / \rho_{61} V_{61}\right) + \overline{D}_1$$

$$a_2^{\phi} = \frac{\langle\rho\rangle_{62}^{2} Az_2}{2}\left(|0,-F_{x2}|\Delta z_0 / \rho_2 V_2 + |0,-F_{x62}|\Delta z_6 / \rho_{62} V_{62}\right) + \overline{D}_2$$

$$a_3^{\phi} = \frac{\langle\rho\rangle_{63}^{3} Az_3}{2}\left(|0,F_{y3}|\Delta z_0 / \rho_3 V_3 + |0,F_{y63}|\Delta z_6 / \rho_{63} V_{63}\right) + \overline{D}_3$$

$$a_4^{\phi} = \frac{\langle\rho\rangle_{64}^{4} Az_4}{2}\left(|0,-F_{y4}|\Delta z_0 / \rho_4 V_4 + |0,-F_{y64}|\Delta z_6 / \rho_{64} V_{64}\right) + \overline{D}_4$$

$$a_5^{\phi} = |0,\overline{F}_{z5}|\frac{\Delta z_0 \langle\rho\rangle_0^{5} Az_5}{\rho_0 V_0} + \overline{D}_5$$

$$a_6^{\phi} = |0,-\overline{F}_{z6}|\frac{\Delta z_6 \langle\rho\rangle_{66}^{6} Az_6}{\rho_6 V_6} + \overline{D}_6$$

$$b3_0^{\phi} = Az_0\left[\langle\rho\rangle_6^{0}\right]^{n}(Az_0 + Az_6)\phi_0^{n} / 2\Delta t + S_{c\phi}\overline{V}_0$$

$$a_0^{\phi}(1) = Az_0\langle\rho\rangle_6^{0}(\Delta z_0 + \Delta z_6) / 2\Delta t$$
$$+ \frac{\langle\rho\rangle_6^{0} Az_0\Delta z_6}{\rho_6 V_6}\left(|0,\overline{F}_{z6}| + \frac{1}{2}|0,F_{x62}| + \frac{1}{2}|0,-F_{x61}| + \frac{1}{2}|0,F_{y64}| + \frac{1}{2}|0,-F_{y63}|\right)$$
$$+ \frac{\langle\rho\rangle_6^{0} Az_0\Delta z_0}{\rho_0 V_0}\left(|0,-\overline{F}_{z5}| + \frac{1}{2}|0,F_{x2}| + \frac{1}{2}|0,-F_{x1}| + \frac{1}{2}|0,F_{y4}| + \frac{1}{2}|0,-F_{y3}|\right)$$
$$+ \overline{D}_1 + \cdots + \overline{D}_6 - S_{p\phi}\overline{V}_0$$

$$a_0^{\phi}(2) = \frac{\langle\rho\rangle_6^{0} Az_0}{2\Delta t}\left[\left(\frac{\rho_0^{n}}{\rho_0}\right)\Delta z_0 + \left(\frac{\rho_6^{n}}{\rho_6}\right)\Delta z_6\right]$$
$$+ \frac{\langle\rho\rangle_6^{0} Az_0\Delta z_6}{\rho_6 V_6}\left(|0,-\overline{F}_{z6}| + \frac{1}{2}|0,-F_{x62}| + \frac{1}{2}|0,F_{x61}| + \frac{1}{2}|0,-F_{y64}| + \frac{1}{2}|0,F_{y63}| + F_{z0}\right)$$
$$+ \frac{\langle\rho\rangle_6^{0} Az_0\Delta z_0}{\rho_0 V_0}\left(|0,\overline{F}_{z5}| + \frac{1}{2}|0,-F_{x2}| + \frac{1}{2}|0,F_{x1}| + \frac{1}{2}|0,-F_{y4}| + \frac{1}{2}|0,F_{y3}| - F_{z0}\right)$$
$$+ \overline{D}_1 + \cdots + \overline{D}_6 - S_{p\phi}\overline{V}_0$$

---

5 Pressure Equation

The pressure appearing in the momentum equation (Eq. 4.38) is unknown and must be determined from the conservation-of-mass equation. In this section, we present the derivation of the pressure equation.

The conservation-of-mass equation for the cell around point 0 (Fig. 9) can be derived from Eq. 4.32 by substituting $\phi = 1$, diffusion strength $D = 0$, and $S = 0$:

$$V_0\left(\frac{\partial \rho}{\partial t}\right) - (A_x u)_{i-1/2}\langle\rho\rangle_0^1 + (A_x u)_{i+1/2}\langle\rho\rangle_2^0 - (A_y v)_{j-1/2}\langle\rho\rangle_0^3 + (A_y v)_{j+1/2}\langle\rho\rangle_4^0 - (A_z w)_{k-1/2}\langle\rho\rangle_0^5 + (A_z w)_{k+1/2}\langle\rho\rangle_6^0 = \delta_0 . \tag{5.1}$$

Here, $V_0 = \gamma_v \Delta x \Delta y \Delta z$ is the fluid volume of the main control volume, δ_0 is the mass residual of the continuity equation, $\langle\rho\rangle$ is the upwind density, u, v, and w are the normal velocities at the surface of the control volume, and A is the flow area. We define the flow area as the product of surface area and surface porosity.

When mass is precisely conserved, the right side of Eq. 5.1 vanishes, i.e., $\delta = 0$. However, because Eq. 5.1 is solved by an iterative-solution procedure, the mass residual δ, in general, may not be zero.

To convert the indirect specification of pressure in the continuity equation to an explicit form, we write the momentum Eq. 4.38 as

$$\phi = \hat{\phi} - d^{\phi}\Delta(\delta P) \qquad (\phi = u, v, w), \tag{5.2a}$$

where

$$\delta P = P^{n+1} - P^{n}, \tag{5.2b}$$

$$\hat{\phi} = \frac{\alpha \sum_{\ell=1}^{6} a_{\ell}^{\phi}\phi_{\ell} + b1_0^{\phi} + b2_0^{\phi} + b3_0^{\phi} - d^{\phi}\Delta P^{n}}{a_0^{\phi}}. \tag{5.2c}$$

The reason that δP (instead of P) is used in Eq. 5.2a is to speed the convergence. This is particularly helpful when the change in pressure is small compared to the absolute pressure of the system.

For example, the z-direction velocity w at the north surface of the main control volume is expressed as

$$w_6 = \hat{w}_6 - d_6^{w}(\delta P_6 - \delta P_0) , \tag{5.3a}$$

where

$$\hat{w}_6 = \frac{\alpha \sum_{\ell=1}^{6} a_\ell^w w_\ell + b1_0^w + b2_0^w + b3_0^w - d_6^w \left(P_6^n - P_0^n\right)}{a_0^w}, \tag{5.3b}$$

$$d_6^w = \frac{2\overline{V}_6^w}{a_0^w(\Delta z_0 + \Delta z_6)}, \tag{5.3c}$$

and

$$\overline{V}_6^w = (\Delta z_0 + \Delta z_6) \Big/ \left(\frac{\Delta z_0}{V_0} + \frac{\Delta z_6}{V_6}\right). \tag{5.3d}$$

With similar definitions for $\hat{u}$, $\hat{v}$, d, and $\overline{V}$, the other velocities appearing in Eq. 5.1 can be expressed as

$$u_1 = \hat{u}_1 - d_1^u(\delta P_0 - \delta P_1),$$

$$u_2 = \hat{u}_2 - d_2^u(\delta P_2 - \delta P_0),$$

$$v_3 = \hat{v}_3 - d_3^v(\delta P_0 - \delta P_3),$$

$$v_4 = \hat{v}_4 - d_4^v(\delta P_4 - \delta P_0),$$

and

$$w_5 = \hat{w}_5 - d_5^w(\delta P_0 - \delta P_5), \tag{5.4}$$

where

$$d_1^u = \frac{2\overline{V}_1^u}{a_0^u(\Delta x_0 + \Delta x_1)},$$

$$d_2^u = \frac{2\overline{V}_2^u}{a_0^u(\Delta x_0 + \Delta x_2)},$$

$$d_3^v = \frac{2\overline{V}_3^v}{a_0^v(\Delta y_0 + \Delta y_3)},$$

$$d_4^v = \frac{2\overline{V}_4^v}{a_0^v(\Delta y_0 + \Delta y_4)},$$

and

$$d_5^w = \frac{2\overline{V}_5^w}{a_0^w(\Delta z_0 + \Delta z_5)}. \tag{5.5}$$

The characteristic volumes are defined as

$$\overline{V}_1^u = (\Delta x_0 + \Delta x_1) \Big/ \left(\frac{\Delta x_0}{V_0} + \frac{\Delta x_1}{V_1}\right).$$

$$\overline{V}_2^u = (\Delta x_0 + \Delta x_2) \Big/ \left(\frac{\Delta x_0}{V_0} + \frac{\Delta x_2}{V_2} \right),$$

$$\overline{V}_3^v = (\Delta y_0 + \Delta y_3) \Big/ \left(\frac{\Delta y_0}{V_0} + \frac{\Delta y_3}{V_3} \right),$$

$$\overline{V}_4^v = (\Delta y_0 + \Delta y_4) \Big/ \left(\frac{\Delta y_0}{V_0} + \frac{\Delta y_4}{V_4} \right),$$

and

$$\overline{V}_5^w = (\Delta z_0 + \Delta z_5) \Big/ \left(\frac{\Delta z_0}{V_0} + \frac{\Delta z_5}{V_5} \right), \tag{5.6}$$

Here, the subscripts 1 .... 6 for velocities refer to the surfaces of the main control volume. Substitution of Eqs. 5.3 and 5.4 into Eq. 5.1 yields

$$a_0^p \delta P_0 - \sum_{\ell=1}^{6} a_\ell^p \delta P_\ell - b_0^p = \delta_0 . \tag{5.7}$$

The coefficients of Eq. 5.7 are listed in Table 16. These coefficients form a symmetric matrix.

Equation 5.7 is the required pressure equation. It can be solved by using any one of the matrix solvers described in Sec. 10.4.

6 Turbulence Modeling

6.1 Background of Turbulence Modeling

The subject of turbulence has attracted countless researchers for more than 80 years. In 1895, Reynolds proposed that a fluid particle in turbulent flow is in randomly unsteady motion. He averaged the Navier-Stokes equation over a time scale that is long compared to the turbulent time scale and derived the equations that describe the mean turbulent motion. In spite of the long time span and large research effort since then, the problem of turbulence has not been resolved completely, for the reasons discussed below.

The appearance of the time-averaged correlations, such as $\rho\overline{u'v'}$ in the governing equations, gives rise to the so-called "closure" problem (more unknowns than equations available for the solution of unknowns). Here, ρ denotes fluid density, u' and v' are the fluctuating velocity components in the coordinate directions x and y, and the overbar denotes the time averaging. The correlations u'v' are known as Reynolds stresses.

Another difficulty is that the constituents of the turbulence phenomenon normally take place in scales of motion that are of very small orders of magnitude in size, while the whole flow domain may extend over meters or even kilometers. Important details of turbulence are small-scale in character (although it is not the details but the time-averaged consequences that are of interest in practical application). As a result, the computational nodes required to resolve small-scale motions of turbulence will require far more storage capacity

Table 16. Coefficients of pressure equation (Eq. 5.7)

$$a_1^p = \left(\frac{A_x}{a_0^u}\right)_{i-1/2} \langle\rho\rangle_0^1 \left(\frac{2\overline{V}_1^u}{\Delta x_0 + \Delta x_1}\right)$$

$$a_2^p = \left(\frac{A_x}{a_0^u}\right)_{i+1/2} \langle\rho\rangle_2^0 \left(\frac{2\overline{V}_2^u}{\Delta x_0 + \Delta x_2}\right)$$

$$a_3^p = \left(\frac{A_y}{a_0^v}\right)_{j-1/2} \langle\rho\rangle_0^3 \left(\frac{2\overline{V}_3^v}{\Delta y_0 + \Delta y_3}\right)$$

$$a_4^p = \left(\frac{A_y}{a_0^v}\right)_{j+1/2} \langle\rho\rangle_4^0 \left(\frac{2\overline{V}_4^v}{\Delta y_0 + \Delta y_4}\right)$$

$$a_5^p = \left(\frac{A_z}{a_0^w}\right)_{k-1/2} \langle\rho\rangle_0^5 \left(\frac{2\overline{V}_5^w}{\Delta z_0 + \Delta z_5}\right)$$

$$a_6^p = \left(\frac{A_z}{a_0^w}\right)_{k+1/2} \langle\rho\rangle_6^0 \left(\frac{2\overline{V}_6^w}{\Delta z_0 + \Delta z_6}\right)$$

$$a_0^p = a_1^p + a_2^p + a_3^p + a_4^p + a_5^p + a_6^p$$

$$b_0^p = -V_0\left(\frac{\partial\rho}{\partial t}\right)_0 + (A_x\hat{u})_{i-1/2}\langle\rho\rangle_0^1 - (A_x\hat{u})_{i+1/2}\langle\rho\rangle_2^0 + (A_y\hat{v})_{j-1/2}\langle\rho\rangle_0^3 - (A_y\hat{v})_{j+1/2}\langle\rho\rangle_4^0 + (A_z\hat{w})_{k-1/2}\langle\rho\rangle_0^5 - (A_z\hat{w})_{k+1/2}\langle\rho\rangle_6^0$$

than is available with current computers. The corresponding computer running time also will be infeasibly long.

An alternative approach to resolving these difficulties is to employ some form of turbulence modeling in which we solve only the time-averaged equations of motion, along with a set of transport equations of turbulence quantities, e.g., k, the turbulence kinetic energy, ε, the rate of dissipation of k, etc. Even this approach requires a significant amount of numerical computation. It is only in the last 20 years, with the recent advances in computer power, that this alternative turbulence modeling approach has been feasible.

Many turbulence models have been proposed to resolve the above-mentioned difficulties by providing solvable equations for computation of turbulent flows. The central idea in most of the turbulence models, except the Reynolds-stress model or algebraic stress modeling, is the use of an artificial turbulent viscosity μ_{tur} to account for the additional diffusional flux due to the turbulent motion. To do that, the Reynolds stress term is expressed as

$$-\rho\,\overline{u'v'} = \mu_{tur}\left(\frac{\partial u}{\partial x}+\frac{\partial v}{\partial y}\right)-\frac{1}{3}\rho\left(\overline{u'^2}+\overline{v'^2}+\overline{w'^2}\right). \tag{6.1}$$

We must note here that the turbulent viscosity μ_{tur} is a property of the local state of turbulence and not a physical property of the fluid. The turbulence model in this category is therefore generally referred to as a viscosity model.

The very early and still popular model among these viscosity models is the Prandtl's mixing length hypothesis.[57] Prandtl's mixing length model is the simplest turbulence model since it does not require solution of any transport equation of turbulence parameters. In his mixing length hypothesis, Prandtl assumes that

$$\mu_{tur} = \rho \ell^2 \frac{\partial u}{\partial y}, \tag{6.2}$$

where ℓ is the mixing length that represents the length scale of the turbulent flow. It is known that ℓ can have different forms for different type of flows. For example, in the boundary layer of a single wall,

$$\ell = Ky, \tag{6.3}$$

where K is the von Karman constant (0.42) and y is the distance from the wall. For some free turbulent flows, such as jets or mixing layers,

$$\ell = c\delta, \tag{6.4}$$

where δ is the jet half-width, and c is an empirical constant. Even though the mixing length hypothesis is easy to use and gave fairly good results for some simple flows, it has the following disadvantages:

- It cannot predict successfully more complicated flows in practical applications, such as recirculating flows that occur frequently in engineering systems.
- It implies that the effective viscosity and the effective thermal conductivity vanish where the velocity gradient is zero. This is generally not true and can lead to erroneous results.

Finally, it should be noted that the mixing length hypothesis does not take into account the effects of convection and diffusion on turbulence, and we shall see that it is a special case of the more general k-ε two-equation turbulence model.

In 1945, Prandtl suggested a more general approach than the mixing-length hypothesis.[58] His new approach is generally referred to as a one-equation turbulence model. In this model, the turbulent viscosity is assumed to be a function of the square root of the turbulence kinetic energy k:

$$\mu_{tur} = \rho \ell k^{1/2}. \tag{6.5}$$

To determine the value of k, Prandtl suggested that a transport equation of k be solved, thus taking into account the influence of neighboring regions on the local turbulence energy. As shown in Eq. 6.5, the turbulent viscosity is related to the turbulent kinetic

energy k, instead of a mean velocity gradient. This alleviated the problem encountered in the mixing length hypothesis where the effects of turbulence vanish when the mean velocity gradient is zero. For example, on the centerline of a pipe, although the mean velocity gradient is zero, the turbulence energy is not. Therefore, the turbulent viscosity does not vanish at the centerline of the pipe. Even though the one-equation turbulence model generally produces more reliable results than the mixing length hypothesis (at the expense of more computation), in practice, the model offers only a small advantage over the mixing length hypothesis since the length scale in Eq. 6.5 still must be specified. Furthermore, the effect of transport of the length scale is not accounted for in the one-equation turbulence model. The difficulty of trying to specify a length scale in complicated flow situations for the one-equation turbulence model leads to the development of a two-equation turbulence model that is the main subject of this chapter.

There are several two-equation turbulence models (k-ε model, k-ℓ model, k-W model, etc.). Here, the symbol k is the kinetic energy of turbulence, ε is the dissipation rate of turbulence energy, ℓ is a macroscopic length scale of turbulence, and W is interpreted as the time-averaged square of the velocity fluctuations. Among the two-equation models, the k-ε model, as proposed by Harlow and Nakayama[59] and Jones and Launder,[60] is the most widely used.

The next level in turbulence modeling is represented by the complex Reynolds stress models.[61-64] These models are still in the development stages.

In COMMIX-1C, as in COMMIX-1B, we have adopted the k-ε two-equation turbulence model of Harlow and Nakayama[59] and Jones and Launder[60] for the following reasons:

- The k-ε two-equation turbulence model is the most widely used and tested model. This will provide the user with some confidence in the results of COMMIX-1C when it is used to predict turbulent flows.
- The k-ε two-equation turbulence model has some generality and can be applied to various types of turbulent flows, including internal flows and free shear flows. This generality fits well in the COMMIX code, which is itself a general-purpose code.

It should be noted that only the k-ε two-equation turbulence model is retained in COMMIX-1C in an attempt to simplify the code structure by eliminating seldom-used options. This is different from COMMIX-1B, where three options are available for calculating turbulent flows, i.e., the Prandtl mixing length hypothesis, the one-equation turbulence model, and the k-ε two-equation model. Because the Prandtl mixing length hypothesis and the one-equation turbulence model are special cases of the more general k-ε two-equation turbulence model, there is no loss of generality in dealing with various types of turbulent flows in COMMIX-1C compared to COMMIX-1B. However, the reader should be aware of both the limitations and the merits of the Prandtl mixing length hypothesis and the one-equation turbulence model. It is our opinion that understanding the mixing length hypothesis and the one-equation turbulence model is a prerequisite to understanding the more complicated and more general k-ε two-equation turbulence model and is, therefore, highly recommended.

Finally, we have retained the constant diffusivity model in COMMIX-1C. Strictly speaking, the constant diffusivity model is not a turbulence model. We find it useful sometimes in performing scoping calculations since it does not require the solution of additional transport equations.

6.2 Constant Turbulent Diffusivity Model

This is a very simplified turbulence model in which the turbulent viscosity and the turbulent conductivity are assumed to be constant. The value of turbulent viscosity is a user-prescribed single input constant.

It is preferable to prescribe values of turbulent viscosity and turbulent conductivity obtained from experimental data. If the experimental information is not available, then turbulent viscosity can be estimated with the following equation suggested by Sha and Launder:[65]

$$\mu_{tur} = 0.007 c_\mu \rho U_{max} \ell \,, \tag{6.6}$$

where

$$c_\mu = 0.1 \qquad \text{for } Re_{max} > 2000,$$

$$c_\mu = 0.1(0.001 Re_{max} - 1) \qquad \text{for } 1000 \le Re_{max} \le 2000,$$

and

$$c_\mu = 0 \qquad \text{for } Re_{max} < 1000, \tag{6.7}$$

Here,

$$U_{max} = \text{Max}(u,v,w) \quad \text{and} \tag{6.8}$$

$$Re_{max} = \text{Max}(Re_x, Re_y, Re_z) \,, \tag{6.9}$$

the mixing length scale

$$\ell = C_\ell D_h \,, \tag{6.10}$$

the coefficient

$$C_\ell = 0.4 \,, \tag{6.11}$$

and D_h is the hydraulic diameter.

If information about turbulent conductivity λ_{tur} is not available and not prescribed, we can approximate it with the following relation:

$$\lambda_{tur} = \frac{c_p \mu_{tur}}{\sigma_h}$$

$$= \frac{c_p \mu_{tur}}{0.8\left[1 - \exp\left(-6 \times 10^{-5} Re Pr^{1/3}\right)\right]^{-1}} \,. \tag{6.12}$$

where σ_h is the turbulent Prandtl number, Re is the characteristic Reynolds number, and $Pr = C_p\mu/\lambda$ is the molecular Prandtl number. Equation 6.12 is based on the proposal of Nijsing and Eifler.[66]

Again, it must be emphasized that the constant diffusivity model is, strictly speaking, not a turbulence model. It does save computing time compared to the two-equation turbulence model and is used only for scoping calculations.

6.3 k-ε Two-Equation Turbulence Model

The derivations of the transport equations for k and ε are well documented in the literature, e.g., Launder and Spalding,[67] Sha and Launder,[65] and Arpaci and Larsen.[68] Here, we will only briefly summarize the results. In this section, k and ε are defined by the following equations:

$$k = \frac{1}{2}\left(\overline{u'^2+v'^2+w'^2}\right) \tag{6.13}$$

and

$$\varepsilon = \nu\overline{\frac{\partial u_i'}{\partial x_j}\frac{\partial u_i'}{\partial x_j}} . \tag{6.14}$$

6.3.1 Transport Equation for k

The transport equation for turbulence kinetic energy, k, can be written as

$$\rho\frac{\partial k}{\partial t} + \rho u_j\frac{\partial k}{\partial x_j} = -\rho\overline{u_i'u_j'}\frac{\partial u_i}{\partial x_j} + \overline{\rho' u_i'}\,g_i - \mu\overline{\frac{\partial u_i'}{\partial x_j}\left(\frac{\partial u_i'}{\partial x_j}+\frac{\partial u_j'}{\partial x_i}\right)}$$

$$\text{A} \qquad \text{B} \qquad \text{C}$$

$$+\frac{\partial}{\partial x_j}\left[\mu\left(\frac{\partial k}{\partial x_j}+\overline{\frac{\partial u_i'u_j'}{\partial x_i}}\right) - \rho\overline{\frac{u_i'u_i'u_j'}{2}} - \overline{pu_i'}\,\delta_{ij}\right] . \tag{6.15}$$

$$\text{D}$$

Equation 6.15 is the exact form of the transport equation for k. Here, the terms are

A: source due to mean shear,

B: buoyancy interactions,

C: loss of k through viscous dissipation, and

D: diffusive transport of k and randomizing action of the pressure-strain correlation.

We can see that Eq. 6.15 has a closure problem. Using the standard closure relations, Eq. 6.15 reduces to

$$\rho\frac{\partial k}{\partial t} + \rho\, u_j\frac{\partial k}{\partial x_j} = P_k + G_k - \rho\varepsilon + \frac{\partial}{\partial x_j}\left[\left(\frac{\mu_{tur}}{\sigma_k} + \mu_{tam}\right)\frac{\partial k}{\partial x_j}\right]. \tag{6.16}$$

Here,

$$P_k = \mu_{tur}\left[\frac{\partial u_i}{\partial x_j}\left(\frac{\partial u_i}{\partial x_j} + \frac{\partial u_j}{\partial x_i}\right)\right] \tag{6.17}$$

is the source due to mean shear, and

$$G_k = -\frac{\mu_{tur}}{\rho\sigma_h}\frac{\partial\rho}{\partial T}\left(\frac{\partial T}{\partial x_j}\, g_j\right) \tag{6.18}$$

is the source due to thermal buoyancy, where σ_h is the turbulent Prandtl number for the energy equation and has a recommended value of 0.9. The term containing σ_k in Eq. 6.16 represents the diffusion of k. σ_k is called the turbulent Prandtl number for k. Launder et al.[63] have recommended the value 1.0 for σ_k.

6.3.2 Transport Equation for ε

The exact form of the transport equation for ε is obtained by taking the derivative of Eq. 6.1 with respect to x_j, and multiplying it by

$$2\nu\left(\frac{\partial u_i'}{\partial x_j} + \frac{\partial u_j'}{\partial x_i}\right). \tag{6.19}$$

The resulting equation is discussed in detail by Daly and Harlow,[69] Hanjalic and Launder,[62] and Lumley and Khajeh-Nouri.[70] The only feasible approach toward devising an ε equation is to apply both intuition and intelligent dimensional analysis. The ε equation contains several empirical coefficients that require adjusting to account for different behaviors of different shear flows. The equation proposed by Jones and Launder[60] and by Daly and Harlow[70] is

$$\rho\frac{\partial\varepsilon}{\partial t} + \rho\, u_j\frac{\partial\varepsilon}{\partial x_j} = C_1\frac{\varepsilon}{k}(P_k + G_k) - C_2\frac{\rho\varepsilon^2}{k} + \frac{\partial}{\partial x_j}\left[\left(\frac{\mu_{tur}}{\sigma_\varepsilon} + \mu_{tam}\right)\frac{\partial\varepsilon}{\partial x_j}\right]. \tag{6.20}$$

Here, the source terms P_k and G_k have the same form as Eq. 6.17 and Eq. 6.18, respectively; the second term on the right is the dissipation term; and the last term represents diffusion. The variable σ_ε is the turbulent Prandtl number for ε; the recommended value[68] is 1.3. The coefficient of the production term C_1 is normally chosen by reference to near-wall turbulence, whereas the coefficient C_2 is determined from the decay of grid turbulence. The values of C_1 and C_2 recommended by Launder et al.[71] are 1.44 and 1.92, respectively.

6.3.3 k-ε Two-Equation Turbulence Model

In the k-ε two-equation turbulence model, we first solve the transport equation for turbulence kinetic energy k (Eq. 6.16) and the dissipation rate of turbulence kinetic energy ε (Eq. 6.20). After obtaining the values of k and ε, we compute the turbulent viscosity μ_{tur} using the relation

$$\mu_{tur} = \left(\frac{C_D \rho k^2}{\varepsilon} \right), \tag{6.21}$$

Here, C_D is a constant having the recommended value 0.09. After computing turbulent viscosity, we compute the thermal conductivity using the relation

$$\lambda_{tur} = \frac{C_p \mu_{tur}}{\sigma_h} \tag{6.22}$$

For turbulent flow, the diffusivity in the governing conservation equation (2.1) is considered as a time-averaged value. Therefore, the viscosity μ and thermal conductivity λ in the momentum and energy equations are replaced by the effective transport coefficients of momentum and energy, respectively. Thus,

$$\mu = \mu_{eff} = \mu_{lam} + \mu_{tur} \tag{6.23}$$

and

$$\lambda = \lambda_{eff} = \lambda_{lam} + \lambda_{tur}. \tag{6.24}$$

Here, the subscripts lam and tur stand for laminar (molecular) and turbulent properties.

In Sec. 6.1, we remarked that the Prandtl's mixing length hypothesis is a special case of the k-ε two-equation turbulence model. We shall now proceed to demonstrate this. For steady-state, one-dimensional flow near a wall, the effects of convection and diffusion are usually negligible; turbulence production is balanced by dissipation. Equation 6.16 reduces to

$$\mu_{tur} \left(\frac{\partial u}{\partial y} \right)^2 = \rho \varepsilon. \tag{6.25}$$

Multiplying Eq. 6.21 by Eq. 6.25,

$$\mu_{tur}^2 \left(\frac{\partial u}{\partial y} \right)^2 = C_D \rho^2 k^2. \tag{6.26}$$

Since

$$\tau = \mu_{tur} \frac{\partial u}{\partial y}, \tag{6.27}$$

Equation 6.26 can be written as

$$\tau = C_D^{1/2} \rho k , \tag{6.28}$$

which expresses the result that the turbulent shear stress is directly proportional to the turbulence kinetic energy in local equilibrium turbulence. This important relationship is supported by experiments on flows near walls.

From dimensional considerations,[67] the dissipation rate ε can be expressed as

$$\varepsilon = C_D \, k^{3/2} / \ell . \tag{6.29}$$

Substituting Eqs. 6.21 and 6.29 into Eq. 6.25 and after further rearrangement,

$$C_D k = \left(\frac{\partial u}{\partial y} \right)^2 \ell^2 . \tag{6.30}$$

Eliminating k between Eqs. 6.28 and 6.30 gives

$$\tau = C_D^{1/2} \rho \ell^2 \left(\frac{\partial u}{\partial y} \right)^2 . \tag{6.31}$$

Equation 6.31 can be recognized as equivalent to the Prandtl's mixing-length hypothesis expressed by Eq. 6.2. Thus, the mixing-length hypothesis can be deduced from the transport equation for the turbulence kinetic energy by neglecting the contributions from convection and diffusion. Its application is limited to local equilibrium turbulent flows that usually occur near walls. Consequently, as we shall see, the results of local equilibrium turbulence model play an important role in the wall function development to be described in Sec. 6.5.

6.4 Boundary Conditions for Turbulent Transport Equations

There are three types of boundaries: (1) a line or surface (plane) of symmetry, (2) inlet and outlet boundaries, and (3) a solid wall. The first two boundaries are discussed here, and a solid wall boundary is discussed in Sec. 6.5.

6.4.1 Symmetry Boundary

The simplest boundary is the line or plane of symmetry; at a symmetry line, the normal velocity is zero. The gradients of scalar quantities k and ε normal to the symmetry line are also zero.

6.4.2 Inlet and Outlet Boundaries

At the outlet plane (free boundary), the gradient of turbulence quantities is assumed to be zero. Thus, at the outlet plane,

$$\partial k / \partial z = 0,$$

and

$$\partial\varepsilon/\partial z = 0, \tag{6.30}$$

where z represents flow direction at the outlet.

The inlet plane requires special treatment. Both the inlet turbulence kinetic energy k_{in} and the inlet dissipation rate ε_{in} should be obtained from measurements if available. If measurements are not available at the inlet plane, the following procedure may be used to estimate k_{in} and ε_{in}. If the inlet velocity is uniform and equal to u_{in},

$$k_{in} = 0.001\, u_{in}^2 \tag{6.31}$$

and

$$\varepsilon_{in} = C_D\, k_{in}^{3/2} / \ell_{in}, \tag{6.32}$$

where ℓ_{in} is a length scale at the inlet. ℓ_{in} is usually assumed to be equal to the smaller of 0.42 y or 0.1 δ, where y denotes the distance to the nearest wall and δ is the width of the shear layer. If the profile of the mean velocity at the inlet plane is known, then k_{in} can be estimated from

$$k_{in} = 3\ell_{in}^2 \left[\left(\frac{\partial v_{in}}{\partial y} \right)^2 + \left(\frac{\partial u_{in}}{\partial z} \right)^2 \right], \tag{6.33}$$

where u_{in} is the mean velocity component in the main flow (x) direction. The inlet dissipation rate ε_{in} is again estimated by using Eq. 6.32.

It should be noted that k_{in} and ε_{in} are user-specified input parameters for COMMIX-1C. If the user does not specify k_{in} and ε_{in}, COMMIX-1C assumes that the inlet k and ε are negligibly small ($k = 10^{-16}$ and $\varepsilon = 10^{-10}$).

6.5 Wall Function Treatment

In the immediate vicinity of a solid wall, there is a large variation in the values of turbulence properties. Therefore, to predict the correct values of momentum flux, energy flux, and the gradients of k and ε, we apply a special treatment called the wall-function treatment. In this procedure, we implicitly account for steep variation near a wall and avoid the need for a fine mesh. This approach fits well with COMMIX since, in most engineering applications, one rarely has the luxury of resolving the fine details in a boundary layer due primarily to the high cost of computation in using a fine mesh system.

In the literature, there are several different treatments of wall function.[72] It appears that at the present time, no single wall function treatment can claim superiority in both generality and accuracy for a variety of turbulent flows. In view of this, we have developed the wall-function model in COMMIX-1C based on the following guidelines:

1. Simplicity.

2. Minimizing numerical difficulties.

3. Wide range of applicability.

The first two guidelines are straightforward. The third guideline will become clear later.

There are basically two approaches in treating the cells adjacent to the walls. The first one is that both the k and ε are calculated algebraically for the cells next to the walls. Therefore, transport equations for k and ε are not solved for wall-adjacent cells. The second approach is to calculate ε algebraically and solve the transport equation for k for cells adjacent to walls. In COMMIX-1C, we have adopted the first approach, i.e., both k and ε are solved algebraically, because of its simplicity (guideline 1).

There are also two types of wall function models; a two-layer model and a three-layer model. Again, we have chosen the simpler two-layer wall function model and modified it slightly to meet the guidelines described previously.

6.5.1 A Two-Layer Wall Function Model

In a general purpose code such as COMMIX, one may frequently have to deal simultaneously with laminar and turbulent flows at different locations of a system. Also, during a transient simulation, different flow regimes may occur at the same location but at different times. Provision must be made in the code to handle these situations even though the accuracy of the results may deteriorate in a certain range of the relevant parameters (such as Reynolds number). Thus, in COMMIX-1C, we have made provision to calculate flows with Reynolds numbers ranging from very small (laminar) to very large (highly turbulent). This is what we mean by a wide range of applicability in guideline 3.

Figures 10 and 11 show the two-layer wall function model used in COMMIX-1C, where P is the node adjacent to the wall, y_P is the distance from P to the wall, and y_ℓ is the thickness of the viscous sublayer. The distance y_P is fixed when the user finishes modeling the geometry (and mesh system). The thickness of the viscous sublayer y_ℓ, however, is not a constant and often cannot be easily determined beforehand. This is why we have made provision in COMMIX-1C to accommodate both situations shown in Figs. 10 and 11. The distributions of k and ε are assumed to be the same in both figures.

When $Y_P > Y_\ell$, the first node is in the fully turbulent zone (Fig. 10). The velocity at node P is given by the law of the wall in the fully turbulent region

$$u_p = (u_\tau / K)\, \ell n\left(E\, y_p^+\right), \tag{6.34}$$

where

$$u_\tau = (\tau_w/\rho)^{1/2} \tag{6.35}$$

$$y^+ = y u_\tau / \nu . \tag{6.36}$$

E is a constant equal to 9.0, K is the von Karman constant (K = 0.42), and ν is the kinematic viscosity. Equation 6.34 can be written as

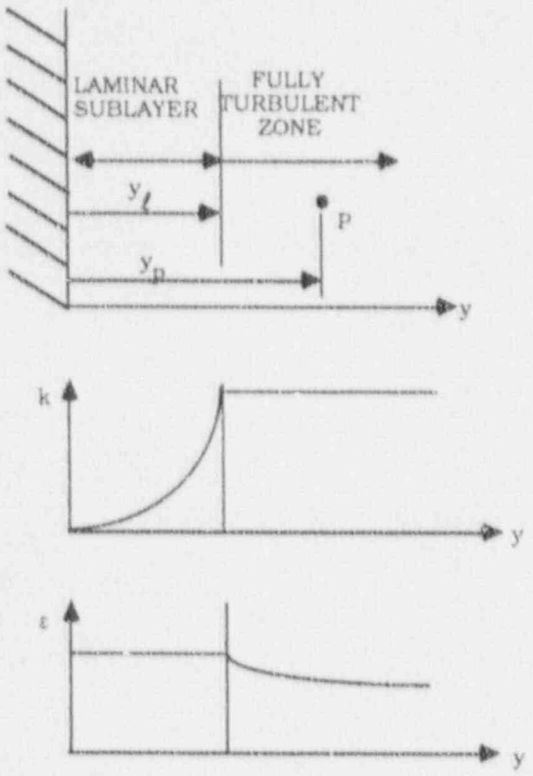

Fig. 10. Two-layer wall function model ($y_P > y_\ell$)

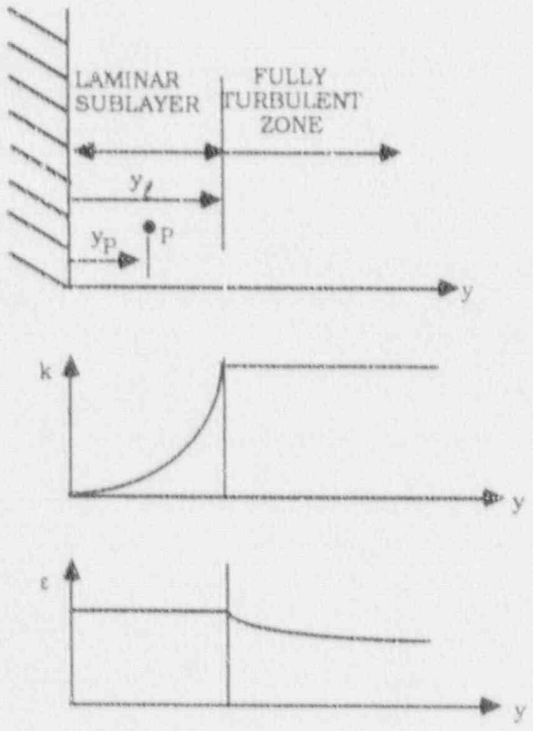

Fig. 11. Two-layer wall function model ($y_P \leq y_\ell$)

$$u_\tau = K u_P / \ell n(E\, y_P^+). \tag{6.34a}$$

The turbulence kinetic energy k at node P can be calculated by using Eq. 6.28, which is rewritten as

$$k_P^3 = u_\tau^2 / C_D^{1/2}. \tag{6.37}$$

The turbulence dissipation rate ε at node P is calculated by using an equation similar to Eq. 6.29

$$\varepsilon_P = C_D^{3/4} k_P^{3/2} / (K y_P)$$

$$= u_\tau^3 / (K y_P). \tag{6.38}$$

When $Y_P \leq Y_\ell$, the node P is in the laminar sublayer (Fig. 11). The velocity at node P is given by the law of the wall in the laminar sublayer

$$u_P = u_\tau y_P^+, \tag{6.39}$$

which can be rewritten as

$$u_\tau = (\nu\, u_P / y_P)^{1/2}. \tag{6.39a}$$

The turbulence kinetic energy at node P is calculated by

$$k_P = k_\ell (y_P / y_\ell)^2, \tag{6.40}$$

where k_ℓ is the turbulence kinetic energy at $y = y_\ell$. We assume that Eq. 6.28 for local equilibrium turbulence applies at the edge of the laminar sublayer ($y = y_\ell$) and Eq. 6.40 becomes

$$k_P = u_\tau^2 (y_P / y_\ell)^2 / C_D^{1/2}. \tag{6.40a}$$

It should be noted that the assumption of local equilibrium at the edge of the laminar sublayer may not be strictly valid. It is known[38] that local equilibrium applies when $30 < y^+ < 50$. We adopt it here to simplify the calculation. It should also be noted that we assume that the turbulence kinetic energy k is constant outside the laminar sublayer (Fig. 10). This assumption greatly simplifies the numerical calculation (guideline 1) since no extrapolation is needed.

The turbulence dissipation rate ε at node P is calculated by using Eq. 6.38 and assuming that the dissipation rate in the laminar sublayer is constant and equal to that at $y = y_\ell$.

$$\varepsilon_P = u_\tau^3 / k y_\ell \tag{6.41}$$

The assumption of constant ε in the laminar sublayer is in agreement with most wall function models in the literature. The assumption of ε_P equal to ε at $y = y_\ell$ is different from those in the literature. The reason for making the last assumption is to make ε continuous

so that numerical difficulties associated with discontinuous functions can be avoided (guideline 2).

6.5.2 Evaluating k and ε for Cells Adjacent to Walls

In the computer code, the following paths are followed to determine the proper values of k and ε for cells adjacent walls. The key is to determine whether the node adjacent to a wall is in the laminar sublayer or in the turbulent zone. The relevant scaling parameter is the frictional velocity u_τ, which appears in the equations for k, ε, and the velocity distribution given by the law of the wall in Sec. 6.5.1.

The preliminary step is to evaluate the dimensionless thickness of the laminar sublayer y_ℓ^+. This is accomplished by matching the velocity at the edge of the viscous sublayer ($y = y_\ell$) to that from the law of the wall,

$$y_\ell^+ = \frac{1}{\kappa}\ell n\left(E\, y_\ell^+\right), \tag{6.42}$$

where

$$y_\ell^+ = y_\ell u_\tau / \nu, \tag{6.43}$$

$\kappa = 0.42$, and $E = 9$. It should be noted that y_ℓ^+ depends only on the constants κ and E. The value of y_ℓ^+ turns out to be 10.924. Then we proceed to calculate k_P and ε_P as follows:

Step 1 – Calculate y_ℓ based on a guessed value of u_τ

The value of u_τ can be estimated by either the laminar sublayer relationship (Eq. 6.39a), or the local equilibrium turbulence relationship (Eq. 6.37). In the code, we take the larger of the two as the guessed value of u_τ,

$$u_\tau^2 = \max\left(\frac{\nu u_P}{y_P}, C_D^{1/2} k_P\right). \tag{6.44}$$

Then, y_ℓ is calculated by

$$y_\ell = y_\ell^+ / u_\tau,$$

where y_ℓ^+ is calculated previously and has a value of 10.924.

Step 2 – Compute k_P and ε_P by comparing y_P with y_ℓ

If $y_P > y_\ell$

This indicates the node P is in the turbulent zone, and we recompute the frictional velocity u_τ iteratively by using the law of wall in the turbulent zone

$$u_\tau = \kappa u_P / \ell n(E y_P u_\tau / \nu). \tag{6.45}$$

Then, compute k_P and ε_P according to Eqs. 6.37 and 6.38

$$k_P = u_\tau^2 / C_D^{1/2}$$

$$\varepsilon_P = u_\tau^3 / K y_P .$$

If $y_P \le y_\ell$

This indicates that the node P is in the laminar sublayer, and we recompute u_τ by using Eq. 6.39a,

$$u_\tau = (\nu u_P / y_P)^{1/2} .$$

Then, compute k_P and ε_P according to Eqs. 6.40a and 6.41

$$k_P = u_\tau^2 (y_P / y_\ell)^2 / C_D^{1/2}$$

$$\varepsilon_P = u_\tau^3 / K y_\ell .$$

The algebraically computed k_P and ε_P of wall adjacent cells are then used in the solution of the transport equations of k and ε for other cells. If the results do not satisfy the convergence criteria, Steps 1 and 2 are repeated until convergence is reached.

6.6 Solution Procedure for Calculating Turbulent Flows

The procedure for calculating turbulent flows is similar to that described in Chapter 10, except that there are two additional transport equations (k and ε) to be solved. These two equations are solved after the pressure equation and before the energy equation. Table 17 summarizes a solution procedure for calculating turbulent flows.

6.7 Discussion

There are a total of eight constants employed in the k-ε two-equation turbulence model. Table 18 provides a summary of these constants. The values listed in this table are the default values used in COMMIX-1C. These values may or may not be slightly different from those used in other k-ε two-equation turbulence models. If users wish to use values other than those listed in Table 18, they may input these parameters (input preparation is described in Volume II).

The wall function model described in Sec. 6.5 is different from and simpler than most other models in the literature. We have thoroughly tested this model against the data for fully developed pipe flow and for two-dimensional single-sudden-expansion (backward-facing step).[73] The results indicate that the current k-ε two-equation turbulence model compares favorably with the data of fully developed pipe flow at high Reynolds numbers, while the agreement is less favorable for the backward-facing-step problem, particularly near the reattachment zone. These observations are in agreement with assessment of other two-equation turbulence models.[74]

We have also tested the k-ε two-equation turbulence model against data of a circular buoyant jet.[73] Both the calculated centerline velocity and centerline temperature

Table 17. Fully implicit (SIMPLEST-ANL) solution sequence (α = 1) for turbulent flows

1. *Calculate* velocity–pressure relation coefficients from the previous iterate values of u, v, w, and μ_{eff}:

$$\hat{\phi}, d^{\phi}; (\phi = u, v, w).$$

2. *Calculate* pressure equation coefficients using $\hat{\phi}, d^{\phi}$:

$$a_0^P, a_\ell^P, b_0^P .$$

3. *Solve* pressure equation for new-time, new-iterate pressure δP:

$$a_0^P \delta P_0 = \sum a_\ell^P \delta P_\ell + b_0^P .$$

4. *Calculate* new-time, new iterate velocities u, v, w from velocity–pressure relations:

$$\phi = \hat{\phi} - d^{\phi} \Delta \delta P; (\phi = u, v, w).$$

5. *Calculate* coefficients for k and ε equations using new-time new-iterate velocities:

$$a_0^k, a_\ell^k, b_0^k \; ; \; a_0^\varepsilon, a_\ell^\varepsilon, b_0^\varepsilon$$

6. *Solve* k and ε equations for new-time, new-iterate k and ε:

$$a_0^k k_0 = \sum a_\ell^k k_\ell + b_0^k \; ; \; a_0^\varepsilon \varepsilon_0 = \sum a_\ell^\varepsilon \varepsilon_\ell + b_0^\varepsilon$$

7. *Calculate* new-time, new-iterate μ_{eff} and λ_{eff}:

$$\mu_{tur} = C_D \rho k^2 / \varepsilon, \; \lambda_{tur} = C_P \mu_{tur} / \sigma_h$$

$$\mu_{eff} = \mu_{lam} + \mu_{tur}, \; \lambda_{eff} = \mu_{lam} + \mu_{tur}$$

8. *Calculate* energy equation coefficients using new-time, new-iterate velocities and λ_{eff}:

$$a_0^h, a_\ell^h, b_0^h .$$

9. *Solve* energy equation for new-time, new-iterate enthalpy h:

$$a_0^h h_0 = \sum a_\ell^h h_\ell + b_0^h .$$

10. *Check* for convergence of u, v, w, h, k, ε; if not converged, return to Step 1.

Table 18. Summary of constants employed in k-ε two-equation turbulence model

Symbol	Value	Appearance (Equation)
σ_h	0.9	6.18
σ_k	1.0	6.16
σ_ε	1.3	6.20
C_1	1.44	6.20
C_2	1.92	6.20
C_D	0.09	6.21
K	0.42	6.34 and 6.42
E	9.0	6.34 and 6.42

distributions compare favorably with data for a densimetric Froude number of 5. The buoyant jet is a free shear flow and therefore is not affected by the wall function model.

Finally, it should be noted that the k-ε two-equation turbulence model described in this section is, strictly speaking, only valid for isotropic turbulence at very high Reynolds numbers. Even though the code will perform calculations for flows at lower Reynolds numbers, the results are less reliable and must be examined and interpreted very carefully. This is because the k-ε two-equation turbulence model does not automatically degenerate to the low Reynolds flow and is the inherent limitation of most turbulence models. The users must be aware of this limitation. However, as mentioned previously, the k-ε two-equation turbulence model is the most widely used and tested turbulence model. Our assessment is that this model does have some generality in treating a variety of turbulent flows encountered in engineering systems, even though the accuracy may vary from one type of flow to another.

7 Flow-Modulated Skew-Upwind Discretization Scheme

7.1 Introduction

In fluid-dynamic calculations, the pure-upwind difference scheme is generally preferred over the central-difference scheme to discretize convective terms. The reason is that for high-Peclet number flows, the pure-upwind scheme prevents instability and provides a more accurate solution than that obtained with the central-difference scheme. However, it has been observed that for flows inclined to grid lines, the pure-upwind scheme causes increased numerical diffusion. To reduce numerical diffusion, we have developed and implemented a flow-modulated skew-upwind discretization (FMSUD) scheme. This scheme is currently implemented in the energy equation only. To keep the

discussion manageable, the demonstrations and derivations that follow are based on the assumption of unidirectional flow in an arbitrary direction (i.e., there is no velocity gradient anywhere in the flow domain). However, this assumption will be removed as shown in Sec. 7.4.3. In fact, the implementation of FMSUL in the energy equation is for all flow conditions.

7.2 Pure-Upwind Difference Scheme

7.2.1 One-Dimensional

Because of its stabilizing effect, the pure-upwind difference scheme is used extensively in one-dimensional hydrodynamic computer programs.[75] The basic concept is briefly discussed here with reference to Fig. 12.

It is easy to difference the model equation

$$\frac{\partial}{\partial x}(u\phi) = 0 \tag{7.1}$$

at node i, where ϕ is some scalar and u is the velocity. Equation 7.1 can be differenced at center node i as

$$\frac{(u\phi)_{i+1/2} - (u\phi)_{i-1/2}}{\Delta x} = 0, \tag{7.2}$$

where the subscript $i \pm 1/2$ refers to the values of $(u\phi)$ at the cell edges. In a staggered mesh system, ϕ and u are not known at the same points. If it is assumed that ϕ is continuous, Eq. 7.2 can be approximated as

$$\frac{(u\phi)_{i+1/2} - (u\phi)_{i-1/2}}{\Delta x} \cong \frac{u_{i+1/2}\phi_i - u_{i-1/2}\phi_{i-1}}{\Delta x} \tag{7.3a}$$

for the case $u_{i \pm 1/2} > 0$, and

$$= \frac{u_{i+1/2}\phi_{i+1} - u_{i-1/2}\phi_i}{\Delta x} \tag{7.3b}$$

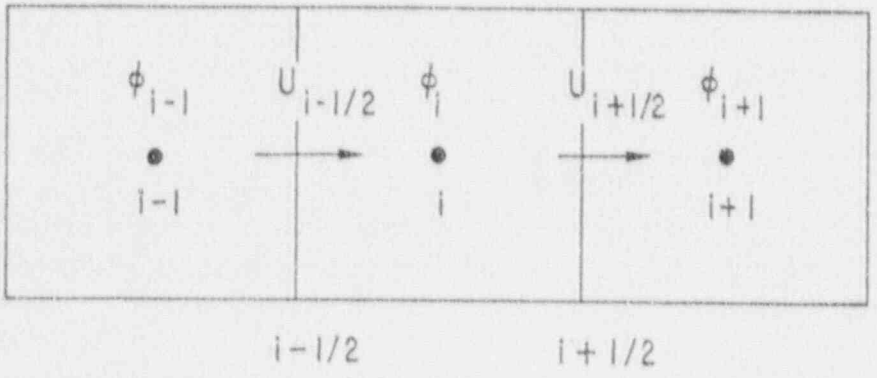

Fig. 12. One-dimensional upwind or donor cell

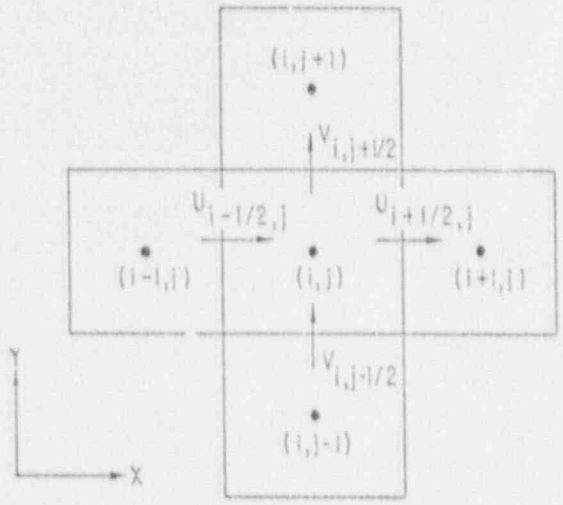

Fig. 13. Two-dimensional upwind or donor cell

for $u_{i\pm1/2} < 0$. That is, the values of ϕ are considered "donated" (or upwinded) to the cell edge, depending on the signs of $u_{i\pm1/2}$.

7.2.2 Two-Dimensional

Now consider the two-dimensional situation shown in Fig. 13. The application of the one-dimensional pure-upwind difference scheme to the two-dimensional model equation

$$\frac{\partial}{\partial x}(u\phi) + \frac{\partial}{\partial y}(v\phi) = 0 \tag{7.4}$$

produces

$$\begin{aligned}\frac{\partial(u\phi)}{\partial x} &= \frac{(u\phi)_{i+1/2,j} - (u\phi)_{i-1/2,j}}{\Delta x} \\ &\equiv \frac{\left(u_{i+1/2,j}\phi_{i,j}\right) - \left(u_{i-1/2,j}\phi_{i-1,j}\right)}{\Delta x}\end{aligned} \tag{7.5}$$

and

$$\begin{aligned}\frac{\partial(v\phi)}{\partial y} &= \frac{(v\phi)_{i,j+1/2} - (v\phi)_{i,j-1/2}}{\Delta y} \\ &\equiv \frac{\left(v_{i,j+1/2}\phi_{i,j}\right) - \left(v_{i,j-1/2}\phi_{i,j-1}\right)}{\Delta y},\end{aligned} \tag{7.6}$$

assuming u and v are both positive. This extension assumes that the velocities are locally one-dimensional, i.e., each cell face is associated with only one velocity component, as shown in Fig. 13. Extension to other combinations of signs of u and v, as well as to three dimensions, are straightforward.

7.2.3 Numerical Diffusion

This apparently straightforward application of the one-dimensional pure-upwind concept to two and three dimensions has been identified as one of the main sources of numerical diffusion when the streamline is at an angle to the grid lines.[76-78] It has been shown that the numerical diffusion coefficient for a two-dimensional steady-state situation can be approximated by

$$\Gamma_{\text{false}} = \frac{\rho U \Delta x \, \Delta y \sin 2\theta}{4\left(\Delta y \sin^2\theta + \Delta x \cos^2\theta\right)}, \tag{7.7}$$

where U is the velocity and θ is the angle between the velocity U and the x coordinate. It can be observed that numerical diffusion for the upwind difference scheme is affected by velocity, mesh size, and angle between the local streamlines and the grid lines. Equation 7.7 indicates that numerical diffusion is most serious when $\theta = 45°$. It is also clear from Eq. 7.7 that numerical diffusion does not exist for a one-dimensional flow or a two-dimensional flow when the local streamlines are parallel (or perpendicular) to grid lines ($\theta = 0$ and 90°).

Note that the term "numerical diffusion" is highly misunderstood among the practitioners of numerical analysis. Accordingly, we get different interpretations from different practitioners. The concept of numerical diffusion can be described as follows. If we subtract the finite-difference approximation from its partial differential equation in a Taylor-series expanded form, the resulting equation is generally termed a "truncation error." Here, we are assuming that a Taylor-series expanded form is an accurate representation of the partial differential equation under consideration.

The truncation error usually contains many odd and even derivative terms. The effect of even derivative terms is generally to reduce all gradients in the solution, whether physically correct or artificially induced. This effect, called dissipation, is often looked on as if we have introduced an artificial diffusivity. This is why dissipation is often referred to as false, artificial, or numerical diffusion. The odd derivative terms, on the other hand, have a tendency to produce an oscillatory solution. This effect is termed dispersion.

The lowest-order term of the truncation error defines the order of the numerical scheme. In general, if the lowest-order term in the truncation error is an even derivative, the dissipative error will predominate; if it is an odd derivative, the dispersive error will predominate.

When we use an upwind-differencing scheme, the lowest-order term in the truncation error is a first-order even derivative of the order $0(\Delta x)$. The effect of upwind differencing is therefore to distort sharp gradients by dissipation, as shown in Fig. 14b. In the case of central differencing, the even-derivative term is cancelled, so the lowest-order term is a second-order odd derivative of the order $0(\Delta x^2)$. The effect of central differencing is therefore dispersive, as shown in Fig. 14c.

Since a pure-upwind scheme introduces dissipation, we need not consider it as inaccurate or a misrepresentation of reality. On the contrary, for convection diffusion flows parallel to grid lines and at high Peclet numbers, the pure-upwind scheme actually gives a better and more stable solution than would be obtained from a central-differencing scheme.

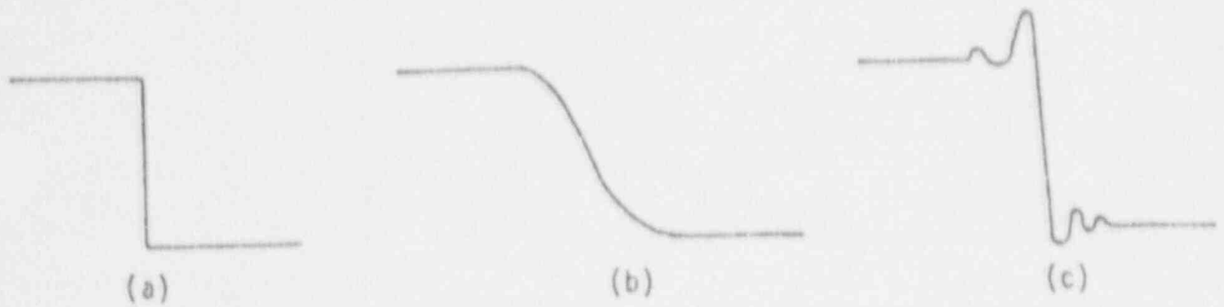

Fig. 14. Effects of dissipation and dispersion: (a) exact solution; (b) numerical solution distorted primarily by dissipation errors (typical of first-order methods); (c) numerical solution distorted primarily by dispersion errors (typical of second-order methods)

However, for flows inclined to grid lines, we need modification to reduce numerical diffusion.

In Sec. 7.3, we shall show some numerical examples so that the reader can better understand what numerical diffusion is when the upwind difference scheme is used and when the flow is at an angle to the grid lines.

The cause of numerical diffusion for the upwind difference scheme is the result of treating the flow across each control volume face as locally one-dimensional (Fig. 13). This approach apparently does not take into account the multidimensional nature of the flow when it is inclined at an angle to the grid lines. To do so, it is necessary to involve more neighbors in the discretization equation. We shall describe this approach in more detail later.

7.2.4 Reducing Numerical Diffusion

The apparent ways to reduce numerical diffusion are to

- Reduce the velocity.
- Orient the grid so that the grid lines more or less align with the flow direction (reducing θ).
- Use very fine mesh.
- Use smaller time-steps for transient problems, but correlate with mesh size so that it will not impair diffusion-controlled stability criteria.
- Use higher-order finite-difference approximations.
- Extend the upwind difference scheme to involve more neighbors in the discretization equation.

The first two ways of reducing numerical diffusion are often not possible since the user does not have the freedom in choosing the magnitude and the direction of the local

velocities. The third and the fifth methods may not be practical. It is not practical to use very fine mesh when one is trying to analyze a large, complex, real engineering system. Higher-order finite-difference approximation will be much more involved, and its implementation in COMMIX would require major code modifications. Furthermore, the procedure would become computationally more expensive. It appears that the last method, i.e., extending the upwind difference scheme to involve more neighbors in the discretization equation, is the only practical and feasible way to reduce numerical diffusion in COMMIX calculations at the present time. In the literature, this type of discretization method is called the skew-upwind difference (SUD) scheme. We shall briefly describe various skew-upwind difference schemes available in the literature before we move on to the main subject of this chapter, i.e., the flow-modulated skew-upwind discretization (FMSUD) scheme.

7.3 Review of Skew-Upwind Difference Schemes

7.3.1 Two-Dimensional Skew-Upwind Difference Scheme

The two-dimensional SUD scheme was first proposed by Raithby.[76] The main idea is to perform differencing in the direction of local streamlines. This requires that the values of the upstream scalar quantity be known. By purely geometrical consideration, Raithby assumed that the upstream value of the scalar quantity is a linear interpolation of that particular variable evaluated at two neighboring grid points. Thus, Raithby's SUD scheme is able to reduce numerical diffusion caused by assuming the flow to be locally one-dimensional in the upwind difference scheme. However, the Raithby SUD scheme has employed arbitrary cutoffs for the geometrical interpolation. Furthermore, Raithby's SUD scheme is known to have undershoots and overshoots under certain conditions. The situation is best illustrated by the numerical example described below.

Figure 15 shows the known exact solution for the isotherms (constant-temperature lines) of a two-dimensional flow with negligible thermal diffusivity. The horizontal axis can be considered as the entrance of uniform velocity with mass flow rate m_y at a uniform temperature of 100°C. The vertical axis can be considered as the entrance of uniform velocity with mass flow rate m_x at a uniform temperature of 0°C. If $m_x = m_y$ and $\Delta x = \Delta y$, the resultant velocity is uniform everywhere and is inclined at an angle of 45° with respect to the x axis. Since there is no numerical diffusion (exact solution) and there is no physical diffusion (negligible thermal diffusivity), a sharp interface should prevail along the diagonal beginning from the origin. Above this interface, the fluid temperature should be 0°C everywhere. Below this interface, the fluid temperature should be 100°C everywhere. This is the result shown in Fig. 15. The isotherms are concentrated near the diagonal parallel to the flow direction and are plotted in 5°C intervals. The reason that the hot/cold interface has a finite width instead of being a single line is the result of the mesh size used in the computation. It can be observed that the width of the interface region is equal to the length of the diagonal of a computational cell. If the size of the computational cell is reduced, the width of this interface region will be reduced correspondingly. It can be observed that all the isotherms are parallel to each other and are inclined at an angle of 45° with respect to the horizontal axis. The nonparallel behavior of the isotherms near the two corners is due to the edge effect, which extends 1/2 cell from the boundaries and is

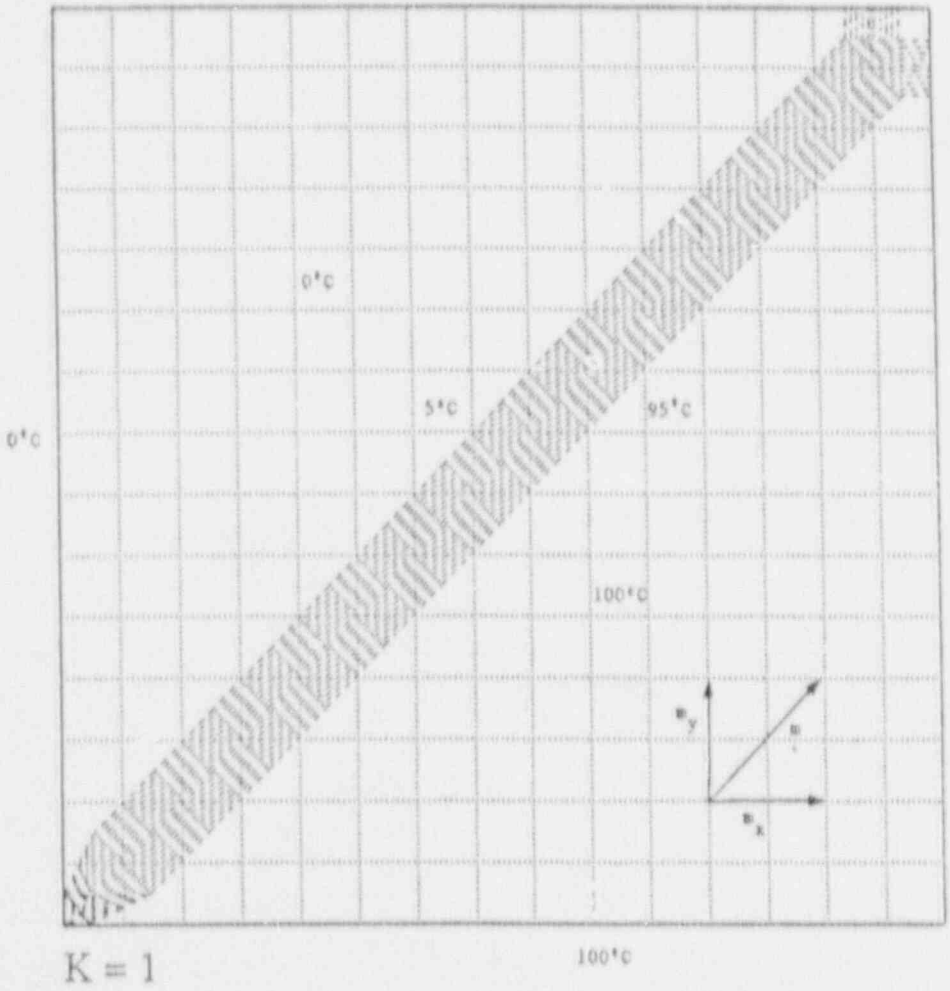

Fig. 15. Isotherms of two-dimensional flow with $m_x = m_y$ (exact solution)

inherent in the plotting package of COMMIX. The important thing to keep in mind is that the results of an acceptable numerical scheme should approach that of the exact solution shown in Fig. 15.

Figure 16 shows the calculated isotherms by using the pure upwind-difference scheme. Again, the horizontal mass flow rate m_x is set equal to the vertical mass flow rate m_y and the mesh size is identical to that shown in Fig. 15. It is obvious that the isotherms are no longer concentrated near the diagonal in the flow direction and are spread over a wide region. Moreover, the isotherms shown in Fig. 16 are no longer parallel. Thus, one can conclude that significant numerical diffusion occurred by using the upwind difference scheme to calculate the flow inclined at an angle to the grid lines.

Figure 17 shows the plot of the isotherms calculated by using Raithby's SUD scheme. Again, the flow is inclined at an angle of 45° with respect to the horizontal axis, and other conditions are identical to that shown in Fig. 15. It is evident that the Raithby SUD scheme is able to eliminate numerical diffusion completely for this particular case (i.e., a two-dimensional unidirectional flow inclined at an angle of 45° to the grid lines) because the

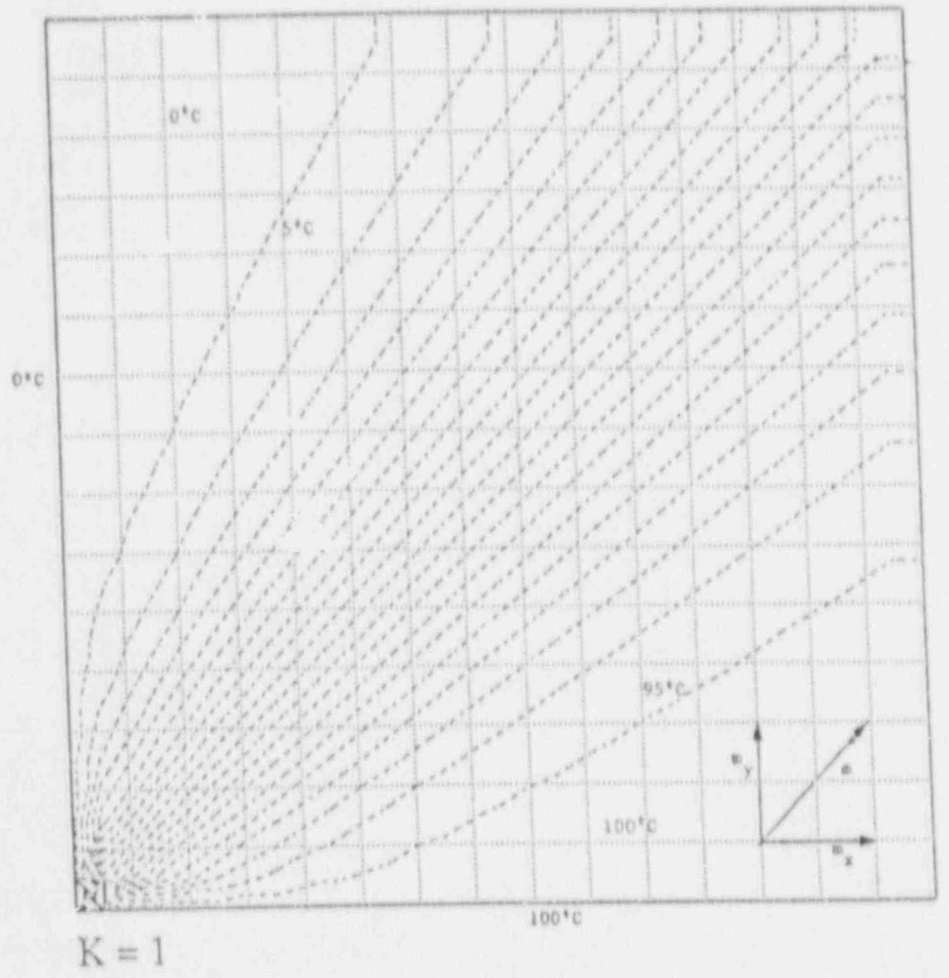

Fig. 16. Isotherms of two-dimensional flow with $m_x = m_y$ (upwind difference)

result shown in Fig. 17 is identical to that shown in Fig. 15. However, as we shall demonstrate, the Raithby SUD scheme does not offer unqualified improvement over the pure upwind difference scheme if the resultant velocity is not inclined at an angle of 45° to the grid lines.

Figure 18 shows the isotherms of a two-dimensional flow with $m_y = 2\ m_x$ calculated by using the pure upwind difference scheme. As expected, significant numerical diffusion exists and the isotherms spread over a wide region. Figure 19 shows the results of a similar calculation except that the Raithby SUD scheme is used instead of the pure upwind difference scheme. It can be observed that in some areas, the Raithby SUD scheme does reduce numerical diffusion by narrowing the distance between isotherms, but it also creates a strange pattern of isotherms over an even wider area. The temperatures in this region can be higher than 100°C (in other cases, it can be lower than 0°C), which is unrealistic. The temperature anywhere in the computational domain should be bounded between 0 and 100°C because there is no heat source/sink anywhere in the domain. This type of overshoot (or undershoot) is obviously not acceptable and is the main shortcoming of the Raithby SUD scheme.

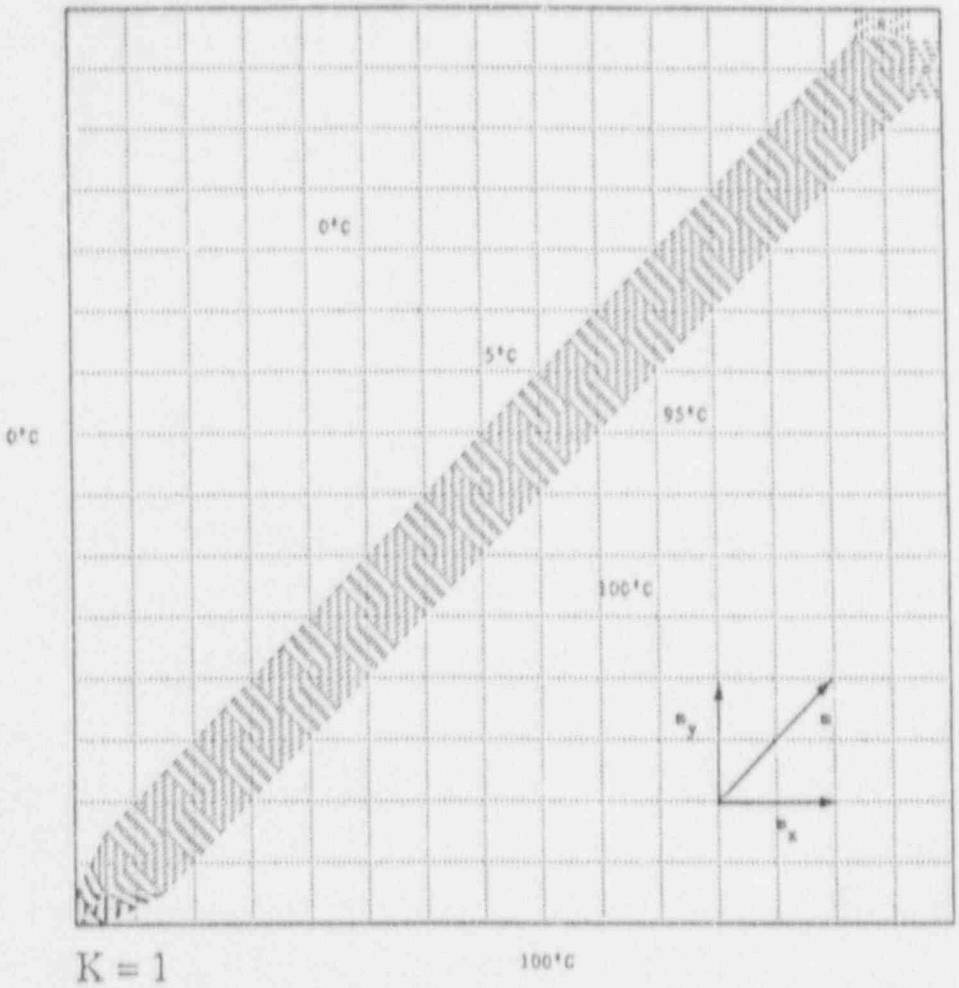

Fig. 17. Isotherms of two-dimensional flow with $m_x = m_y$ (Raithby skew-upwind difference)

More recently, Hassan et al.[79] proposed a mass-flow-weighted SUD scheme for calculating two-dimensional flows. This scheme is an improvement over the Raithby SUD scheme because it can eliminate the overshoot/undershoot observed in the Raithby SUD scheme while retaining the exact 45° solution. We shall describe in more detail the two-dimensional mass-flow-weighted SUD scheme of Hassan et al. in Sec. 7.4 because it forms the basis of the flow-modulated SUD scheme. Here, we present only the calculated results of the same problem shown in Figs. 18 and 19 by using Hassan's SUD scheme.

Figure 20 shows that the overshoot (or undershoot) is indeed absent when the mass-flow-weighted SUD scheme is used. Also, it can be observed, by comparing Fig. 20 to Fig. 18, that Hassan's SUD scheme is able to reduce numerical diffusion caused by the pure upwind difference scheme, although some numerical diffusion is still present.

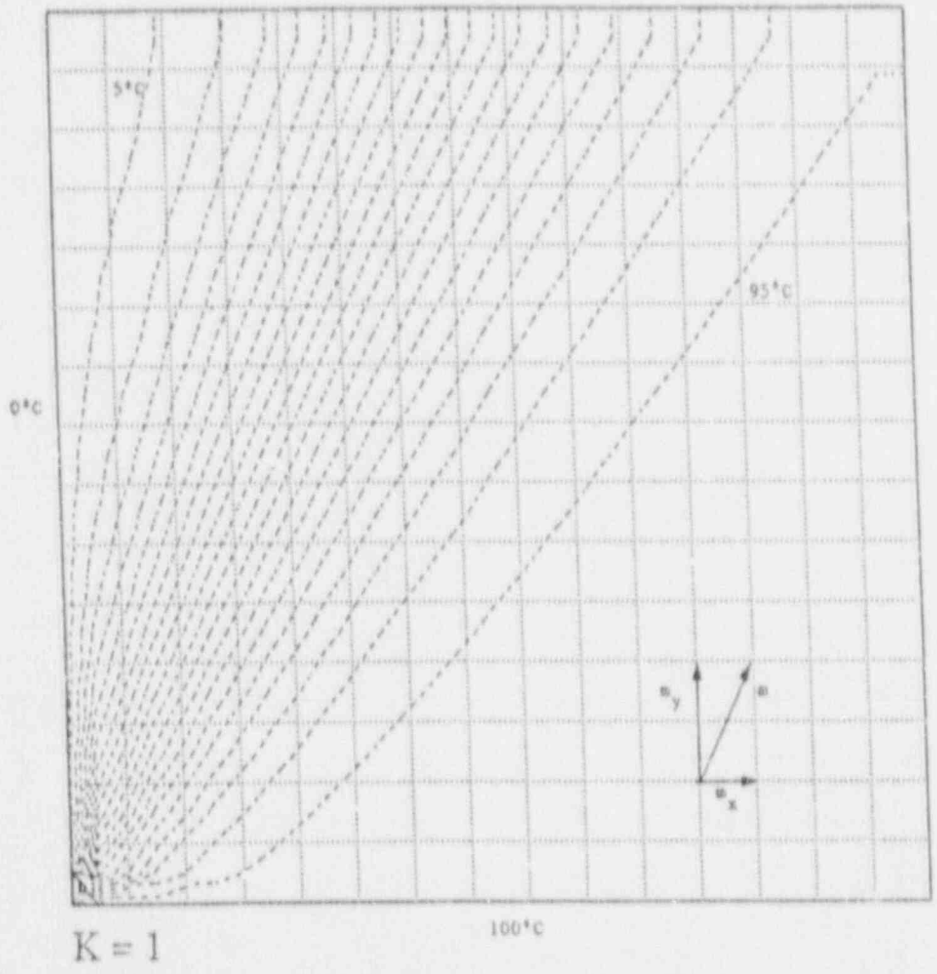

Fig. 18. Isotherms of two-dimensional flow with $m_y = 2\ m_x$ (upwind difference)

7.3.2 Three-Dimensional Skew-Upwind Difference Schemes

Three types of SUD schemes have been employed for three-dimensional applications:

- Extended Raithby.
- Volume-weighted.
- Mass-flow-weighted.

The extended Raithby scheme is a straightforward extension of the two-dimensional Raithby SUD scheme to three-dimensional problems. This was accomplished and documented in COMMIX-1B. The volume-weighted SUD scheme was developed at ANL and was implemented and documented in COMMIX-1B in 1985. The mass-flow-weighted SUD scheme is an extension of the two-dimensional SUD scheme proposed by Hassan et al. and is implemented in an earlier version of COMMIX by Hassan.[80] We will not describe the

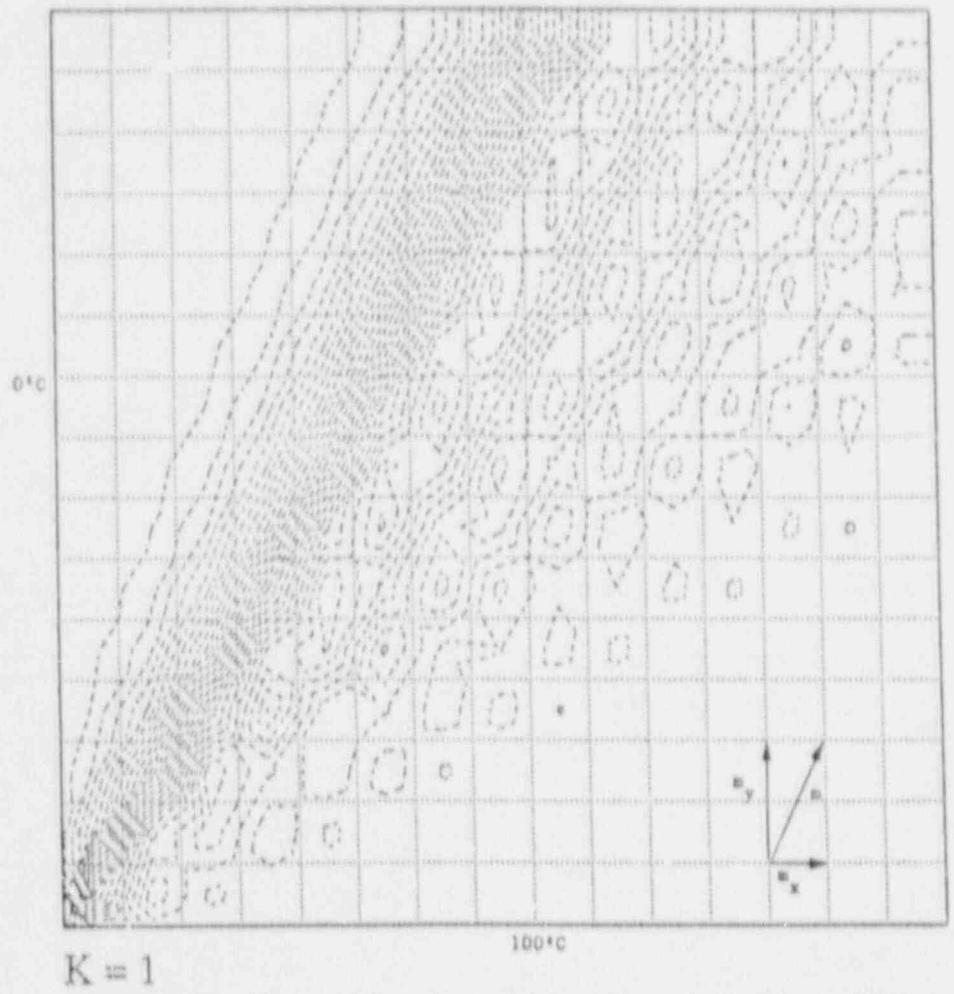

Fig. 19. Isotherms of two-dimensional flow with $m_y = 2\ m_x$ (Raithby skew-upwind difference)

mathematical details of these numerical schemes; instead, we present below a numerical example and comment briefly on the major features of each of these schemes.

Figure 21 shows the isotherms of a three-dimensional flow with uniform velocity ($m_x = m_y = m_z$) calculated by using the exact solution. The horizontal axis can be considered as flow entering in the y direction at a uniform temperature of 0°C and the vertical axis can be considered as flow entering the x direction, also at a uniform temperature of 0°C. Figure 21 represents the first plane (k=1) in the z direction and therefore can be considered as the bottom (lowest elevation) of the flow channel. The flow entering from the bottom is at a uniform temperature of 100°C. Thermal diffusivity is assumed to be negligible. It can be observed that the isotherms are concentrated near the entrances and are parallel to either the x or the y axis except near the three corners where the edge effect mentioned previously is present. Figure 22 shows the isotherms calculated by the exact solution at a higher elevation (k = 4). As expected, the isotherms remain concentrated in a narrow band, and the width of the band is proportional to the mesh size used in the computation. The hot and cold regions are clearly defined.

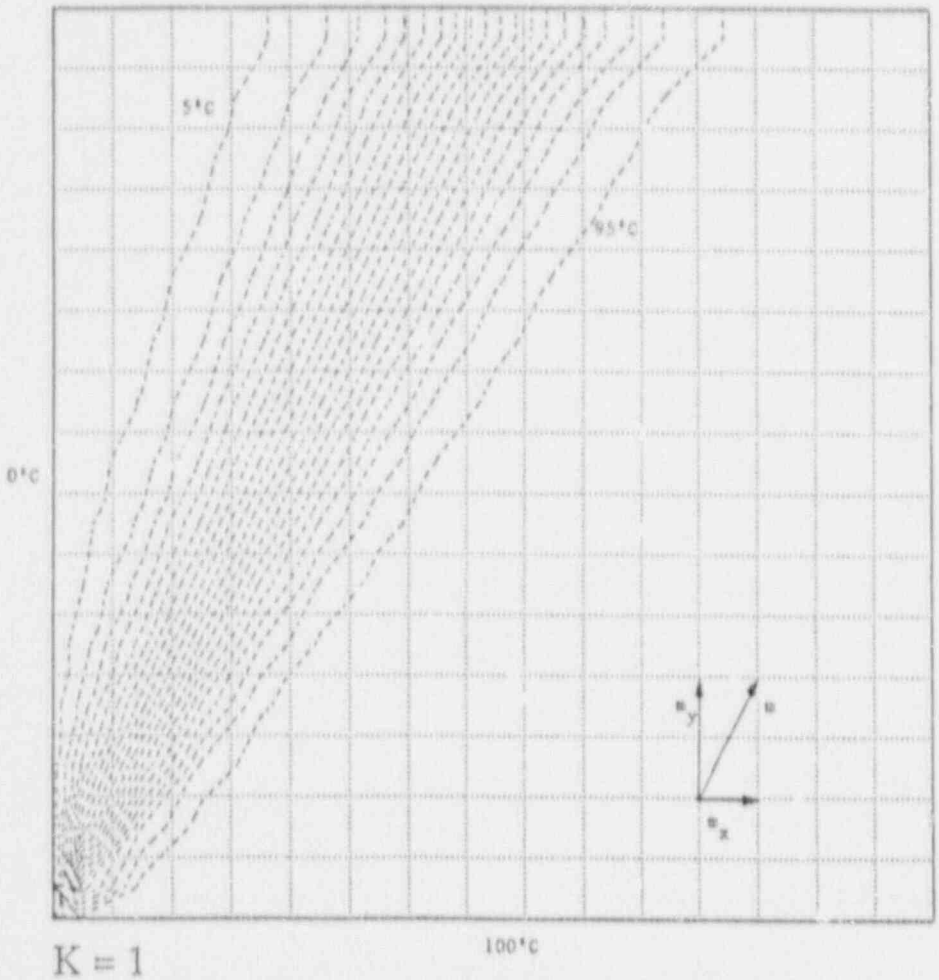

Fig. 20. Isotherms of two-dimensional flow with $m_y = 2\ m_x$ (mass-flow-weighted skew-upwind difference of Hassan et al.)

Figures 23 and 24 show the isotherms of the same problem calculated by using the pure upwind difference scheme. It can be observed that numerical diffusion is present even at the lowest elevation (Fig. 23). At a higher elevation, the effect of numerical diffusion has propagated through the entire plane and a hot/cold interface no longer exists (Fig. 24).

Figures 25 and 26 show the isotherms of the three-dimensional flow calculated by using the extended Raithby SUD scheme. Although the three-dimensional Raithby SUD scheme is able to reduce numerical diffusion, significant undershoot/overshoot occurred (Fig. 26). The result is similar to that of the two-dimensional problem described in Sec. 7.3.1. The undershoot/overshoot is not realistic and is therefore not acceptable from the physical standpoint.

The volume-weighted SUD scheme implemented in COMMIX-1B is an improvement over the extended Raithby SUD scheme. The volume-weighted SUD scheme needs no artificial cutoffs and therefore is less restrictive than the Raithby SUD scheme as far as undershoots and overshoots are concerned. Even though the volume-weighted SUD

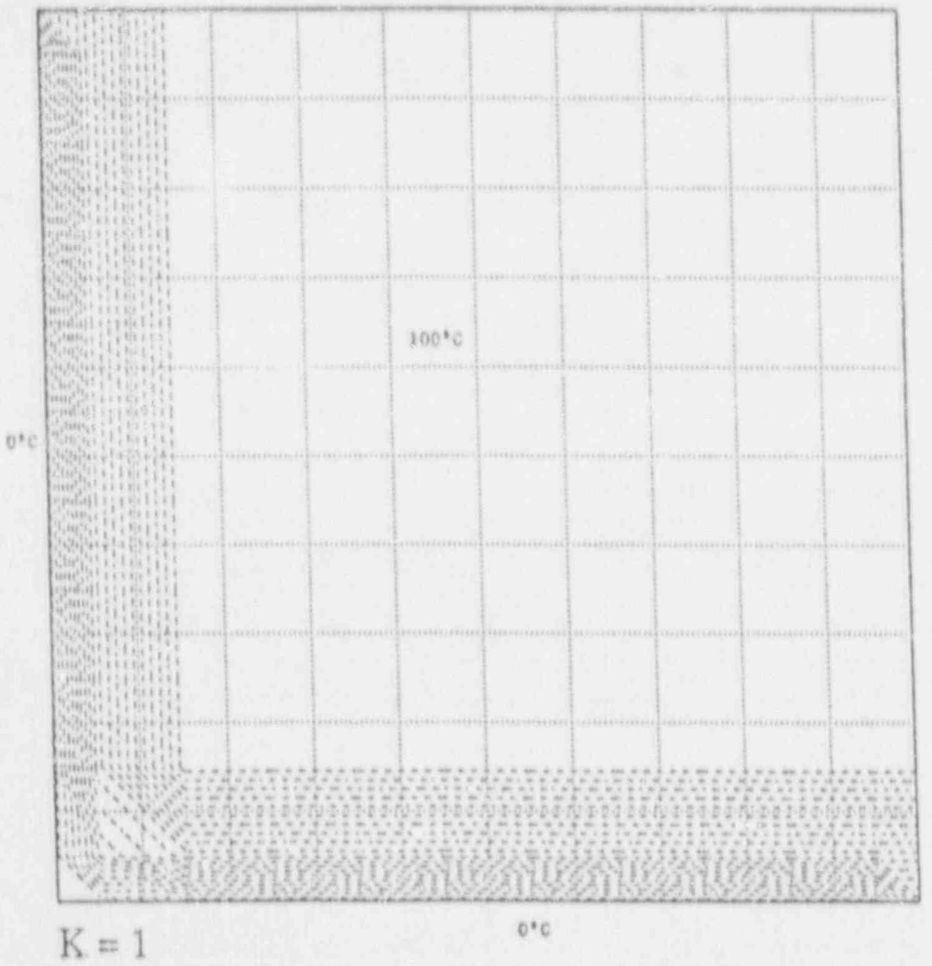

Fig. 21. Isotherms at lowest elevation (k = 1) of a three-dimensional flow with $n_x = m_y = m_z$ (exact solution)

scheme was able to reduce numerical diffusion and was successful in simulating steady-state thermal mixing problems with flow oblique to grid lines, stability (no undershoots and overshoots) cannot be guaranteed over the entire domain.

The three-dimensional mass-flow-weighted SUD scheme is an extension of the two-dimensional mass-flow-weighted SUD scheme. As described in Sec. 7.3.1, the two-dimensional mass-flow-weighted SUD scheme is able to reduce numerical diffusion and prevent overshoots and undershoots. The three-dimensional mass-flow-weighted SUD scheme proposed and implemented by Hassan[80] has been demonstrated to reduce numerical diffusion when the flow is oblique to grid lines. However, derivation of the discretized equations involves ad hoc assumptions in Hassan's mass-flow-weighted SUD scheme. Furthermore, closer examination of the discretized equations indicates that it is possible to have negative coefficients that may lead to undershoots and overshoots under certain conditions (for example, it can be demonstrated that if $m_y = 2\ m_x$, and $m_z = 3\ m_x$, the coefficient a_1 in Hassan's mass-flow-weighted SUD scheme becomes negative).

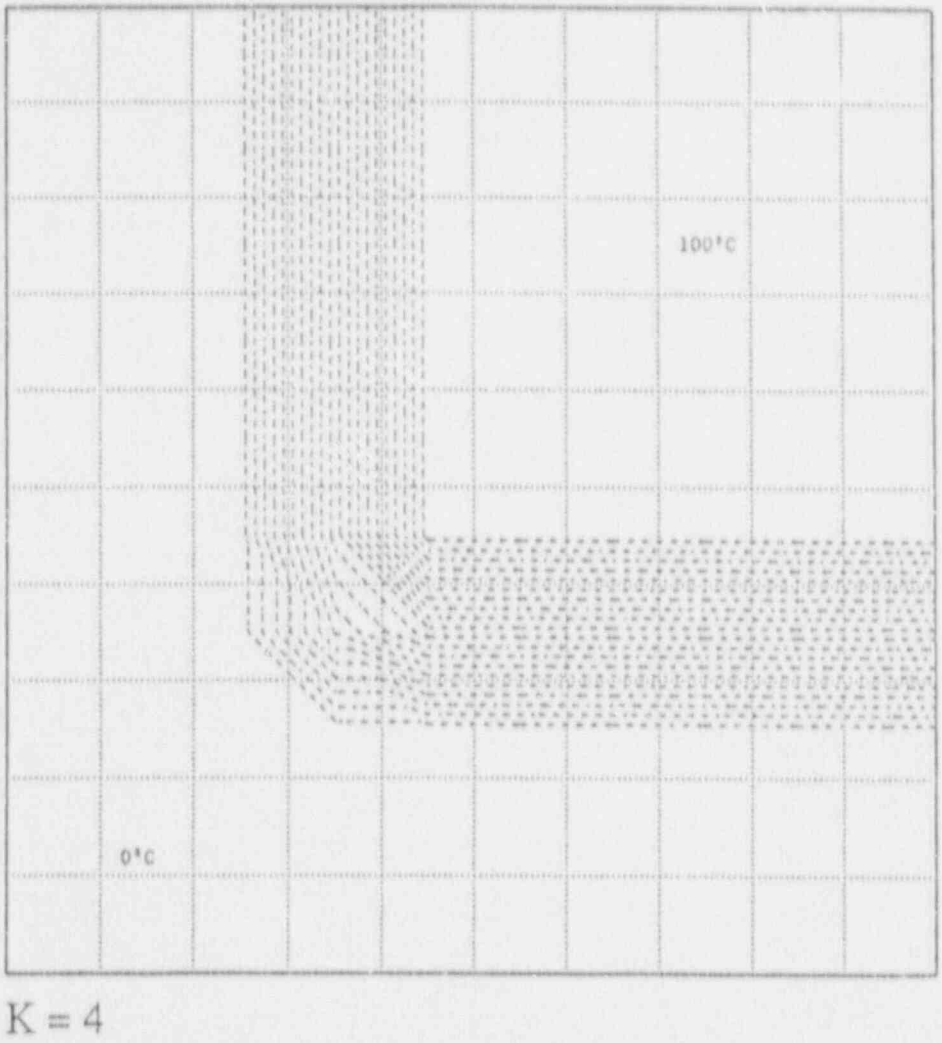

Fig. 22. Isotherms at higher elevation (k = 4) of a three-dimensional flow with $m_x = m_y = m_z$ (exact solution)

7.4 Flow-Modulated Skew-Upwind Discretization Scheme

The FMSUD scheme is implemented only in the energy equation of COMMIX-1C. Our objective is to develop a scheme that is relatively simple to implement, permits the use of coarser mesh for given accuracy, has acceptable numerical diffusion, and perhaps most important, prevents the occurrence of physically unrealistic results (undershoots and overshoots) in the entire computation domain. Our primary interest is the three-dimensional FMSUD scheme because COMMIX is a three-dimensional code. However, we will begin by describing the two-dimensional FMSUD scheme, which is relatively simple and easy to understand and sets the stage for the development of the three-dimensional FMSUD scheme. For relative simplicity, as in previous discussions, only arbitrary unidirectional situations will be considered and demonstrated. As mentioned before, the assumption of unidirectional flow will be removed as shown in Sec. 7.4.3.

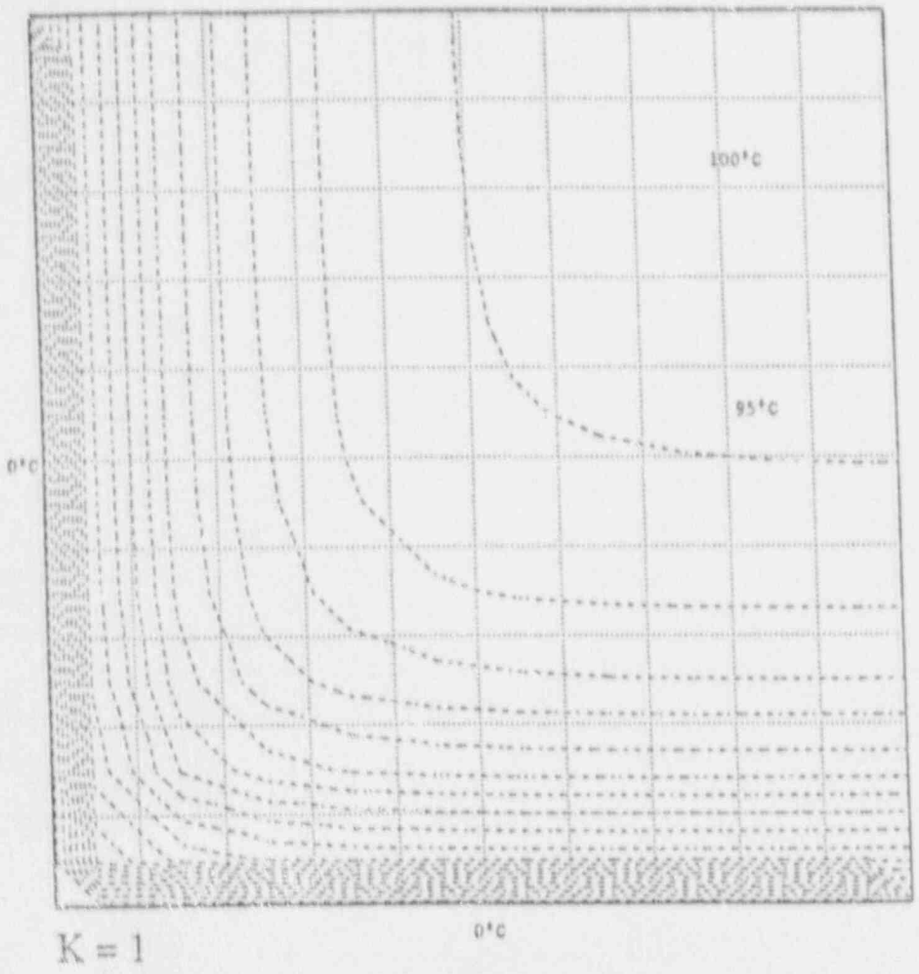

Fig. 23. Isotherms at lowest elevation (k = 1) of a three-dimensional flow with $m_x = m_y = m_z$ (upwind-difference)

Certain basic rules ensure that the discretization method is stable and does not produce physically unrealistic solutions such as undershoots and overshoots.[77] We shall briefly outline two of these rules that are of paramount importance and relevant to the development of the FMSUD scheme. As shown in Chapter 4, the general form of the discretized equation is

$$a_o \phi_o = \Sigma a_i \phi_i + b. \tag{7.8}$$

Since we are dealing with the energy equation only, the general variable ϕ can be replaced by the enthalpy h and Eq. 7.8 becomes

$$a_o h_o = \Sigma a_i h_i + b. \tag{7.9}$$

The two basic rules can simply be expressed as

1. $a_i \geq 0$ (7.10)

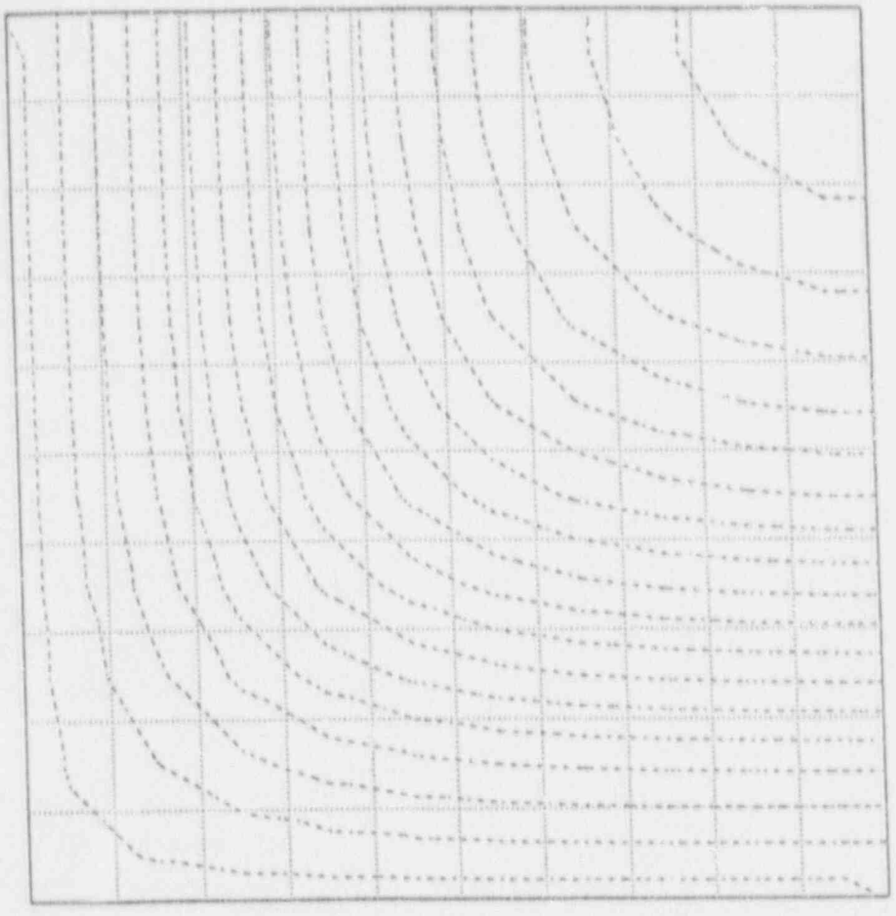

Fig. 24. Isotherms at higher elevation (k = 4) of a three-dimensional flow with $m_x = m_y = m_z$ (upwind-difference)

2. $a_0 = \Sigma\, a_i$ (7.11)

Rule 1 guarantees that all the coefficients in Eq. 7.9 are positive. This means that the influence of the neighboring points on a given grid point is positive, i.e.,

$$\frac{\partial h_0}{\partial h_i} \geq 0. \tag{7.12}$$

The requirement of positive coefficients is intended to eliminate the possibility of undershoots and overshoots that are physically unrealistic. Rule 2 is based on the consideration that the discretized equation should be able to accommodate the arbitrary change in scaling. More detailed discussions of these rules can be found in Ref. 77.

7.4.1 Two-Dimensional FMSUD Scheme

Consider the two-dimensional mesh system shown in Fig. 27. Remember that we are dealing with the energy equation so that only the cell-centered mesh must be

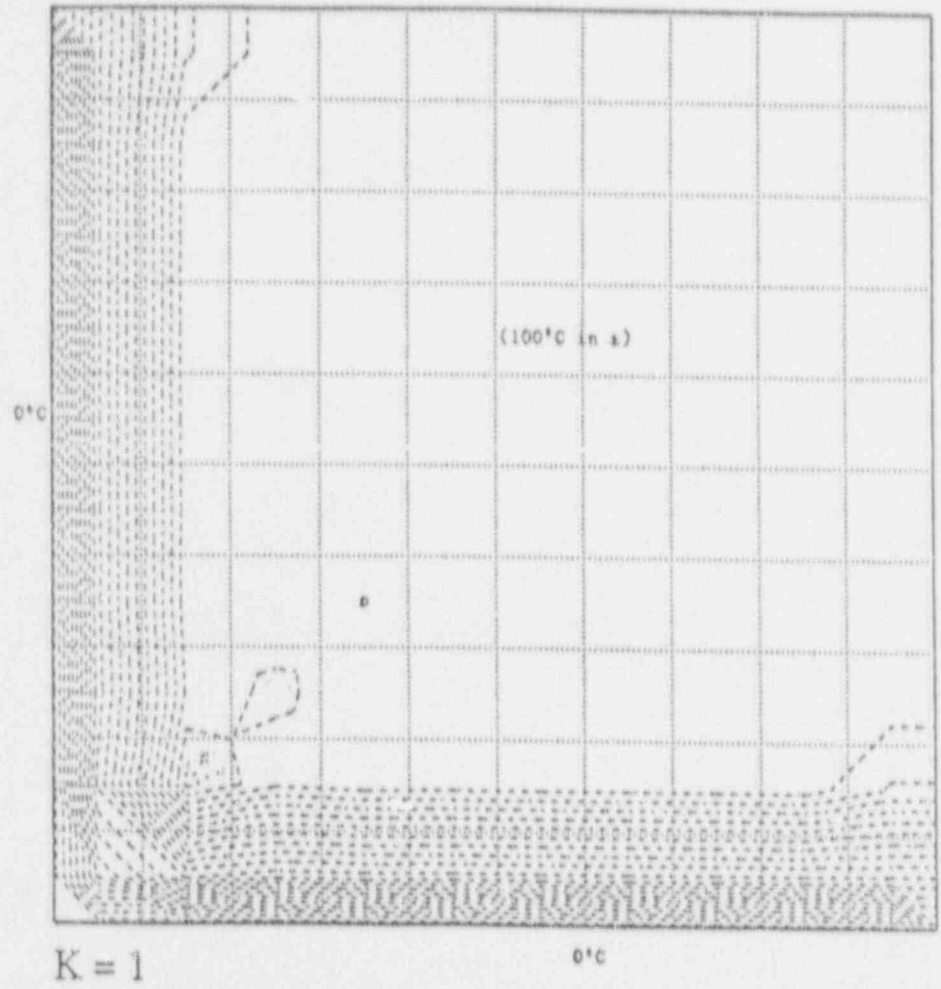

Fig. 25. Isotherms at lowest elevation (k = 1) of a three-dimensional flow with $m_x = m_y = m_z$ (extended Raithby skew-upwind difference)

considered (the main control volume referred to in Chapter 4). Since the flow is uniform everywhere, the mass flow rate in a given direction does not change and both m_x and m_y are positive. This is shown in Fig. 27, where m_x and m_y denote the mass flow rate in x and y direction, respectively. The center cell is denoted by the subscript o, while the neighboring cells due west, east, south, and north are denoted by the subscripts 1, 2, 3, and 4, respectively. The corner cells are represented by 13, 24, etc., as shown in Fig. 27. The enthalpy h at the four faces surrounding the center cell o is represented by the symbol < > at their corresponding locations. We express the cell facial quantities in terms of the cell center quantities by the following equations:

$$\langle h \rangle_1 = P_{xy}\, h_1 + S_{xy}\, h_{13} \tag{7.13a}$$

$$\langle h \rangle_2 = P_{xy}\, h_0 + S_{xy}\, h_3 \tag{7.13b}$$

$$\langle h \rangle_3 = P_{yx}\, h_3 + S_{yx}\, h_{13} \tag{7.13c}$$

$$\langle h \rangle_4 = P_{yx}\, h_0 + S_{yx}\, h_1 \,. \tag{7.13d}$$

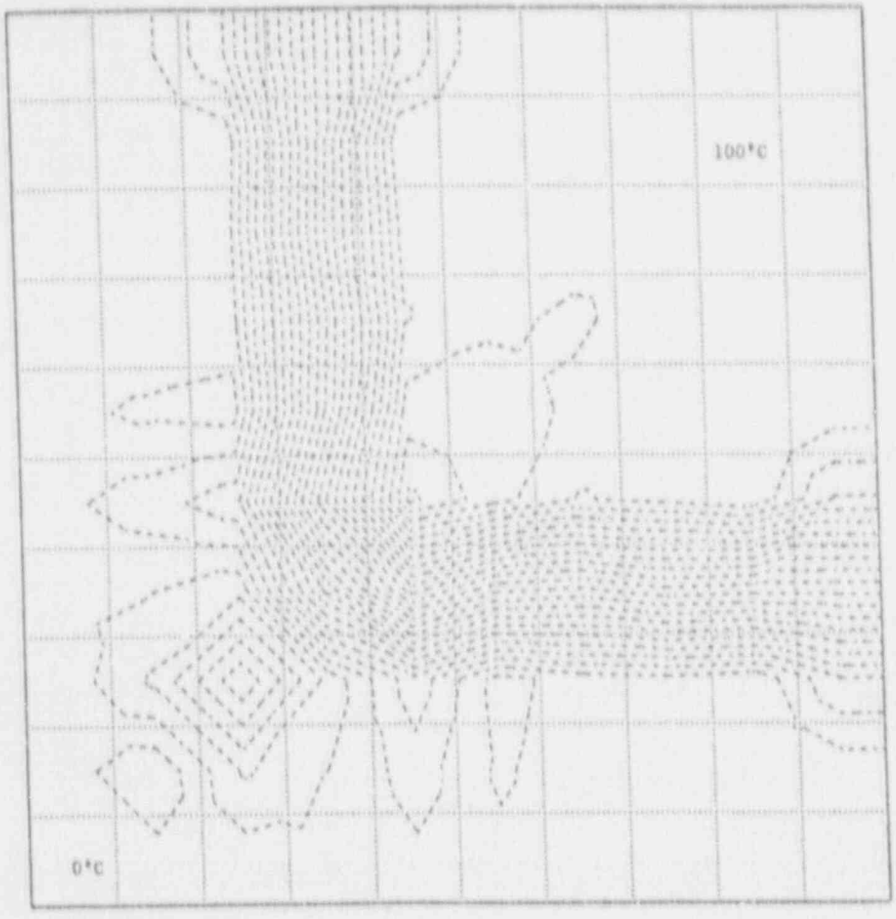

Fig. 26. Isotherms at higher elevation (k = 4) of a three-dimensional flow with $m_x = m_y = m_z$ (extended Raithby skew-upwind difference)

where P (primary) and S (side) are weighting factors and they are functions of the mass flow rates m_x and m_y.

$$P(m_x, m_y) = P_{xy} \qquad \text{(primary)}$$
$$S(m_x, m_y) = S_{xy} \qquad \text{(side)} \tag{7.14}$$

and

$$P_{xy} + S_{xy} = 1. \tag{7.15}$$

If $S_{xy} = 0$, then $P_{xy} = 1$, and Eq. 7.13a becomes

$$\langle h \rangle_1 = h_1 , \tag{7.16}$$

which is the result of the pure upwind difference. Thus, by adding S in Eq. 7.13, we have accounted for the two-dimensional effect. Similarly, the weighting factors P_{yx} and S_{yx} are related.

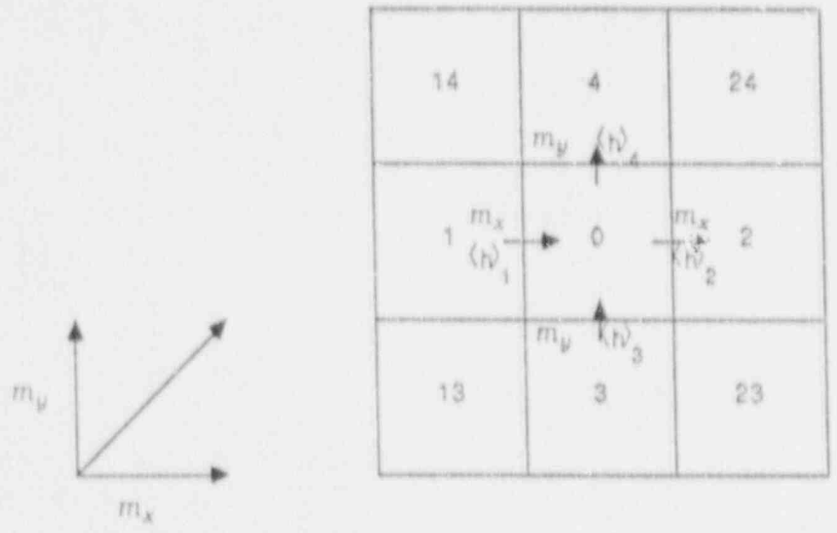

Fig. 27. Mesh system for two-dimensional unidirectional flow

$$P_{yx} + S_{yx} = 1. \tag{7.17}$$

All the weighting factors are greater or equal to zero. By assuming that the transported quantity is conserved, we obtain the following discretized equation for the facial quantities h,

$$m_x\langle h\rangle_2 - m_x\langle h\rangle_1 + m_y\langle h\rangle_4 - m_y\langle h\rangle_3 = 0\ . \tag{7.18}$$

Substituting Eq. 7.13 into Eq. 7.18, and rearranging according to the sparse matrix form expressed by Eq. 7.9 (b = 0 because there is no source term),

$$a_o\, h_o = \Sigma\, a_i h_i \tag{7.19}$$

where the coefficients are given by

$$a_0 = m_x + m_y - m_x\, S_{xy} - m_y\, S_{yx} \tag{7.20}$$

$$a_1 = m_x - m_x\, S_{xy} - m_y\, S_{yx} \tag{7.21}$$

$$a_3 = m_y - m_x\, S_{xy} - m_y\, S_{yx} \tag{7.22}$$

$$a_{13} = m_x\, S_{xy} + m_y\, S_{yx}. \tag{7.23}$$

It can be shown that Eqs. 7.20 to 7.23 satisfy the following relationship:

$$a_o = a_1 + a_3 + a_{13}, \tag{7.24}$$

which is required by rule 2. Substituting Eq. 7.23 into Eqs. 7.20 to 7.22, (eliminating the weighting factors) and recognizing Eq. 7.10,

$$a_o = m_x + m_y - a_{13} \geq 0 \tag{7.25}$$

$$a_1 = m_x - a_{13} \geq 0 \tag{7.26}$$

$$a_3 = m_y - a_{13} \geq 0\ . \tag{7.27}$$

The following condition must be met in order to satisfy Rule 1, i.e., all coefficients must be positive:

$$0 \leq a_{13} \leq \min\,(m_x,\, m_y), \tag{7.28}$$

where min (m_x, m_y) means the smaller of m_x and m_y. It is obvious that if $a_{13} = 0$, then Eqs. 7.26 to 7.27 reduce to

$$a_0 = a_1 + a_3 \tag{7.29}$$

$$a_1 = m_x \tag{7.30}$$

$$a_3 = m_y, \tag{7.31}$$

which are the results of the pure upwind difference. The coefficient a_{13} represents the contribution of the corner cell (Fig. 27) and is the key coefficient to be determined for the present FMSUD scheme. Equations 7.25–7.27 indicate that once a_{13} is determined, all the other coefficients in the discretized equation are determined also. Equation 7.28 provides the lower and upper bounds for the coefficient a_{13}. It is clear that a_{13} is not unique because it can have any value between the lower and upper bounds. We would like to stay away from the lower bound because it is the upwind difference scheme that is known to produce numerical diffusion when the flow is oblique to the grid lines. In the present FMSUD scheme, we assume that a_{13} is equal to the upper bound, i.e., the maximum allowable value without the possibility of obtaining physically unrealistic solutions (undershoots and overshoots). Thus,

$$a_{13} = \min (m_x, m_y) \tag{7.32}$$

Equations 7.23 and 7.32 can be combined to give

$$m_x S_{xy} + m_y S_{yx} = \min (m_x, m_y) \tag{7.33}$$

Equation 7.33 must be satisfied by S_{xy} and S_{yx} for any values of m_x and m_y. It can be shown that the following equations for S_{xy} and S_{yx} provide a solution to Eq. 7.33:

$$S_{xy} = \frac{1}{2}\min\left(1, m_y / m_x\right) \tag{7.34}$$

$$S_{yx} = \frac{1}{2}\min\left(1, m_x / m_y\right). \tag{7.35}$$

Substituting Eqs. 7.34 and 7.35 into the left side of Eq. 7.33,

$$\begin{aligned} & m_x \cdot \frac{1}{2}\min\left(1, m_x / m_y\right) + m_y \cdot \frac{1}{2}\min\left(1, m_x / m_y\right) \\ &= \frac{1}{2}\min\left(m_x, m_y\right) + \frac{1}{2}\min\left(m_x, m_y\right) \\ &= \min\left(m_x, m_y\right), \end{aligned}$$

which is identical to the right side of Eq. 7.33.

Once the weighting factors for the corner cells are determined, i.e., Eqs. 7.34 and 7.35, the weighting factors for the primary cells are calculated by using Eqs. 7.15 and 7.17,

$$P_{xy} = 1 - \frac{1}{2}\min\left(1, m_y / m_x\right) \tag{7.36}$$

$$P_{yx} = 1 - \frac{1}{2}\min\left(1, m_x / m_y\right). \tag{7.37}$$

The coefficients in the discretized equation can then be calculated in terms of these weighting factors.

It is interesting to note the differences among the Raithby,[76] Hassan,[79] and the present flow-modulated two-dimensional SUD schemes. The main difference is in the weighting factor S. The weighting factors employed by the three SUD schemes are

$$\text{Raithby SUD:}\quad S_{xy} = \min\left(1, \frac{1}{2}\frac{m_y}{m_x}\right)$$

$$\text{Hassan SUD:}\quad S_{xy} = \min\left(\frac{1}{2}, \frac{1}{2}\frac{m_y}{m_x}\right)$$

$$\text{FMSUD:}\quad S_{xy} = \frac{1}{2}\min\left(1, \frac{m_y}{m_x}\right).$$

If $m_x = m_y$ (flow is oblique at an angle of 45° to the grid lines), $S_{xy} = \frac{1}{2}$ for all three schemes. This is the reason why the Raithby SUD scheme was able to reproduce the result of the exact solution shown in Fig. 17. If $m_y = 2\,m_x$, then

$$\text{Raithby SUD:}\quad S_{xy} = 1$$

$$\text{Hassan SUD:}\quad S_{xy} = \tfrac{1}{2}$$

$$\text{FMSUD:}\quad S_{xy} = \tfrac{1}{2}.$$

The results of the Hassan SUD scheme and the present FMSUD scheme are the same, but the Raithby SUD scheme gives a weighting factor twice as large as that of the other two schemes. As explained previously, the present FMSUD scheme is based on the criterion of maximum contribution from the corner cell without the possibility of obtaining physically unrealistic solutions. The Raithby SUD scheme apparently violated this basic criterion and the result is shown in Fig. 19, where overshoots and undershoots occurred. The Hassan SUD (and the present FMSUD) scheme was able to eliminate those undershoots and overshoots, as shown in Fig. 20. However, as described earlier, Hassan's results were based on ad hoc assumptions and there was no explicit derivation for the weighting factors.

7.4.2 Three-Dimensional FMSUD Scheme

The three-dimensional FMSUD scheme is a straightforward extension of the two-dimension FMSUD scheme. However, the algebra becomes much more involved. The user need not be too concerned about the algebra as long as he or she understands the basic principle and limitations of the scheme.

Figure 28 shows the mesh system of a three-dimensional uniform flow inclined at an angle to the grid lines. We assume that all the mass flow components are either zero or positive,

$$m_x,\ m_y,\ m_z \geq 0$$

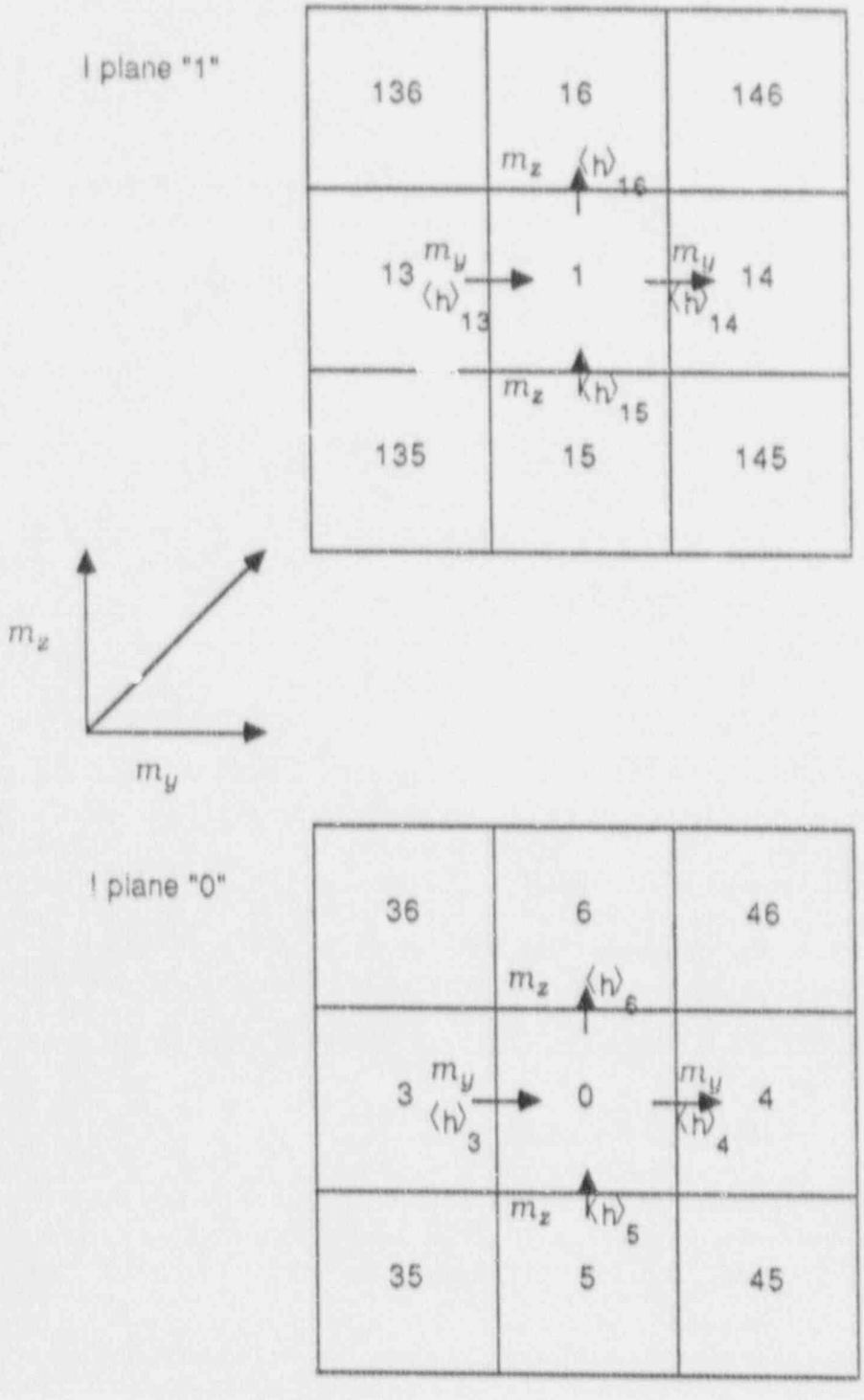

Fig. 28. Mesh system for three-dimensional unidirectional flow inclined at an angle to grid lines

The two mesh systems shown in Fig. 28 represent the plane view at two adjacent elevations. We first define the following weighting factors,

$$P\ (m_x, m_y, m_z) = P_{xyz} \qquad \text{(primary)}$$

$$S\ (m_x, m_y, m_z) = S_{xyz} \qquad \text{(side)}$$

$$C\ (m_x, m_y, m_z) = C_{xyz} \qquad \text{(corner)}$$

Here, the word *primary* means that the weighting factor P is associated with a cell identified by a single-digit number in Fig. 28. The side-weighting factor S is associated with a cell identified by a two-digit number, and the corner-weighting factor C is associated with a cell of three-digit number in Fig. 28. Next, we write down the facial quantities for the enthalpy as we did for the two-dimensional case, and remembering that we now have six faces surrounding a center point:

$$\begin{aligned}
\langle h\rangle_1 &= P_{xyz}\, h_1 + S_{xyz}\, h_{13} + S_{xzy}\, h_{15} + C_{xyz}\, h_{135} \\
\langle h\rangle_2 &= P_{xyz}\, h_0 + S_{xyz}\, h_3 + S_{xzy}\, h_5 + C_{xyz}\, h_{35} \\
\langle h\rangle_3 &= P_{yzx}\, h_3 + S_{yxz}\, h_{13} + S_{yzx}\, h_{35} + C_{yzx}\, h_{135} \\
\langle h\rangle_4 &= P_{yzx}\, h_5 + S_{yxz}\, h_1 + S_{yzx}\, h_5 + C_{yzx}\, h_{15} \\
\langle h\rangle_5 &= P_{zxy}\, h_5 + S_{zxy}\, h_{15} + S_{zyx}\, h_{35} + C_{zxy}\, h_{135} \\
\langle h\rangle_6 &= P_{zxy}\, h_0 + S_{zxy}\, h_1 + S_{zyx}\, h_3 + C_{zxy}\, h_{13}\ .
\end{aligned} \tag{7.38}$$

The weighting factors are related by the following equations:

$$\begin{aligned}
P_{xyz} + S_{xyz} + S_{xzy} + C_{xyz} &= 1 \\
P_{yzx} + S_{yxz} + S_{yzx} + C_{yzx} &= 1 \\
P_{zxy} + S_{zxy} + S_{zyx} + C_{zxy} &= 1.
\end{aligned} \tag{7.39}$$

The discretized steady-state convective transport equation can be written as

$$\begin{aligned}
m_x \langle h\rangle_2 - m_x \langle h\rangle_1 + m_y \langle h\rangle_4 - m_y \langle h\rangle_3 + m_z \langle h\rangle_6 \\
- m_z \langle h\rangle_5 = 0.
\end{aligned} \tag{7.40}$$

Substituting Eqs. 7.38 and 7.39 into Eq. 7.40, rearranging according to the sparse matrix form,

$$a_0\, h_0 = \Sigma\, a_i h_i\ , \tag{7.41}$$

and the coefficients turn out to be as follows:

$$\begin{aligned}
a_0 = {} & m_x - m_x S_{xyz} - m_x S_{xzy} - m_x C_{xyz} \\
& + m_y - m_y S_{yxz} - m_y S_{yzx} - m_y C_{yzx} \\
& + m_z - m_z S_{zxy} - m_z S_{zyx} - m_z C_z
\end{aligned} \tag{7.42}$$

$$a_1 = m_x - m_x S_{xyz} - m_x S_{xzy} - m_x C_{xyz} \quad m_y S_{yxz} - m_z S_{zxy} \tag{7.43}$$

$$a_3 = m_y - m_y S_{yxz} - m_y S_{yzx} - m_y C_{yzx} - m_x S_{xyz} - m_z S_{zyx} \tag{7.44}$$

$$a_5 = m_z - m_z S_{zxy} - m_z S_{zyx} - m_z C_{zxy} - m_x S_{xzy} - m_y S_{yzx} \tag{7.45}$$

$$a_{13} = m_x S_{xyz} + m_y S_{yxz} - m_z C_{zxy} \tag{7.46}$$

$$a_{15} = m_x S_{xzy} + m_z S_{zxy} - m_y C_{yzx} \tag{7.47}$$

$$a_{35} = m_y S_{yzx} + m_z S_{zyx} - m_x C_{xyz} \tag{7.48}$$

$$a_{135} = m_x C_{xyz} + m_y C_{yzx} + m_z C_{zxy}. \tag{7.49}$$

There are a total of eight coefficients for the three-dimensional flow, as compared to a total of four coefficients for the two-dimensional flow. Eliminating the weighting factors in Eqs. 7.42-7.45 by utilizing Eqs. 7.46-7.49, we obtain the following equations that express the primary coefficients (coefficients with a single-digit number) in terms of the side coefficients (coefficients with a double-digit number), and the corner coefficients (coefficients with a triple-digit number):

$$a_0 = m_x + m_y + m_z - a_{13} - a_{15} - a_{35} - 2a_{135} \geq 0 \tag{7.50}$$

$$a_1 = m_x - a_{13} - a_{15} - a_{135} \geq 0 \tag{7.51}$$

$$a_3 = m_y - a_{13} - a_{35} - a_{135} \geq 0 \tag{7.52}$$

$$a_5 = m_z - a_{15} - a_{35} - a_{135} \geq 0 \tag{7.53}$$

and recalling Rule 1 that all the coefficients must be greater than or equal to zero. After closer examination of Eqs. 7.50-7.53, the upper and lower limits can be established for the following coefficients:

$$0 \leq a_{135} \leq \min (m_x, m_y, m_z) \tag{7.54a}$$

$$0 \leq a_{13} \leq \min (m_x, m_y) - a_{135} \tag{7.54b}$$

$$0 \leq a_{15} \leq \min (m_x, m_z) - a_{135} \tag{7.54c}$$

$$0 \leq a_{35} \leq \min (m_y, m_z) - a_{135}. \tag{7.54d}$$

The coefficients given by Eq. 7.54 are not unique. This should not present any problem since most discretized equations are not unique in the first place. We choose to maximize the influence of the corner and side cells. Thus, by adopting the upper limits in Eq. 7.54, we obtain

$$a_{135} = \min (m_x, m_y, m_z) \tag{7.55}$$

$$\begin{aligned} a_{13} &= \min (m_x, m_y) - \min (m_x, m_y, m_z) \\ &= \max [0, \min (m_x, m_y) - m_z] \end{aligned} \tag{7.56}$$

$$\begin{aligned} a_{15} &= \min (m_x, m_z) - \min (m_x, m_y, m_z) \\ &= \max [0, \min (m_x, m_z) - m_y] \end{aligned} \tag{7.57}$$

$$\begin{aligned} a_{35} &= \min (m_y, m_z) - \min (m_x, m_y, m_z) \\ &= \max [0, \min (m_y, m_z) - m_x]. \end{aligned} \tag{7.58}$$

Comparing Eq. 7.55 to Eq. 7.49 gives

$$m_x C_{xyz} + m_y C_{yxz} + m_z C_{zxy} = \min (m_x, m_y, m_z). \tag{7.59}$$

Similarly, by comparing Eqs. 7.46-7.48 to Eqs. 7.56-7.58, we obtain

$$\begin{aligned} m_x S_{xyz} + m_y S_{yxz} - m_z C_{zxy} &= \min (m_x, m_y) - \min (m_x, m_y, m_z) \\ &= \max [0, \min (m_x, m_y) - m_z] \end{aligned} \tag{7.60}$$

$$m_x S_{xzy} + m_z S_{zxy} - m_y C_{yzx} = \min(m_x, m_z) - \min(m_x, m_y, m_z)$$
$$= \max[0, \min(m_x, m_z) - m_y] \quad (7.61)$$

$$m_y S_{yzx} + m_z S_{zyx} - m_x C_{xyz} = \min(m_y, m_z) - \min(m_x, m_y, m_z)$$
$$= \max[0, \min(m_y, m_z) - m_x] . \quad (7.62)$$

Equations 7.59-7.62 must be satisfied by the weighting factors C and S for arbitrary m_x, m_y, and m_z. It can be shown that the following expressions for C and S satisfy Eqs. 7.59 -7.62:

$$C_{xyz} = C(m_x, m_y, m_z) = \frac{1}{3}\min\left(1, \frac{m_y}{m_x}, \frac{m_z}{m_x}\right) \quad (7.63)$$

$$C_{yzx} = \frac{1}{3}\min\left(1, \frac{m_z}{m_y}, \frac{m_x}{m_y}\right) \quad (7.64)$$

$$C_{zxy} = \frac{1}{3}\min\left(1, \frac{m_x}{m_z}, \frac{m_y}{m_z}\right) \quad (7.65)$$

$$S_{xyz} = S(m_x, m_y, m_z) = \frac{1}{2}\left\{\max\left[0, \min\left(1, \frac{m_y}{m_x}\right) - \frac{m_z}{m_x}\right] + \frac{1}{3}\min\left(1, \frac{m_y}{m_x}, \frac{m_z}{m_x}\right)\right\} \quad (7.66)$$

$$S_{xzy} = S(m_x, m_z, m_y) = \frac{1}{2}\left\{\max\left[0, \min\left(1, \frac{m_z}{m_x}\right) - \frac{m_y}{m_x}\right] + \frac{1}{3}\min\left(1, \frac{m_y}{m_x}, \frac{m_z}{m_x}\right)\right\} \quad (7.67)$$

$$S_{yxz} = \frac{1}{2}\left\{\max\left[0, \min\left(1, \frac{m_x}{m_y}\right) - \frac{m_z}{m_y}\right] + \frac{1}{3}\min\left(1, \frac{m_z}{m_y}, \frac{m_x}{m_y}\right)\right\} \quad (7.68)$$

$$S_{zxy} = \frac{1}{2}\left\{\max\left[0, \min\left(1, \frac{m_x}{m_z}\right) - \frac{m_y}{m_z}\right] + \frac{1}{3}\min\left(1, \frac{m_x}{m_z}, \frac{m_y}{m_z}\right)\right\} \quad (7.69)$$

$$S_{yzx} = \frac{1}{2}\left\{\max\left[0, \min\left(1, \frac{m_z}{m_y}\right) - \frac{m_x}{m_y}\right] + \frac{1}{3}\min\left(1, \frac{m_z}{m_y}, \frac{m_x}{m_y}\right)\right\} \quad (7.70)$$

$$S_{zyx} = \frac{1}{2}\left\{\max\left[0, \min\left(1, \frac{m_y}{m_z}\right) - \frac{m_x}{m_z}\right] + \frac{1}{3}\min\left(1, \frac{m_y}{m_z}, \frac{m_x}{m_z}\right)\right\} . \quad (7.71)$$

It is straightforward to demonstrate that the weighting factors C and S satisfy Eqs. 7.59-7.62. For example, the left side of Eq. 7.62 can be reduced to

$$m_y S_{yzx} + m_z S_{zyx} - m_x C_{xyz}$$
$$= \frac{1}{2}\left\{\max\left[0, \min(m_y, m_z) - m_x\right] + \frac{1}{3}\min(m_x, m_y, m_z)\right\}$$
$$+ \frac{1}{2}\left\{\max\left[0, \min(m_z, m_y) - m_x\right] + \frac{1}{3}\min(m_x, m_y, m_z)\right\}$$
$$- \frac{1}{3}\min(m_x, m_y, m_z)$$

$$= \max\left[0, \min(m_y, m_z) - m_x\right],$$

which is identical to the right side of Eq. 7.62.

Once the weighting factors S and C are determined, all the coefficients in the discretized transport equation can be calculated according to Eqs. 7.42–7.49.

The results of three-dimensional flow can be reduced to that of the two-dimensional flow by setting $m_z = 0$ in all equations derived in this section. If $m_z = 0$, then

$$C_{xyz} = 0,$$

$$S_{xyz} = \frac{1}{2}\min\left(1, \frac{m_y}{m_x}\right)$$

$$a_{135} = 0,$$

$$a_{13} = \min(m_x, m_y),$$

$$a_{15} = 0,$$

$$a_{35} = 0,$$

$$a_0 = m_x + m_y - a_{13},$$

$$a_1 = m_x - a_{13},$$

$$a_3 = m_y - a_{13},$$

$$a_5 = 0,$$

These results are identical to those presented in Section 7.4.1 for the two-dimensional flow.

7.4.3 Generalization of the Formulation of the FMSUD Scheme for All Flow Conditions

General Expression of the Coefficients Coupling a Cell with Its 26 Neighboring Cells

The FMSUD methodology can be generalized to treat all flow conditions as follows.

Let us introduce first the definition of Heaviside's function as

$$H(a) = \begin{cases} 1, \text{ if } a > 0 \\ 0, \text{ if } a \le 0 \end{cases} \tag{7.72}$$

for every real number a. Hence,

$$H(-a) = 1 - H(a). \tag{7.73}$$

We consider the enthalpy value $\langle h \rangle_{i-1/2,j,k}$ at the boundary surface between cell 0, around node (i, j, k), and cell 1 around node (i–1, j, k), as shown in Fig. 29. $CX1_\ell$, $SX1_\ell$, and PX1 are coefficients that are products of the weighting factor f and Heaviside function (flow direction). If $u_{i-1/2,j,k} > 0$, the $\langle h \rangle_1$ depends on the enthalpy values of the cells at left; if $u_{i-1/2,j,k} < 0$, the $\langle h \rangle_1$ depends on the enthalpy values of the cells at right.

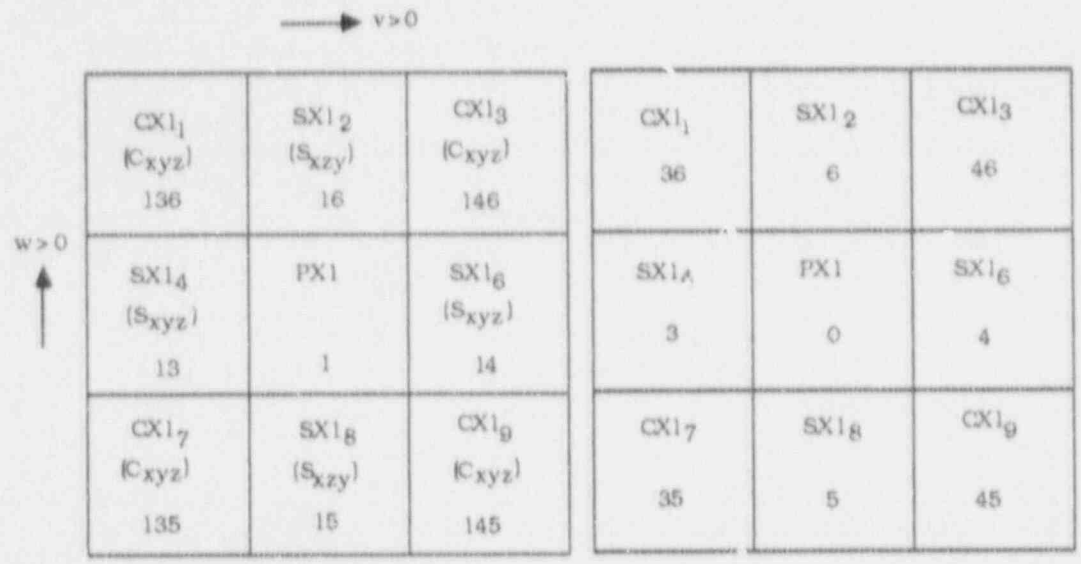

Fig. 29. Cells influencing enthalpy $\langle h \rangle_1$ if $u_{i-1/2,j,k} > 0$ (left) and if $u_{i-1/2,j,k} < 0$ (right). Notation in parentheses corresponds to that of Sec. 7.4.2

In the case of $u_{i-1/2,j,k} > 0$: of the nine cells of the left block, only a maximum of four contribute to $\langle h \rangle_1$. They depend on the sign of $w_1 = w_{i-1/2,j,k}$ and $v_1 = v_{i-1/2,j,k}$ according to the following scheme:

1. If $v_1 > 0$, $w_1 > 0$: cells 13, 1, 135, 15 (quadrant bottom left)
2. If $v_1 < 0$, $w_1 > 0$: cells 14, 1, 145, 15 (quadrant bottom right)
3. If $v_1 > 0$, $w_1 < 0$: cells 136, 1, 13, 16 (quadrant top left)
4. If $v_1 < 0$, $w_1 < 0$: cells 16, 146, 14, 1 (quadrant top right).

For all cases corresponding to $u_1 > 0$, we can write:

$$\begin{aligned}\langle h \rangle_1 = h_{i-1/2,j,k} = {} & CX1_1\, h_{136} + SX1_2\, h_{16} + CX1_3\, h_{146} \\ & + SX1_4\, h_{13} + PX1\, h_1 + SX1_6\, h_{14} \\ & + CX1_7\, h_{135} + SX1_8\, h_{15} + CX1_9\, h_{145} \,. \end{aligned} \tag{7.74}$$

The values of coefficients associated with Eq. 7.74 are as follows:

	$w_1 > 0$ $v_1 > 0$	$w_1 > 0$ $v_1 < 0$	$w_1 < 0$ $v_1 > 0$	$w_1 < 0$ $v_1 < 0$
$CX1_1 = f1\ H(-w)\ H(v)$	0	0	f1	0
$SX1_2 = f2\ H(-w)$	0	0	f2	f2
$CX1_3 = f3\ H(-w)\ H(-v)$	0	0	0	f3
$SX1_4 = f4\ H(v)$	f4	0	f4	0
$PX1 = f5$	f5	f5	f5	f5
$SX1_6 = f6\ H(-v)$	0	f6	0	f6
$CX1_7 = f7\ H(w)\ H(v)$	f7	0	0	0

$SX1_8 = f8\ H(w)$	f8	f8	0	0	
$CX1_9 = f9\ H(w)\ H(-v)$	0	f9	0	0	(7.75)

where both velocities w and v are computed at location (i-1/2,j,k). f_ℓ, $\ell = 1,2,...9$ are weighting factors satisfy the condition

$$\sum_{1}^{9} {}_{\ell} f_\ell = 1 . \tag{7.76}$$

The values of the weighting factor f_ℓ, ($\ell = 1,2,...9$) can be calculated as shown in Sec. 7.4.2. Expressions similar to Eq. 7.75 hold for the coefficients $CX2_\ell$, $SX2_\ell$, and PX2.

Similarly, for $u_1 < 0$, one has

$$\begin{aligned} \langle h \rangle_1 = h_{i-1/2,j,k} = {} & CX1_1\ h_{36} + SX1_2\ h_6 + CX1_3\ h_{46} \\ & + SX1_4\ h_3 + PX1\ h_0 + SX1_6\ h_4 \\ & + CX1_7\ h_{35} + SX1_8\ h_5 + CX1_9\ h_{45} . \end{aligned} \tag{7.77}$$

Equations 7.74 and 7.77 can be combined in a single formula that holds for both $u_1 > 0$ and $u_1 < 0$:

$$\begin{aligned} \langle h \rangle_1 = h_{i-1/2,j,k} = {} & [0,u_1]\ (CX1_1 \bullet h_{136} + SX1_2 \bullet h_{16} + CX1_3 \bullet h_{146} \\ & + SX1_4 \bullet h_{13} + PX1 \bullet h_1 + SX1_6 \bullet h_{14} \\ & + CX1_7 \bullet h_{135} + SX1_8 \bullet h_{15} + CX1_9 \bullet h_{145}) \\ & -[0,-u_1]\ (CX1_1 \bullet h_{36} + SX1_2 \bullet h_6 + CX1_3 \bullet h_{46} \\ & + SX1_4 \bullet h_3 + PX1 \bullet h_0 + SX1_6 \bullet h_4 \\ & + CX1_7 \bullet h_{35} + SX1_8 \bullet h_5 + CX1_9 \bullet h_{45}). \end{aligned} \tag{7.78}$$

For the enthalpy on the opposite face, it holds

$$\begin{aligned} \langle h \rangle_2 = h_{i+1/2,j,k} = {} & [0,u_2]\ (CX2_1 \bullet h_{36} + SX2_2 \bullet h_6 + CX2_3 \bullet h_{46} \\ & + SX2_4 \bullet h_3 + PX2 \bullet h_0 + SX2_6 \bullet h_4 \\ & + CX2_7 \bullet h_{35} + SX2_8 \bullet h_5 + CX2_9 \bullet h_{45}) \\ & -[0,-u_2]\ (CX2_1 \bullet h_{236} + SX2_2 \bullet h_{26} + CX2_3 \bullet h_{246} \\ & + SX2_4 \bullet h_{23} + PX2 \bullet h_2 + SX2_6 \bullet h_{24} \\ & + CX2_7 \bullet h_{235} + SX2_8 \bullet h_{25} + CX2_9 \bullet h_{245}). \end{aligned} \tag{7.79}$$

Similarly, $\langle h \rangle_3$ and $\langle h \rangle_4$ can be expressed as follows:

$$\begin{aligned} \langle h \rangle_3 = h_{i,j-1/2,k} = {} & [0,v_3]\ (CY3_1 \bullet h_{136} + SY3_2 \bullet h_{36} + CY3_3 \bullet h_{236} \\ & + SY3_4 \bullet h_{13} + PY3 \bullet h_3 + SY3_6 \bullet h_{23} \\ & + CY3_7 \bullet h_{135} + SY3_8 \bullet h_{35} + CY3_9 \bullet h_{235}) \\ & -[0,-v_3]\ (CY3_1 \bullet h_{16} + SY3_2 \bullet h_6 + CY3_3 \bullet h_{26} \\ & + SY3_4 \bullet h_1 + PY3 \bullet h_0 + SY3_6 \bullet h_2 \\ & + CY3_7 \bullet h_{15} + SY3_8 \bullet h_5 + CY3_9 \bullet h_{25}). \end{aligned} \tag{7.80}$$

$$\begin{aligned}
\langle h\rangle_4 = h_{i,j+1/2,k} = {} & [0,v_4]\ (CY4_1 \cdot h_{16} + SY4_2 \cdot h_6 + CY4_3 \cdot h_{26} \\
& + SY4_4 \cdot h_1 + PY4 \cdot h_0 + SY4_6 \cdot h_2 \\
& + CY4_7 \cdot h_{15} + SY4_8 \cdot h_5 + CY4_9 \cdot h_{25}) \\
& -[0,-v_4]\ (CY4_1 \cdot h_{146} + SY4_2 \cdot h_{46} + CY4_3 \cdot h_{246} \\
& + SY4_4 \cdot h_{14} + PY4 \cdot h_4 + SY4_6 \cdot h_{24} \\
& + CY4_7 \cdot h_{145} + SY4_8 \cdot h_{45} + CY4_9 \cdot h_{245}). \qquad (7.81)
\end{aligned}$$

The values of the coefficients are given by

	$w_3 > 0$ $u_3 > 0$	$w_3 > 0$ $u_3 < 0$	$w_3 < 0$ $u_3 > 0$	$w_3 < 0$ $u_3 < 0$
$CY3_1$ = f1 H(-w) H(u)	0	0	f1	0
$SY3_2$ = f2 H(-w)	0	0	f1	f2
$CY3_3$ = f3 H(-w) H(-u)	0	0	0	f3
$SY3_4$ = f4 H(u)	f4	0	f4	0
PY3 = f5	f5	f5	f5	f5
$SY3_6$ = f6 H(-u)	0	f6	0	f6
$CY3_7$ = f7 H(w) H(u)	f7	0	0	0
$SY3_8$ = f8 H(w)	f8	f8	0	0
$CY3_9$ = f9 H(w) H(-u)	0	f9	0	0

(7.82)

Similar expressions hold for the coefficients $CY4_\ell$, $SY4_\ell$, and PY4.

Finally, $\langle h\rangle_5$ and $\langle h\rangle_6$ are expressed as follows:

$$\begin{aligned}
\langle h\rangle_5 = h_{i,j,k-1/2} = {} & [0,w_5]\ (CZ5_1 \cdot h_{145} + SZ5_2 \cdot h_{45} + CZ5_3 \cdot h_{245} \\
& + SZ5_4 \cdot h_{15} + PZ5 \cdot h_5 + SZ5_6 \cdot h_{25} \\
& + CZ5_7 \cdot h_{135} + SZ5_8 \cdot h_{35} + CZ5_9 \cdot h_{235}) \\
& -[0,-w_5]\ (CZ5_1 \cdot h_{14} + SZ5_2 \cdot h_4 + CZ5_3 \cdot h_{24} \\
& + SZ5_4 \cdot h_1 + PZ5 \cdot h_0 + SZ5_6 \cdot h_2 \\
& + CZ5_7 \cdot h_{13} + SZ5_8 \cdot h_3 + CZ5_9 \cdot h_{23}). \qquad (7.83)
\end{aligned}$$

$$\begin{aligned}
\langle h\rangle_6 = h_{i,j,k+1/2} = {} & [0,w_6]\ (CZ6_1 \cdot h_{14} + SZ6_2 \cdot h_4 + CZ6_3 \cdot h_{24} \\
& + SZ6_4 \cdot h_1 + PZ6 \cdot h_0 + SZ6_6 \cdot h_2 \\
& + CZ6_7 \cdot h_{13} + SZ6_8 \cdot h_3 + CZ6_9 \cdot h_{23}) \\
& -[0,-w_6]\ (CZ6_1 \cdot h_{146} + SZ6_2 \cdot h_{46} + CZ6_3 \cdot h_{246} \\
& + SZ6_4 \cdot h_{16} + PZ6 \cdot h_6 + SZ6_6 \cdot h_{26} \\
& + CZ6_7 \cdot h_{136} + SZ6_8 \cdot h_{36} + CZ6_9 \cdot h_{236}). \qquad (7.84)
\end{aligned}$$

The values of the coefficients are given by

	$v_5 > 0$ $u_6 > 0$	$v_5 > 0$ $u_5 < 0$	$v_5 < 0$ $u_5 > 0$	$v_5 < 0$ $u_5 < 0$
$CZ5_1$ = f1 H(-v) H(u)	0	0	f1	0
$SZ5_2$ = f2 H(-v)	0	0	f2	f2
$CZ5_3$ = f3 H(-v) H(-u)	0	0	0	f3

$SZ5_4$ = f4 H(u)	f4	0	f4	0	
PZ5 = f5	f5	f5	f5	f5	
$SZ5_6$ = f6 H(-u)	0	f6	0	f6	
$CZ5_7$ = f7 H(v) H(u)	f7	0	0	0	
$SZ5_8$ = f8 H(v)	f8	f8	0	0	
$CZ5_9$ = f9 H(v) H(-u)	0	f9	0	0	(7.85)

Similar expressions hold for the coefficients $CZ6_\ell$, $SZ6_\ell$, and PZ6.

Let us now introduce the following symbols (which generalize the notation of the previous section) to account for the flow rate through the six faces of a computational cell:

$$m_{x1} = (\rho u A)_{i-1/2,j,k}$$
$$m_{x2} = (\rho u A)_{i+1/2,j,k}$$
$$m_{y3} = (\rho v A)_{i,j-1/2,k}$$
$$m_{y4} = (\rho v A)_{i,j+1/2,k}$$
$$m_{z5} = (\rho w A)_{i,j,k-1/2}$$
$$m_{z6} = (\rho w A)_{i,j,k+1/2} \qquad (7.86)$$

The finite-volume discretization of the convective term of the energy equation yields:

$$m_{x2}{}^{+} < h >_2 - m_{x1}{}^{+} < h >_1 + m_{y4}{}^{+} < h >_4$$
$$- m_{y3}{}^{+} < h >_3 + m_{z6}{}^{+} < h >_6 - m_{z5}{}^{+} < h >_5 . \qquad (7.87)$$

Substituting the expressions of $<h>_\ell$, where $\ell = 1,2,\ldots 6$ into Eq. 7.87 gives

$$a_0 h_0 + \sum_{j=1}^{26} (-a_j) h_j , \qquad (7.88)$$

where the central coefficient a_0 and the 26 coefficients a_j of the neighboring cells are given by

$$a_0 = |0, m_{x2}| PX2 + |0, -m_{x1}| PX1 + |0, m_{y4}| PY4$$
$$+ |0, -m_{y3}| PY3 + |0, m_{z6}| PZ6 + |0, -m_{z5}| PZ5 \qquad (7.89/1)$$

$$a_1 = |0, m_{x1}| PX1 - |0, m_{y4}| SY4_4 - |0, -m_{y3}| SY3_4$$
$$- |0, m_{z6}| SZ6_4 - |0, -m_{z5}| SZ5_4 \qquad (7.89/2)$$

$$a_2 = |0, -m_{x2}| PX2 - |0, m_{y4}| SY4_6 - |0, -m_{y3}| SY3_6$$
$$- |0, m_{z6}| SZ6_6 - |0, -m_{z5}| SZ5_6 \qquad (7.89/3)$$

$$a_3 = -|0, m_{x2}| SX2_4 - |0, -m_{x1}| SX1_4 + |0, m_{y3}| PY3$$
$$- |0, m_{z6}| SZ6_8 - |0, -m_{z5}| CZ5_7 \qquad (7.89/4)$$

$$a_4 = -|0, m_{x2}|\ SX2_6 - |0, -m_{x1}|\ SX1_6 + |0, -m_{y4}|\ PY4 - |0, m_{z6}|\ SZ6_2 - |0, -m_{z5}|\ SZ5_2 \quad (7.89/5)$$

$$a_5 = -|0, m_{x2}|\ SX2_8 - |0, -m_{x1}|\ SX1_8 - |0, m_{y4}|\ SY4_8 - |0, -m_{y3}|\ SY3_8 + |0, m_{z5}|\ PZ5 \quad (7.89/6)$$

$$a_6 = -|0, m_{x2}|\ SX2_2 - |0, -m_{x1}|\ SX1_2 - |0, m_{y4}|\ SY4_2 - |0, -m_{y3}|\ SY3_2 + |0, -m_{z6}|\ PZ6 \quad (7.89/7)$$

$$a_{13} = |0, m_{x1}|\ SX1_4 + |0, m_{y3}|\ SY3_4 - |0, m_{z6}|\ CZ6_7 - |0, -m_{z5}|\ CZ5_7 \quad (7.89/8)$$

$$a_{35} = -|0, m_{x2}|\ CX2_7 - |0, -m_{x1}|\ CX1_7 + |0, m_{y3}|\ SY3_8 + |0, m_{z5}|\ SZ5_8 \quad (7.89/9)$$

$$a_{36} = -|0, m_{x2}|\ CX2_1 - |0, -m_{x1}|\ CX1_1 + |0, m_{y3}|\ SY3_2 + |0, -m_{z6}|\ SZ6_8 \quad (7.89/10)$$

$$a_{24} = |0, -m_{x2}|\ SX2_6 + |0, -m_{y4}|\ SY4_6 - |0, m_{z6}|\ CZ6_3 - |0, -m_{z5}|\ CZ5_3 \quad (7.89/11)$$

$$a_{46} = -|0, m_{x2}|\ CX2_3 - |0, -m_{x1}|\ CX1_3 + |0, -m_{y4}|\ SY4_2 + |0, -m_{z6}|\ SZ6_2 \quad (7.89/12)$$

$$a_{23} = |0, -m_{x2}|\ SX2_4 + |0, m_{y3}|\ SY3_6 - |0, -m_{z5}|\ SZ5_6 - |0, m_{z6}|\ CZ6_5 \quad (7.89/13)$$

$$a_{14} = |0, m_{x1}|\ SX1_6 + |0, -m_{y4}|\ SY4_4 - |0, m_{z6}|\ CZ6_1 - |0, -m_{z5}|\ CZ5_1 \quad (7.89/14)$$

$$a_{45} = -|0, m_{x2}|\ SX2_9 - |0, -m_{x1}|\ CX1_9 + |0, -m_{y4}|\ SY4_8 + |0, m_{z5}|\ SZ5_2 \quad (7.89/15)$$

$$a_{15} = |0, m_{x1}|\ SX1_8 - |0, m_{y4}|\ CY4_7 - |0, -m_{y3}|\ CY3_7 + |0, m_{z5}|\ SZ5_4 \quad (7.89/16)$$

$$a_{16} = |0, m_{x1}|\ SX1_2 - |0, m_{y4}|\ CY4_1 - |0, -m_{y3}|\ CY3_1 + |0, -m_{z6}|\ SZ6_4 \quad (7.89/17)$$

$$a_{25} = |0, -m_{x2}|\ SX2_8 - |0, m_{y4}|\ CY4_9 - |0, -m_{y3}|\ CY3_9 + |0, m_{z5}|\ SZ5_6 \quad (7.89/18)$$

$$a_{26} = |0, -m_{x2}|\, SX2_2 - |0, m_{y4}|\, CY4_3 - |0, -m_{y3}|\, CY3_3 + |0, -m_{z6}|\, CZ6_6 \quad (7.89/19)$$

$$a_{135} = |0, m_{x1}|\, CX1_7 + |0, m_{y3}|\, CY3_7 + |0, m_{z5}|\, CZ5_7 \quad (7.89/20)$$

$$a_{136} = |0, m_{x1}|\, CX1_1 + |0, m_{y3}|\, CY3_1 + |0, -m_{z6}|\, CZ6_7 \quad (7.89/21)$$

$$a_{235} = |0, -m_{x2}|\, CX2_7 + |0, m_{y3}|\, CY3_9 + |0, m_{z5}|\, CZ5_9 \quad (7.89/22)$$

$$a_{236} = |0, -m_{x2}|\, CX2_1 + |0, m_{y3}|\, CY3_3 + |0, -m_{z6}|\, CZ6_9 \quad (7.89/23)$$

$$a_{145} = |0, m_{x1}|\, CX1_9 + |0, -m_{y4}|\, CY4_7 + |0, m_{z5}|\, CZ5_1 \quad (7.89/24)$$

$$a_{146} = |0, m_{x1}|\, CX1_3 + |0, -m_{y4}|\, CY4_1 + |0, -m_{z6}|\, CZ6_1 \quad (7.89/25)$$

$$a_{245} = |0, -m_{x2}|\, CX2_9 + |0, -m_{y4}|\, CY4_9 + |0, m_{z5}|\, CZ5_3 \quad (7.89/26)$$

$$a_{246} = |0, -m_{x2}|\, CX2_3 + |0, -m_{y4}|\, CY4_3 + |0, -m_{z6}|\, CZ6_3 \quad (7.89/27)$$

Verification of the Generalized Equations for Special Flow Conditions

Upwind Finite Volume Formulation. If the primary coefficients PX1, PX2, PY3, PY4, PZ5, and PZ6 are equal to one, the side and corner coefficients must be equal to zero. Thus, the general equation, Eq. 7.89, reduces to

$$a_0\ (\text{upwind}) = |0, m_{x2}| + |0, -m_{x1}| + |0, m_{y4}| + |0, -m_{y3}| + |0, m_{z6}| + |0, -m_{z5}| \quad (7.90a)$$

$$a_1 = |0, m_{x1}| \quad (7.90b)$$

$$a_2 = |0, -m_{x2}| \quad (7.90c)$$

$$a_3 = |0, m_{y3}| \quad (7.90d)$$

$$a_4 = |0, -m_{y4}| \quad (7.90e)$$

$$a_5 = |0, m_{z5}| \quad (7.90f)$$

$$a_6 = |0, -m_{z6}|, \quad (7.90g)$$

which correspond exactly to the upwind finite-volume formulation.

Uniform Flow with u, v, w Positive and Constant. In this case, the only weighting factors different from zero are:

$$\begin{array}{llll} PX1, & SX1_4, & SX1_8, & CX1_7, \\ PX2, & SX2_4, & SX2_8, & CX2_7, \\ PY3, & SY3_4, & SY3_8, & CY3_7, \\ PY4, & SY4_4, & SY4_8, & CY4_7, \\ PZ5, & SZ5_4, & SZ5_8, & CZ5_7, \\ PZ6, & SZ6_4, & SZ6_8, & CZ6_7. \end{array}$$

The coefficients different from zero are:

$$a_0 = m_{x2} \cdot PX2 + m_{y4} \cdot PY4 + m_{z6} \cdot PZ6$$

$$a_1 = m_{x1} \cdot PX1 - m_{y4} \cdot SY4_4 - m_{z6} \cdot SZ6_4$$

$$a_3 = -m_{x2} \cdot SX2_4 + m_{y3} \cdot PY3 - m_{z6} \cdot SZ6_8$$

$$a_5 = -m_{x2} \cdot SX2_8 - m_{y4} \cdot SY4_8 + m_{z5} \cdot PZ5$$

$$a_{13} = m_{x1} \cdot SX1_4 + m_{y3} \cdot SY3_4 - m_{z6} \cdot CZ6_7$$

$$a_{15} = m_{x1} \cdot SX1_8 - m_{y4} \cdot CY4_7 + m_{z5} \cdot SZ5_4$$

$$a_{35} = -m_{x2} \cdot CX2_7 + m_{y3} \cdot SY3_8 + m_{z5} \cdot SZ5_8$$

$$a_{135} = m_{x1} \cdot CX1_7 + m_{y3} \cdot CY3_7 + m_{z5} \cdot CZ5_7, \qquad (7.91)$$

which are identical to the coefficients given in Sec. 7.4.2.

7.4.4 Results and Discussion

The three-dimensional FMSUD scheme described in Sec. 7.4.2 has been implemented in the energy equation of COMMIX-1C for all flow conditions. The derivation presented in Sec. 7.4.2 with the assumption of unidirectional flow is merely for demonstration of the concept of the FMSUD scheme and this assumption has been removed in Sec. 7.4.3. The implemented weighting factors for all flow situations remain to be tested. We have performed calculations of the three-dimensional problem described in Sec. 7.3.2 to test this newly implemented scheme. The calculated isotherms are shown in Figs. 30 and 31 for two different elevations. It can be observed that numerical diffusion is reduced significantly compared to the results of upwind-difference (Figs. 23 and 24). Perhaps even more important is that the present FMSUD scheme does not produce undershoots or overshoots anywhere in the computation domain. This is a significant improvement over the extended Raithby SUD scheme shown in Figs. 25 and 26. The results shown in Figs. 30 and 31 are certainly encouraging. The final test of the FMSUD scheme will depend upon the results of using this scheme to calculate various types of flows in engineering applications when the streamlines are oblique to the grid lines. User feedback will be an important part of this process.

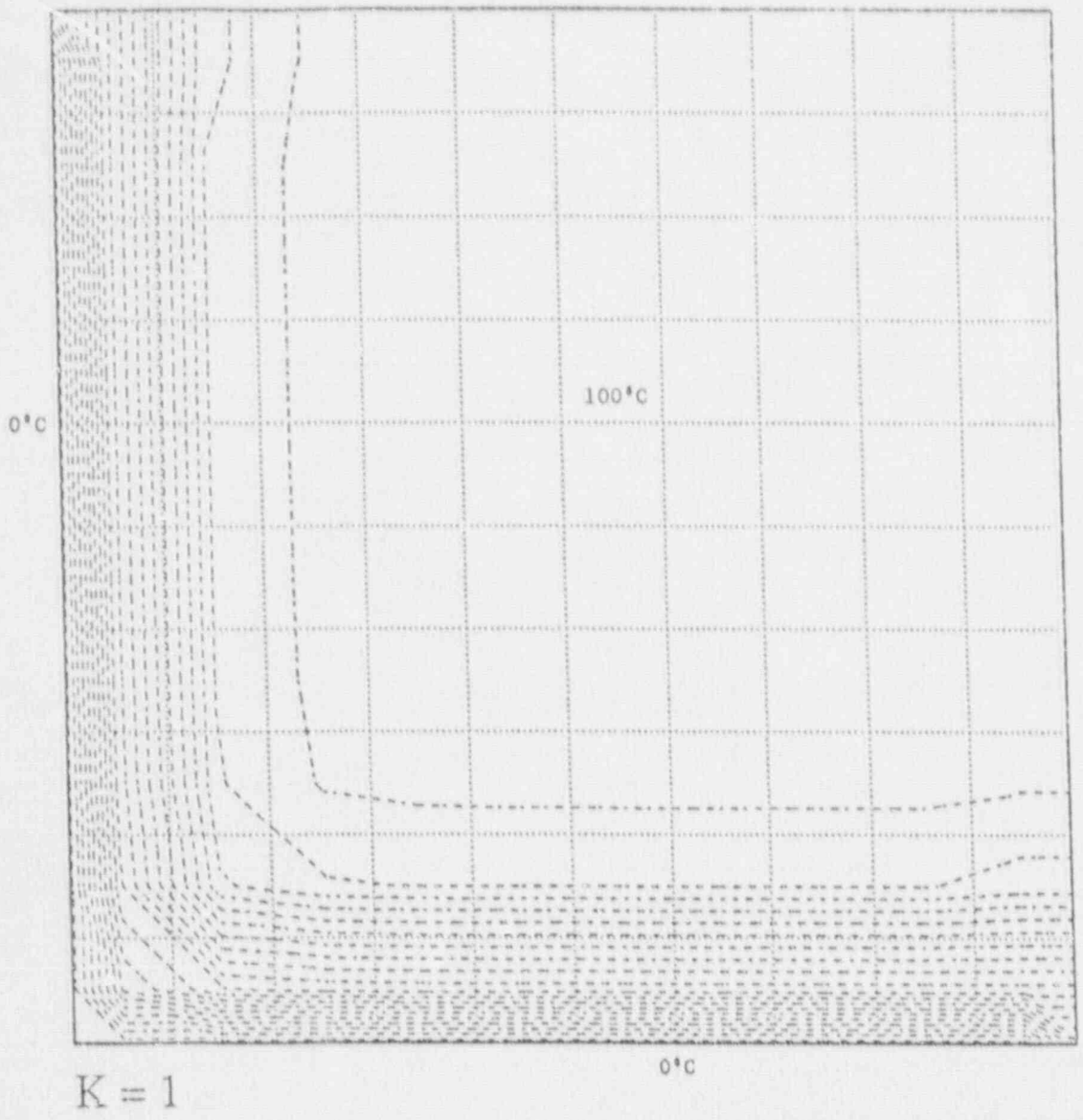

Fig. 30. Isotherms at lowest elevation (k = 1) of a three-dimensional flow with $m_x = m_y = m_z$ (FMSUD)

In summary, we have developed a three-dimensional, flow-modulated skew-upwind discretization (FMSUD) scheme for the energy equation. Our objectives are to reduce numerical diffusion and prevent the occurrence of undershoots and overshoots which are physically unrealistic. Preliminary calculations indicate that the results are encouraging and that we are moving in the right direction. The mathematics is rather involved in the derivation of all the equations. However, the user need not be too concerned about the detailed mathematical derivations. The important thing is to understand the basic principles and the limitations of this new scheme. It is very easy to use this scheme in COMMIX-1C. All that is required is a single statement in the input data. Descriptions of input preparation are provided in Volume II of this report.

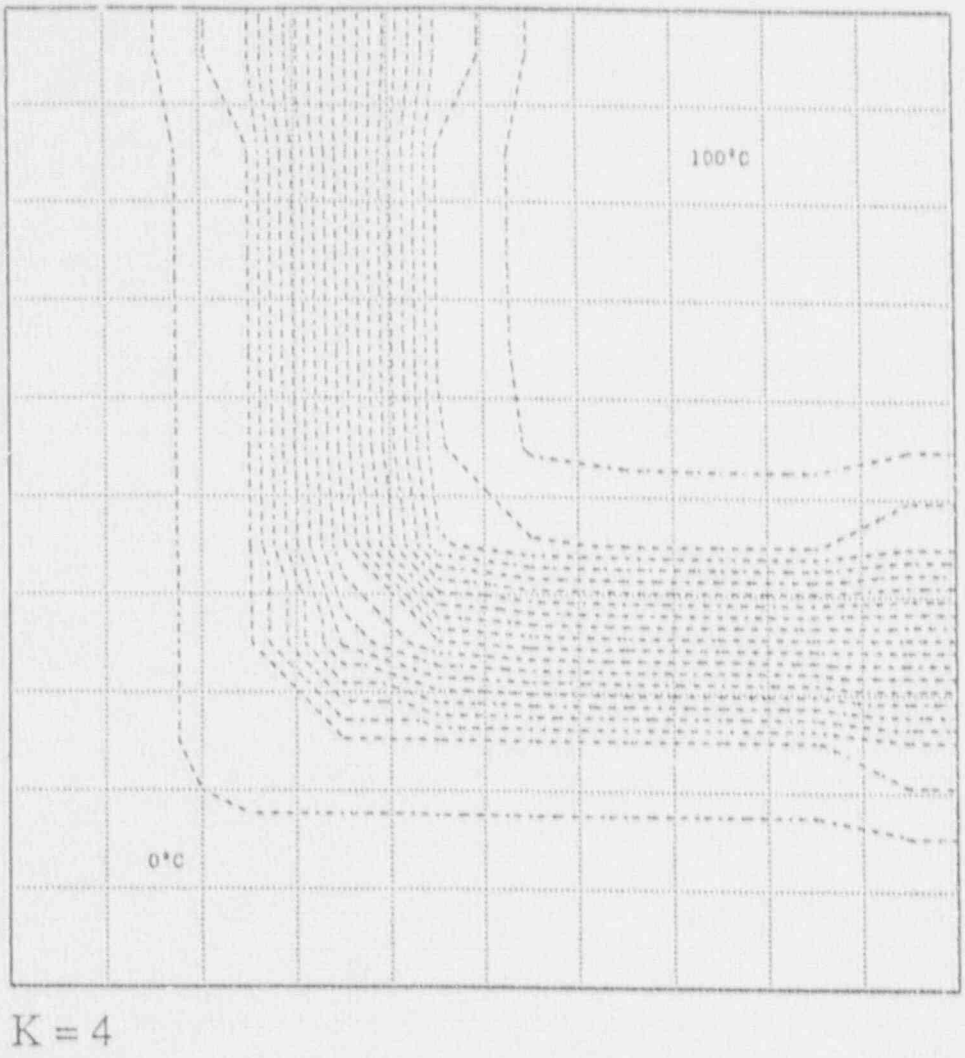

Fig. 31. Isotherms at higher elevation (k = 4) of a three-dimensional flow with $m_x = m_y = m_z$ (FMSUD)

8 Supplementary Physical Models

To broaden the scope of COMMIX-1C applications and to more accurately account for phenomena that affect thermal-hydraulic simulation, a number of supplementary physical models have been incorporated into COMMIX-1C.

8.1 Rigorous Fluid Property Routines

There are four fluid property packages in COMMIX-1C, i.e., water liquid, water vapor, sodium liquid, and sodium vapor. All four property packages are developed and formulated in a modular fashion to accommodate replacement by any other fluid property package. The input description on use of these fluid packages is given in Volume II of this report.

8.2 Simplified Fluid Property Option

Besides the rigorous fluid property packages, another option is available to the user. This option is known as a simplified property option. This option applies to both fluid and solid materials. Enthalpy, density, thermal conductivity, and viscosity are assumed to have the following functional form:

$$h = C_{0h} + C_{1h}T + C_{2h}T^2 + C_{3h}P,$$

$$\rho = C_{0\rho} + C_{1\rho}T + C_{2\rho}P/(T + 273.15),$$

$$k = C_{0k} + C_{1k}T + C_{2k}T^2,$$

and

$$\mu = C_{0\mu} + C_{1\mu}T + C_{2\mu}/(T + 273.15), \tag{8.1}$$

where T is temperature in degrees C, P is pressure in Pascals, and C_0, C_1, C_2, and C_3 are constant coefficients to be specified by the user. The default values for these constants are zero. We found the simplified property option quite useful in many applications because it takes very little time in preparing and inputting the coefficients in Eq. 8.1. It should be noted that for liquids and solid materials, the pressure dependence of the property does not apply, and the corresponding coefficients should be set to zero. A detailed description of inputting the simplified property option is given in Volume II of this report.

8.3 Heat-Transfer Correlations

To calculate the heat transfer between fluid and solid surfaces (either the solid boundaries of a flow domain or the surfaces of internal structures), a heat-transfer coefficient model is required in the code. In the model implemented in COMMIX, all heat transfer coefficient correlations are assumed to have the following form:

$$Nu = C_1 + C_2 Re^{C_3} Pr^{C_4}, \tag{8.2}$$

Here Nu is the Nusselt number, Re is the Reynolds number, Pr is the Prandtl number, and C_1, C_2, C_3, and C_4 are the constant coefficients for a given correlation number NH. The user can prescribe several correlations by inputting different values of coefficients C_1, C_2, C_3, and C_4. The Nusselt number and Reynolds number are based on the characteristic lengths of the system under consideration. These characteristic lengths are input and must be prescribed by the user.

8.4 Structure/Fluid Momentum Interaction

As described before, the solid structures in a flow domain interact with fluid and influence the momentum distribution. In the porous-media formulation employed in COMMIX, these interactions are modeled with the use of distributed resistances that appear in the source term of the momentum equations (Table 1). This section describes how the calculation of distributed resistance, also known as force structure, is carried out, and how a wide range of generality and flexibility is provided in COMMIX.

8.4.1 Force Structure Modeling

In COMMIX-1C, the pressure drop due to stationary solid structures is expressed in the following general form:

$$\Delta p = c_1 \frac{L}{D} \rho v^2 f . \tag{8.3}$$

The distributed resistance R, which represents pressure drop per unit length, has the form

$$R = c_1 \rho \frac{v|v|}{D} f . \tag{8.4}$$

Here, L(Δx, Δy, or Δz) is the length of the cell, D is the hydraulic diameter, and c_1 is the coefficient, depending on the form of the equation desired. The values of c_1 and D depend on the geometry and type of structure and must be provided by the user.

There may be more than one structure in a flow domain of interest. Submerged structures usually have different geometries and so require different values for the parameters c_1 and D. In COMMIX, we have provided this flexibility; details are given in Volume II.

The friction factor f in Eq. 8.4 is a function of the Reynolds number and is assumed to be of the form

$$f = a_{\ell am} Re^{b_{\ell am}} + c_{\ell am} \tag{8.5}$$

for $Re \leq Re_{tr}$ and

$$f = a_{tur} Re^{b_{tur}} + c_{tur} \tag{8.6}$$

for $Re > Re_{tr}$. Here, Re is the Reynolds number, and a, b, and c are constants. The subscripts ℓam, tur, and tr stand for laminar, turbulent, and transition. COMMIX has the flexibility of permitting as many correlations as the user desires. Each correlation requires seven input numbers: $a_{\ell am}$, $b_{\ell am}$, $c_{\ell am}$, a_{tur}, b_{tur}, c_{tur}, and Re_{tr}.

To simplify the specification of which fluid cells interact with which structure, a specific input arrangement has been implemented in COMMIX; details are presented in Volume II of this report.

A report[81] has been prepared that provides a convenient collection of resistance correlations that are most commonly needed by COMMIX users. This collection of resistance correlations is included as an appendix in Volume II.

8.4.2 Friction-Factor Library

Occasionally, the COMMIX-1C user may find that the desired correlation is not of a form directly suitable for input as described in Sec. 8.4.1. The user is then faced with two choices:

- Approximate the correlation to fit the input form, or
- Use the friction-factor library.

The friction-factor library has been created to accommodate up to 50 different additional correlations. Currently, only seven correlations, as described in Table 19, have been added to the library.

An ambitious user who wishes to define his or her own correlation may first examine the code to see what correlation numbers are free and available. Then, with other library correlations as a guide, the new correlation can be inserted appropriately in the code and recompiled. Every effort has been made to modularize this part of the subroutine so that a user has minimum difficulty in inserting new correlations in the code.

8.5 Structure/Fluid Thermal Interaction

8.5.1 Introduction

As described earlier, solid structures near or submerged in fluid can interact with the fluid and influence momentum and energy distributions. The momentum interaction is taken into account by using the force structure modeling described in Sec. 8.4. In this section, we describe the structure/fluid thermal interaction when the temperatures of the solid structures are different from the fluid temperatures. Fluid/structure thermal interaction is modeled by distributed heat sources that appear in the source term of the energy equation (see Table 1).

The fluid/structure thermal interaction consists primarily of the heat transfer between a structure and surrounding fluid and the heat transfer within a solid structure. In COMMIX-1C, we model these interactions by using the so-called thermal-structure module.

The heat transfer to fluid from a structure is calculated by solving the one-dimensional heat conduction equation for the structure. This assumes that heat conduction in the other two directions is negligible. The COMMIX thermal structure model has the following features:

- The model considers all internal structures. The input determines the total number of structures.
- A structure can be planar, cylindrical, or spherical, with either one surface (e.g., solid cylinder or sphere) or two surfaces (plane or annular cylinder) having thermal interactions with surrounding fluid. The axis of alignment of the structure can be aligned with any of the three coordinate axes.
- Each structure can consist of more than one type of material, each separated by a gap.
- Temperature dependence of thermal conductivity and specific heat of structures are incorporated.

Table 19. Friction factor library

Correlation Number	Description	Correlation	CLENTH (hydraulic diameter, m)	REYLEN (length used to compute Reynolds number)
90	CRBR fuel	$f = \frac{81.7}{Re}\sqrt{1-\chi} + \frac{0.48}{Re^{0.25}}\sqrt{\chi}$ $\chi = 0;\ Re \leq 400$ $\chi = (Re - 400)/4600;\ 400 < Re < 5000$ $\chi = 1;\ Re \geq 5000$	3.25×10^{-3}	3.25×10^{-3}
91	CRBR blanket assembly	$f = \frac{99}{Re}\sqrt{1-\chi} + \frac{0.48}{Re^{0.25}}\sqrt{\chi}$ $\chi = 0;\ Re \leq 400$ $\chi = (Re - 400)/4600;\ 400 < Re < 5000$ $\chi = 1;\ Re \geq 5000$	3.39×10^{-4}	3.39×10^{-4}
92	Direct reactor heat exchanger	$f = \frac{A}{Re^{0.32}}$ $A = 0.171 + 0.012\,(P/D) - 0.07e^{-50(P/D-1)}$ $P/D = 1.84$	0.1055	0.1055
93	CRBR chimneys	$f = \frac{64}{Re}\sqrt{1-\chi} + \frac{0.3164}{Re^{0.25}}\sqrt{\chi}$ $\chi = 0;\ Re \leq 1200$ $\chi = (Re - 1200)/2800;\ 1200 < Re < 4000$ $\chi = 1;\ Re \geq 4000$	0.127	0.127

94	FFTF pin Bundle	$f = \frac{84}{Re}$; $Re \leq 1000$ $f = 1.075 f_c \left[1 + 0.1746 \left(\frac{1000}{Re} \right)^2 + 0.0745 \left(\frac{1000}{Re} \right)^4 \right]$ $\frac{1}{\sqrt{f_c}} = -0.8686 \log_e \left(\frac{2.51}{Re\sqrt{f_c}} \right)$	3.95×10^{-3}	3.95×10^{-3}
95	CRBR control assembly	$f = \frac{60.68}{Re}\sqrt{1-\chi} + \frac{0.48}{Re^{0.25}}\sqrt{\chi}$ $\chi = 0$; $Re \leq 400$ $\chi = (Re - 400)/4600$; $400 < Re < 5000$ $\chi = 0$; $Re \geq 5000$	3.48×10^{-3}	3.48×10^{-3}
96	Mixed convection through vertical rod bundles	If $Gr/Re \leq 2000$ $f = f_0$ If $Gr/Re > 15000$ $f = 2f_0$ If $15{,}000 > Gr/Re > 2000$ $f = [5.917 \times 10^{-9} (Gr/Re)^2 - 2.367 \times 10^{-5} (Gr/Re) + 1.023] \times f_0$ where $f_0 = \frac{24.7}{Re^{0.773}}$ $Re = \frac{\rho v De}{\mu}$ $Gr = \frac{1}{4} \frac{g\rho}{\mu^2} Pr\, Re\, De^4 \frac{\Delta\rho}{\Delta z}$	$De = \frac{4 \times \text{Flow Area}}{\text{Wetted Perimeter}}$	De

- The effects of gaps in a structure element are accounted for in the model. The gap width and heat-transfer coefficient across a gap are input parameters.
- The heat source in a structure element is considered in the heat conduction equation. The heat source can be transient.
- Each structure is divided into a desired number of axial elements. A set of discretization equations is obtained for each element, through use of the proper boundary conditions. The equations are solved using the Tri-Diagonal Matrix Algorithm. The temperature variations in the element and heat transfer from the element to fluid are calculated.

8.5.2 Thermal Structure Modeling

Geometrical Description

To explain the geometrical features of the model, we consider a cylindrical structure with its axis aligned in the z direction and its length extending over a number of Δz partitions (K levels), as shown in Fig. 32. Although the description and the subsequent formulation are geared toward cylindrical-type structures, the model in COMMIX-1C also is applicable to spherical and slab-type geometries.

Each Δz partition of the structure is referred to as a thermal-structure element. Each element has its own internal temperature distribution as it interacts with surrounding fluid cells. Each element has two surfaces, outer and inner. The outer surface interacts with surrounding fluid. The inner surface can either be adiabatic or can interact with fluid, as shown in Fig. 33. Each element can interact with no more than one fluid cell per element surface, while each fluid cell can interact with more than one structure element; this can be seen in Figs. 34 and 35.

Figure 36 shows the cross section of a typical structure element. The outside surface is considered as surface 1 and the inside as surface 2. Each element can be made up of more than one material. In Fig. 36, there are three materials. Each material region can be subdivided into a number of partitions as shown.

Governing Equation

The transient one-dimensional heat conduction equation is

$$\rho c_p \frac{\partial T}{\partial t} = \frac{1}{A}\frac{\partial}{\partial r}(-Aq) + \dot{q}''' . \tag{8.7}$$

Here, ρ and c_p are the density and specific heat of the material, $\dot{q}'''$ is the heat source per unit volume, q is the surface heat flux per unit area, and A is the cross-sectional area.

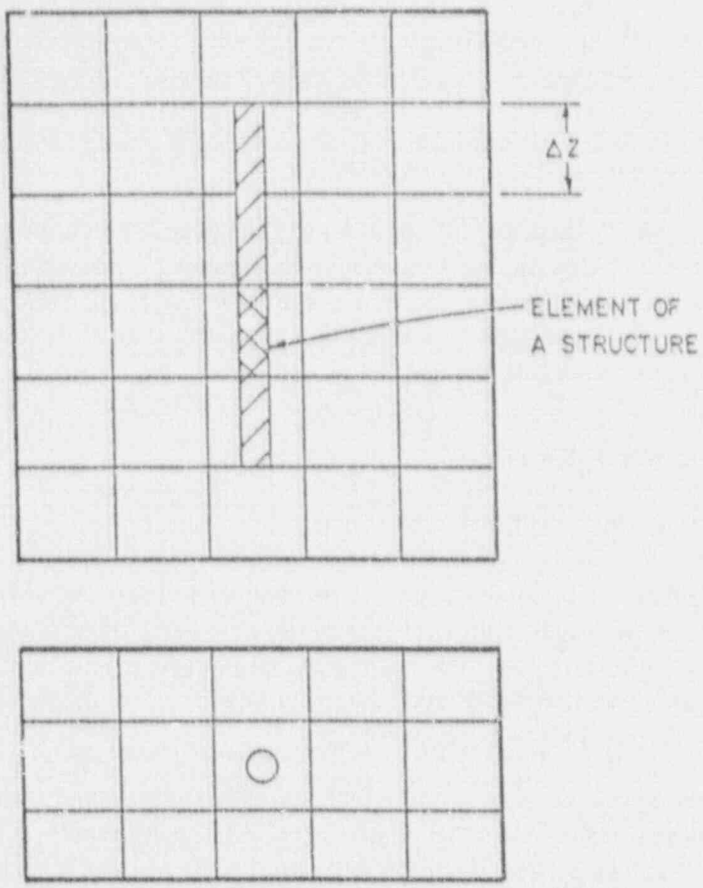

Fig. 32. Flow domain, showing cylindrical structure

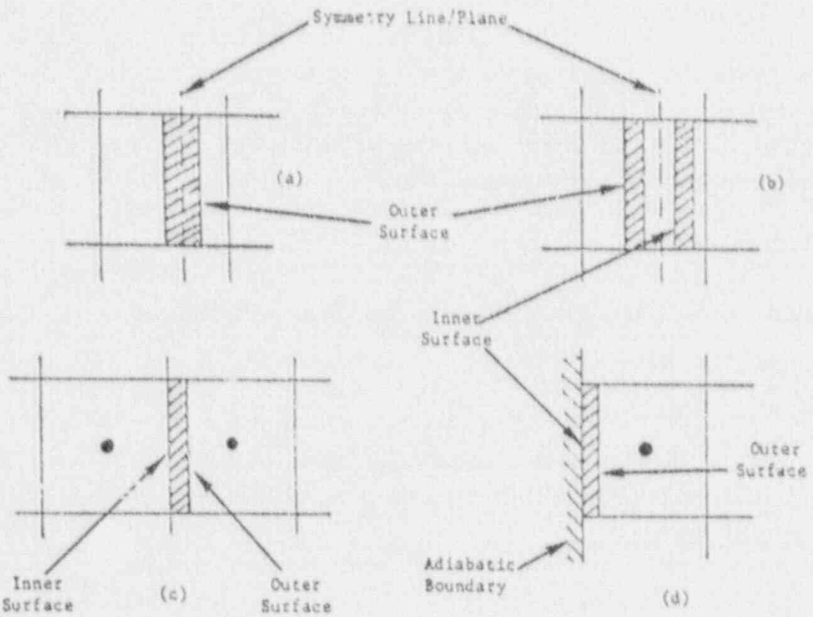

Fig. 33. Element of thermal structure, showing outer and inner surfaces

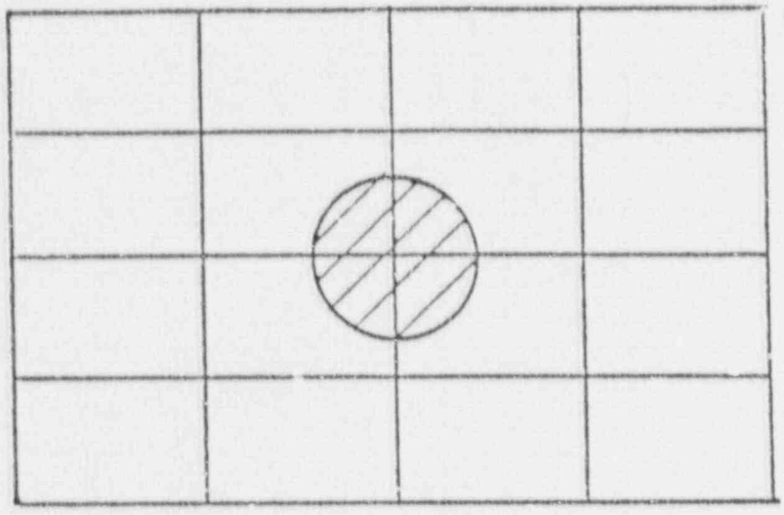

Fig. 34. Four quarter-cylindrical structures, each interacting with one fluid cell

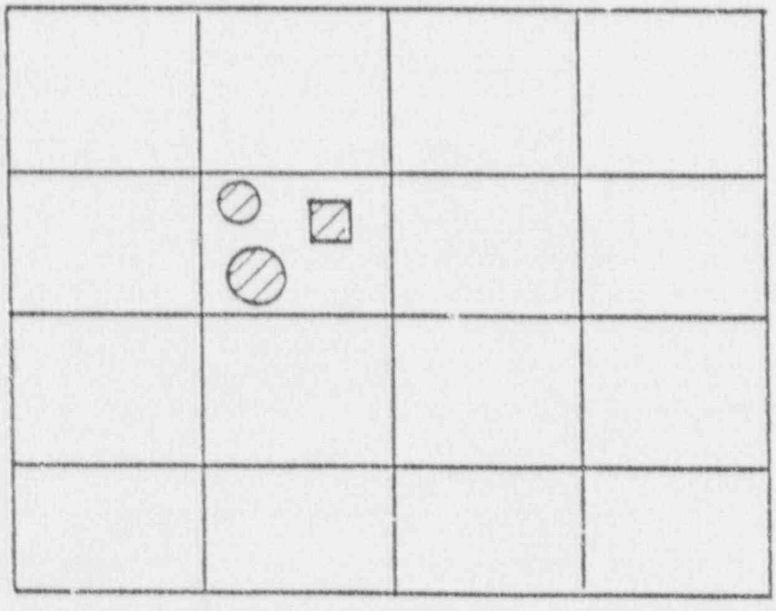

Fig. 35. More than one structure interacting with a single fluid cell

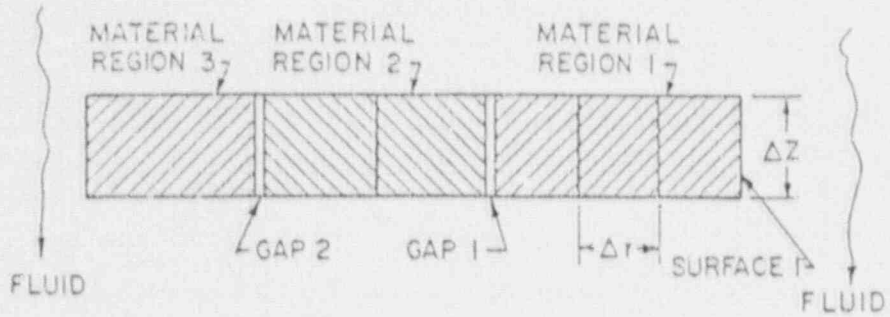

CROSS SECTION A-A

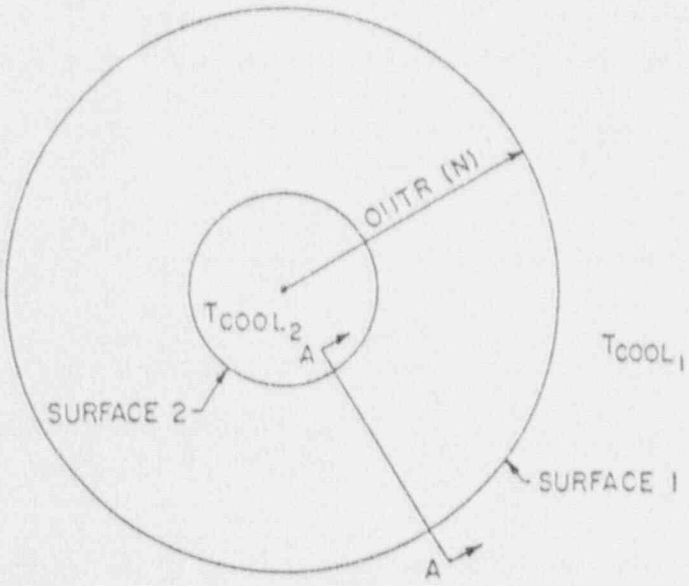

Fig. 36. Typical structure element, showing material regions and gaps

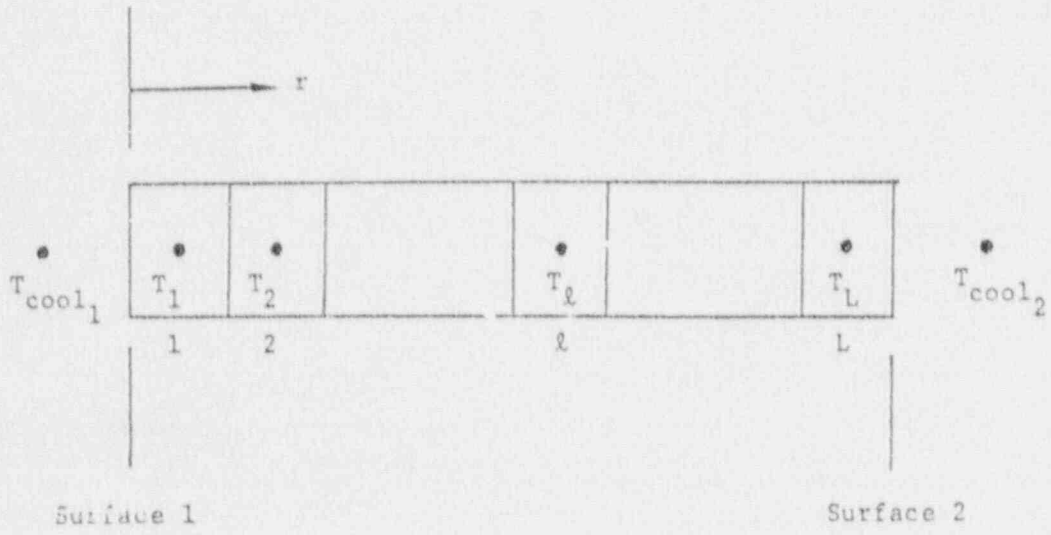

Fig. 37. Cross section of a thermal structure element

Finite-Difference Formulation

Figure 37 shows the cross section of a typical structure element under consideration. Each element is divided into a number of material regions and each material region is subdivided into a number of partitions. Let Δr be the partition size and let L be the total number of partition cells.

Consider the energy balance of cell ℓ, as shown in Fig. 38. The integrated energy equation for the structure in the control volume of cell ℓ gives

$$\frac{\rho c_p V_\ell}{\delta t}\left(T_\ell - T_\ell^n\right) = -\left(A_{\ell+1} q_{\ell+1} - A_\ell q_\ell\right) + \dot{q}''' V_\ell . \tag{8.8}$$

Here, V_ℓ is the cell volume. The heat flux q_ℓ can be expressed in terms of temperature difference:

$$q_\ell = U_\ell\left(T_{\ell-1} - T_\ell\right) = \left(T_{\ell-1} - T_\ell\right)/R_\ell . \tag{8.9}$$

Here, U_ℓ is the overall heat transfer coefficient (conductance) and R_ℓ is the overall thermal resistance between T_ℓ and $T_{\ell-1}$:

$$U_\ell = \frac{1}{R_\ell} = \frac{1}{\left(\frac{\Delta r}{2\lambda}\right)_{\ell-1} + \left(\frac{\Delta r}{2\lambda}\right)_\ell}$$ for conduction between two solid cells of similar material, (8.10)

$$U_\ell = \frac{1}{R_\ell} = \frac{1}{\frac{1}{h} + \left(\frac{\Delta r}{2\lambda}\right)_\ell}$$ for conduction and convection between a fluid cell and a solid cell, (8.11)

and

$$U_\ell = \frac{1}{R_\ell} = \frac{1}{\left(\frac{\Delta r}{2\lambda}\right)_{\ell-1} + \frac{1}{h_{gap}} + \left(\frac{\Delta r}{2\lambda}\right)_\ell}$$ for conduction between two solid cells with different materials. (8.12)

Here, λ is the thermal conductivity, h is the convection heat transfer coefficient, and h_{gap} is the gap conductance between the two materials.

Substituting Eq. 8.9 into 8.8 and rearranging, we obtain

$$\left(a_\ell + b_\ell + b_{\ell+1}\right)T_\ell = b_\ell T_{\ell-1} + b_{\ell+1} T_{\ell+1} + d_\ell , \tag{8.13}$$

where

$$a = \rho c_p V / \delta t , \tag{8.14}$$

$$b = AU = A/R , \tag{8.15}$$

and

$$d = \dot{q}''' V + a T^n . \tag{8.16}$$

Here, T^n and T are the temperatures at time t and $(t + \delta t)$, respectively.

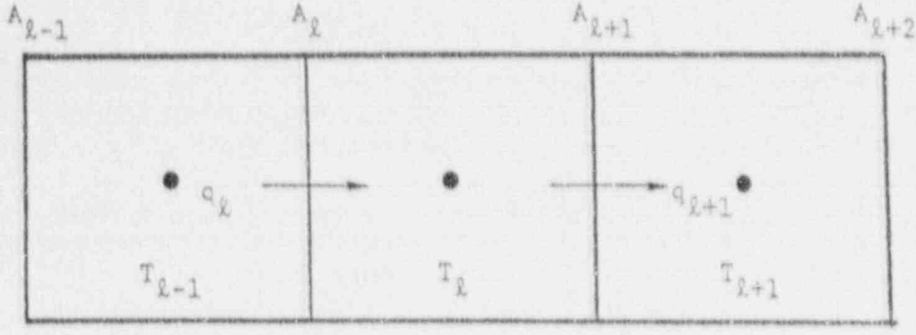

Fig. 38. Energy balance of a partition cell ℓ

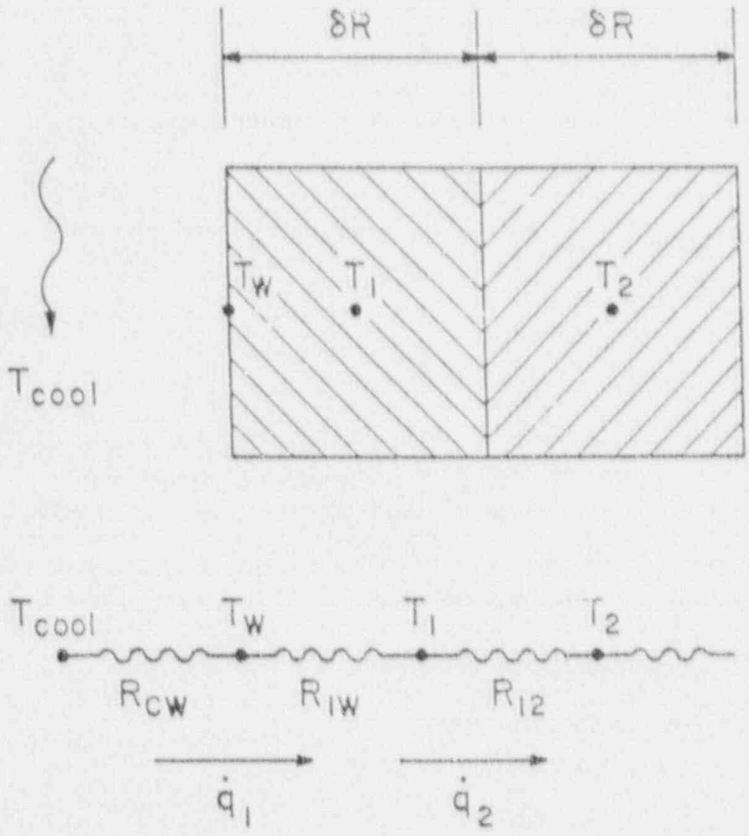

Fig. 39. Energy balance of cell 1 adjacent to coolant

Cell Adjacent to Coolant. For the case of Cell 1 (Fig. 39), adjacent to the fluid, the integrated energy equation for the structure in the cell gives

$$(a_1 + b_1 + b_2)T_1 = b_1 T_{cool_1} + b_2 T_2 + d_1 . \qquad (8.17)$$

Here, a, b, and d have the same meaning, except that b_1 now includes the convective contribution. Therefore,

$$b_1 = \frac{A_1}{R_1} = \frac{A_1}{\frac{1}{h_{cool_1}} + \left(\frac{\Delta r}{2\lambda}\right)_1} . \tag{8.18}$$

Similarly, if the other end of the thermal structure, say Cell L, is in contact with fluid, we get

$$(a_L + b_L + b_{L+1})T_L = b_L T_{L-1} + b_{L+1} T_{cool_2} + d_L , \tag{8.19a}$$

where

$$b_{L+1} = \frac{A_{L+1}}{R_{L+1}} = \frac{A_{L+1}}{\frac{1}{h_{cool_2}} + \left(\frac{\Delta r}{2\lambda}\right)_L} . \tag{8.19b}$$

Cell Adjacent to Different Material. For a cell adjacent to a different material cell, as shown in Fig. 40,

$$(a_\ell + b_\ell + b_{\ell+1})T_\ell = b_\ell T_{\ell-1} + b_{\ell+1} T_{\ell+1} + d_\ell . \tag{8.20}$$

Equation 8.20 is similar to Eq. 8.13, except that the term $b_{\ell+1}$ includes the gap resistance. Thus,

$$b_{\ell+1} = \frac{A_{\ell+1}}{P_{\ell+1}} = \frac{A_{\ell+1}}{\left(\frac{\Delta r}{2\lambda}\right)_\ell + \frac{1}{h_{gap}} + \left(\frac{\Delta r}{2\lambda}\right)_{\ell+1}} . \tag{8.21}$$

End Cell with Adiabatic Boundary Condition. In solid cylindrical or spherical structures, the other end (symmetry line) has the adiabatic boundary condition. The end cell for this boundary condition is shown in Fig. 41. There is no heat transfer, so thermal resistance is infinite and the term b_{L+1} goes to zero. The final equation, therefore, is

$$(a_L + b_L)T_L = b_L T_{L-1} + d_L . \tag{8.22}$$

Solution of the Discretization Equations

We can see from the formulation of the preceding section that there are L number of equations for L number of unknown temperatures.

- Outside Surface Cell ($\ell = 1$)

$$(a_1 + b_1 + b_2)T_1 = b_2 T_2 + d_1 + b_1 T_{cool_1} . \tag{8.23a}$$

- Intermediate Cells ($\ell = 2, \bullet\bullet\bullet\bullet L-1$)

$$(a_\ell + b_\ell + b_{\ell+1})T_\ell = b_\ell T_{\ell-1} + b_{\ell+1} T_{\ell+1} + d_\ell . \tag{8.23b}$$

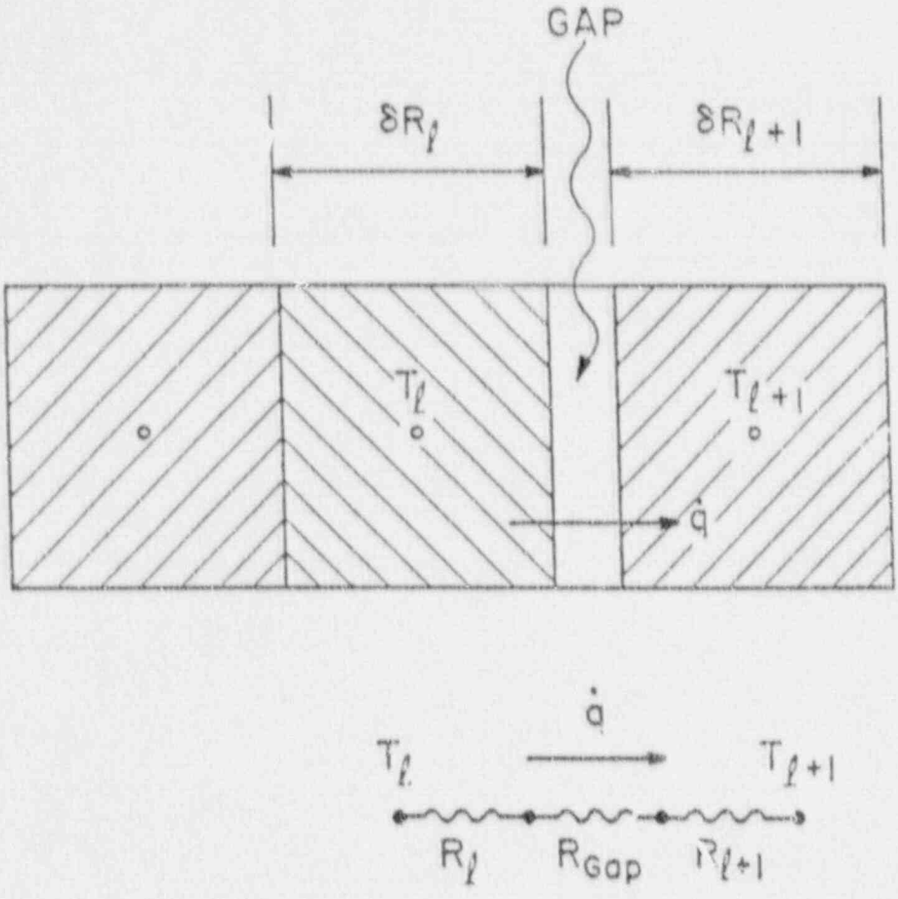

Fig. 40. Cell surrounded by different materials with air gap between them

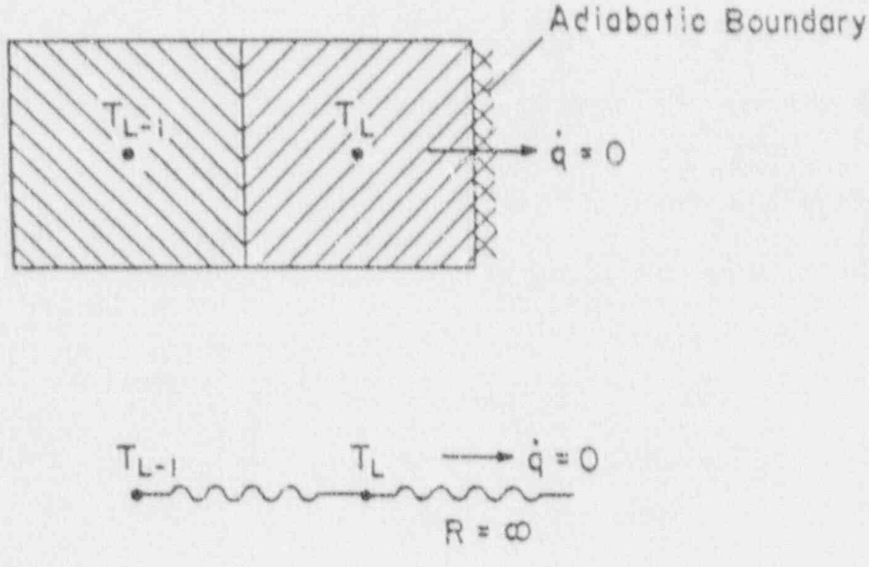

Fig. 41. Cell with adiabatic boundary

- Inside Surface Cell ($\ell = L$)

$$(a_L + b_L + b_{L+1})T_L = b_L T_{L+1} + b_{L+1} T_{cool_2} + d_L \tag{8.23c}$$

if the inside surface is nonadiabatic, and

$$(a_L + b_L)T_L = b_L T_{L-1} + d_L \tag{8.23d}$$

if the inside surface is adiabatic.

Equation 8.23 can be transformed to

$$C_1' T_1 = b_2 T_2 + A_1' \qquad (\ell = 1) \tag{8.24a}$$

$$C_\ell' T_\ell = b_{\ell+1} T_{\ell+1} + A_\ell' \qquad (\ell = 2, \cdots L-1) \tag{8.24b}$$

$$C_L' T_L = b_{L+1} T_{cool_2} + A_L' \qquad (\ell = L; \text{nonadiabatic}) \tag{8.24c}$$

$$C_L' T_L = A_L' \qquad (\ell = L; \text{adiabatic}). \tag{8.24d}$$

Here,

$$A_\ell' = d_\ell + \left(b_\ell A_{\ell-1}' / C_{\ell-1}' \right) \qquad (\ell = 2; \cdots L) \tag{8.25a}$$

and

$$C_\ell' = a_\ell + b_\ell + b_{\ell+1} - \left(b_\ell^2 / C_{\ell-1}' \right) \qquad (\ell = 2; \cdots L) \tag{8.25b}$$

The first set of coefficients is

$$A_1' = d_1 + b_1 T_{cool_1} \tag{8.25c}$$

and

$$C_1' = a_1 + b_1 + b_2 \, . \tag{8.25d}$$

The inside-surface cell temperature is first calculated from Eq. 8.24c or 8.24d. Then the rest of the temperatures are computed using Eqs. 8.24a and 8.24b.

Heat Transfer to Adjacent Fluid

Once the temperature distribution in a structure element is computed, the heat transfer rate to the adjacent fluid is computed from

$$\dot{q} = \frac{A_1}{R_1}(T_1 - T_f)$$

$$= U_1 A_1 (T_1 - T_f) \text{ for outside surface } \left(T_f = T_{cool_1} \right) \tag{8.26}$$

and

$$\dot{q} = \frac{A_{L+1}}{R_{L+1}}(T_L - T_f)$$

$$= U_{L+1} A_{L+1} (T_L - T_f) \text{ for inside surface } \left(T_f = T_{cool_2}\right). \tag{8.27}$$

Here, $\dot{q}$ is the heat transfer rate in watts, U is the overall heat transfer coefficient given by

$$U = \frac{1}{R} = \frac{1}{\frac{1}{h_{cool}} + \left(\frac{\Delta r}{2\lambda}\right)}, \tag{8.28}$$

A is the surface area, T_1 and T_L are the temperatures of the edge partition cells, and T_f is the respective fluid temperature.

The previous derivations are for the calculation of temperature distribution in the thermal structure. We need to derive the expressions for the interaction between the thermal structure and the fluid. This can be achieved by introducing the distributed heat source $\dot{Q}_{rb}$ described in Sec. 2. However, to increase the speed of convergence in COMMIX-1C, we have adopted an implicit treatment of the interaction between the fluid and the thermal structure. The integrated (over the main control volume) heat source term can be expressed as

$$\int S_h \, dxdydz = V_0 \dot{Q} + \frac{\partial \dot{q}}{\partial h_0} \left(h_0 - h_0^n\right), \tag{8.29}$$

where V_0 is the fluid volume, $\dot{Q}$ is the rate of heat generation in the fluid per unit fluid volume, $\dot{q}$ is the heat transfer rate from the thermal structure to the fluid, h_0^n is the enthalpy of the fluid cell adjacent to the thermal structure at old time n, and h_0 is the enthalpy of the fluid cell adjacent to the thermal structure at new time n+1. The superscript n+1 is omitted for convenience. Equation 4.27 can be written for the energy equation as

$$\int S_h \, dxdydz = S_{ch} V_0 + S_{ph} V_0 h_0 . \tag{8.30}$$

Comparing Eq. 8.29 to Eq. 8.30 gives

$$S_{ch} = \dot{Q} - h_0^n \frac{\partial \dot{q}}{\partial h_0} \Big/ V_0 , \tag{8.31}$$

and

$$S_{ph} = \frac{\partial \dot{q}}{\partial h_0} \Big/ V_0 . \tag{8.32}$$

In Eq. 8.30, we have separated the term containing the new time value h_0 from the rest of the terms that are known. When Eq. 8.30 is substituted into the energy equation, the term containing h_0 can be lumped into the left side of the general discretized finite-volume equation (Eq. 4.33). Thus, the effect of the thermal structure has been accounted for when the energy equation is solved. This is what we mean by the implicit treatment of the interaction between the fluid and the thermal structure. However, we need to derive an expression for $(\partial \dot{q} / \partial h_0)$ so that the two coefficients given by Eqs. 8.31 and 8.32 can be calculated.

Consider that case where only the outside surface is in contact with the fluid. At old time n, Eq. 8.26 can be written as

$$\dot{q}_1^n = U_1 A_1 \left(T_1^n - T_{c1}^n\right), \tag{8.33}$$

where T_1 is the temperature for cell 1 and T_{c1} is the coolant temperature adjacent to cell 1. At the new time n+1,

$$\begin{aligned}\dot{q}_1 &= U_1 A_1 (T_1 - T_{c1}) \\ &= U_1 A_1 \left[\left(T_1^n - T_{c1}^n\right) + \left(T_1 - T_1^n\right) - \left(T_{c1} - T_{c1}^n\right)\right] \\ &= \dot{q}_1^n + U_1 A_1 \left(\frac{\partial T_1}{\partial T_{c1}} - 1\right)\left(h_0 - h_0^n\right)/C_{p1}\,,\end{aligned} \tag{8.34}$$

where C_{p1} is the specific heat of the fluid adjacent to the thermal structure. In Eq. 8.34, the variable $\dot{q}_1$, T_1, T_{c1}, and h_0 represent the new time value and we have omitted the superscript n+1 for these variables. From Eq. 8.34, we can obtain the following approximate expression for $(\partial \dot{q}/\partial h_0)$,

$$\frac{\partial \dot{q}_1}{\partial h_0} = \frac{\dot{q}_1 - \dot{q}_1^n}{h_0 - h_0^n} = \frac{U_1 A_1}{C_{p1}} \left(\frac{\partial T_1}{\partial T_{c1}} - 1\right). \tag{8.35}$$

From Eq. 8.24a,

$$\frac{\partial T_1}{\partial T_{c1}} = \frac{1}{C_1'} \left(b_2 \frac{\partial T_2}{\partial T_{c1}} + \frac{\partial A_1'}{\partial T_{c1}}\right). \tag{8.36}$$

From Eq. 8.25c,

$$\frac{\partial A_1'}{\partial T_{c1}} = b_1\,. \tag{8.37}$$

Substituting Eqs. 8.36 and 8.37 into Eq. 8.35,

$$\frac{\partial \dot{q}_1}{\partial h_0} = \frac{U_1 A_1}{C_{p1}} \left(\frac{b_2}{C_1'} \frac{\partial T_2}{\partial T_{c1}} + \frac{b_1}{C_1'} - 1\right). \tag{8.38}$$

$(\partial T_2/\partial T_{c1})$ can be calculated in terms of the following two recurrence equations:

$$\frac{\partial T_\ell}{\partial T_{c1}} = \frac{1}{C_1'} \left(b_{\ell+1} \frac{\partial T_{\ell+1}}{\partial T_{c1}} + \frac{\partial A_\ell'}{\partial T_{c1}}\right) \tag{8.39}$$

and

$$\frac{\partial A_\ell'}{\partial T_{c1}} = \frac{b_\ell}{C_{\ell-1}'} \frac{\partial A_{\ell-1}'}{\partial T_{c1}}\,, \tag{8.40}$$

which are obtained from Eqs. 8.24c and 8.25a. From Eq. 8.24c, we have

$$\frac{\partial T_L}{\partial T_{c1}} = \frac{1}{C_L'} \frac{\partial A_L'}{\partial T_{c1}}\,. \tag{8.41}$$

In summary, $(\partial \dot{q}_i / \partial h_0)$ can be calculated analytically by using Eqs. 8.37-8.41 when the outside surface of the thermal structure is in contact with the fluid.

If only the inside surface of the thermal structure is in contact with the fluid, an equation similar to Eq. 8.35 can be derived:

$$\frac{\partial \dot{q}_{i_L}}{\partial h_0} = \frac{\dot{q}_{i_L} - \dot{q}_{i_L}^n}{h_0 - h_0^n} = \frac{U_L A_L}{C_{PL}} \left(\frac{\partial T_{i_L}}{\partial T_{c2}} - 1 \right), \tag{8.42}$$

$(\partial T_L / \partial T_{c2})$ can be calculated by using Eq. 8.24c:

$$\frac{\partial T_{i_L}}{\partial T_{c2}} = \frac{b_{L+1}}{C_L'}, \tag{8.43}$$

where C_L' is given by Eq. 8.25b ($\ell = L$):

$$C_L' = a_L + b_L + b_{L+1} - \left(b_L^2 / C_{L-1}' \right). \tag{8.25b}$$

The recurrence formula, Eq. 8.25b, can also be used to evaluate C_{L-1}':

$$C_\ell' = a_\ell + b_\ell + b_{\ell+1} - \left(b_\ell^2 / C_{\ell-1}' \right) \quad (\ell = 2, \bullet\bullet\bullet, L-1), \tag{8.25b}$$

because C_1' is known from Eq. 8.25d:

$$C_1' = a_1 + b_1 + b_2 . \tag{8.25d}$$

Thus, if only the inside surface of the thermal structure is in contact with the fluid, $(\partial \dot{q}_{i_L} / \partial h_0)$ can be calculated analytically by using Eqs. 8.42, 8.43, 8.25b, and 8.25d.

9 Initial and Boundary Conditions

9.1 Initial Conditions

Generally, before the solution sequence can begin, all values of variables must be assigned. In COMMIX, we can accomplish this by either

- Continuing a previous run via the restart capability (recommended for all but the first run), or
- Specifying the initial distribution throughout the interior points and boundary of the space under consideration.

When the initialization is not a restart, we must specify initial pressure, temperature, velocity, and turbulence parameters distributions. The determination of these distributions and their subsequent input into the code are generally tedious. In COMMIX, we have provided several simplified input procedures, which make the initialization of velocity, pressure, temperature, and turbulence parameters fairly simple. These procedures are described in Volume II of this report.

9.2 Boundary Conditions

This section describes the boundary conditions for mass, momentum, and energy equations. The boundary conditions for turbulence transport equations have already been described in Sec. 6.4. The surface flux quantities are oriented with respect to the local surface normal that points into the fluid from the boundary surface.

9.2.1 Fluid Velocity Boundary Conditions

The most common physical boundaries in an engineering system are solid impervious wall, inlet, symmetry, and outlet. To accommodate all possible fluid velocity conditions at these four boundaries, we have provided seven boundary conditions options. Here we describe the meaning of these options in mathematical terms. In Table 20, we have summarized all seven fluid velocity boundary options for the four most commonly occurring physical conditions. Volume II tells how to implement them in the input data.

- *Constant Fluid Velocity*

  This boundary condition implies that normal fluid velocity v_n = constant. This option is applicable to a stationary solid surface with zero normal fluid velocity and to an inlet surface with constant inlet fluid velocity.

- *Transient Fluid Velocity*

  This option is applicable when an inlet velocity varies with time, e.g.,

  $$v_n = v_0 f(t) . \tag{9.1}$$

  Here,

  v_n = surface-normal fluid velocity at time, t,

  v_0 = surface-normal fluid velocity at time, t = 0,

  and

  f(t) = transient function.

- *Free Slip*

  The free-slip option means the shear stress at the surface is zero. Also,

  $$v_n = 0.0 . \tag{9.2}$$

  This option is applicable to a symmetry boundary. For a cylindrical coordinate system in COMMIX, the z axis passing through the origin is considered as a symmetry boundary with zero surface area.

Table 20. Fluid velocity boundary options

Boundary/Suitable Option	Option No.	Remarks
Solid Impervious Surface		
Constant velocity	1	Specify normal velocity $v_n = 0$
Inlet		
Constant velocity	1	Specify inlet velocity
Transient velocity	2	Specify inlet velocity and appropriate transient function
Symmetry		
Free Slip	3	Axis through origin in cylindrical coordinate is a symmetrical surface
Outlet		
Continuative mass flow	4	General outlet condition
Continuative momentum	5	Suitable when areas are equal
Continuative velocity	6	Suitable when areas and densities are equal
Uniform velocity	7	Suitable when outlet is finely divided (Fig. 42)

- *Continuative Mass Flow Outlet*

This option is for an outlet surface as illustrated in Fig. 42. Here, ℓ and m are the outlet boundary cells and $\ell+1$ and m−1 are the neighboring cells. The continuative mass flow outlet implies that normal surface velocity at the outlet must be such as to balance the mass flow, i.e.,

$$(v_n)_{\ell-1/2} = \frac{(\rho A)_{\ell+1/2}}{(\rho A)_{\ell-1/2}} u_{\ell+1/2} \tag{9.3a}$$

and

$$(v_n)_{m+1/2} = -\frac{(\rho A)_{m-1/2}}{(\rho A)_{m+1/2}} u_{m-1/2} \,. \tag{9.3b}$$

The sign difference between Eqs. 9.3a and 9.3b is due to the COMMIX convention that surface-normal is directed into the flow domain.

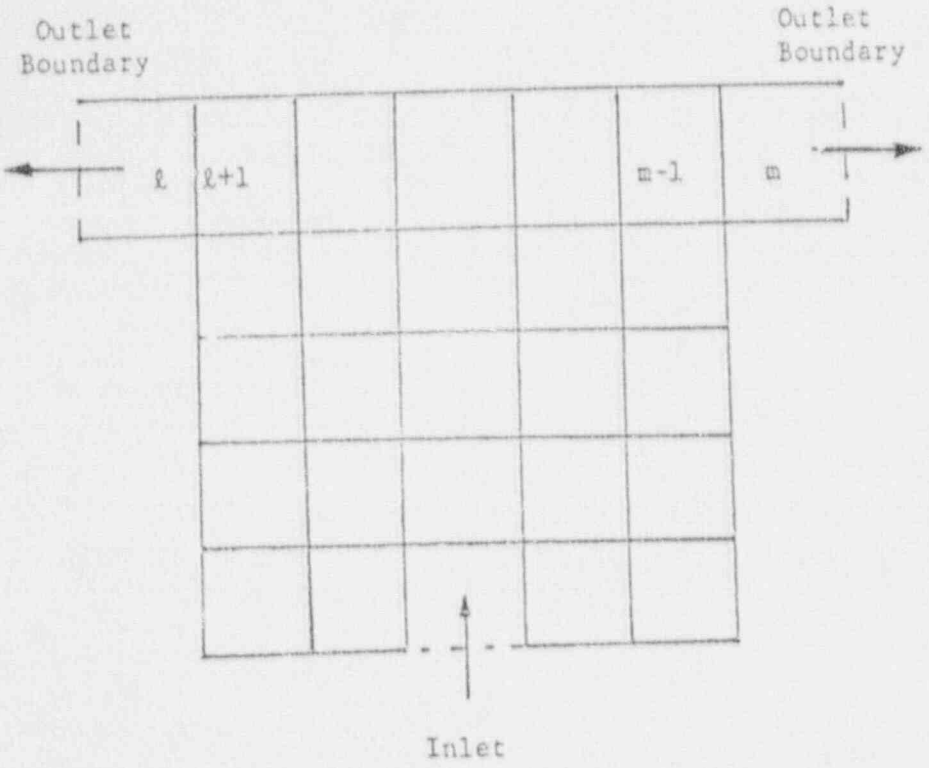

Fig. 42. Near-boundary cells

- *Continuative Momentum Outlet*

When an outlet area is the same as the neighboring surface area, Eq. 9.3a simplifies to

$$(v_n)_{\ell-1/2} = \frac{(\rho u)_{\ell+1/2}}{\rho_{\ell-1/2}}. \tag{9.4}$$

We call this option continuative momentum because it appears that we are eq ‘ng neighboring and outlet momentum fluxes.

- *Continuative Velocity Outlet*

If we have a constant area and equal densities, Eq. 9.3a simplifies to

$$(v_n)_{\ell-1/2} = (u)_{\ell+1/2}. \tag{9.5}$$

We call this option continuative velocity because it appears that we are equating neighboring and outlet velocities.

- *Uniform Velocity Outlet*

The uniform velocity outlet boundary condition option sets the normal velocity for all surface elements of a surface to the same value. This value is computed so that the total mass flow through a surface is the same as that obtained from the continuative mass flow outlet boundary condition. Mathematically,

$$(v_n) = \frac{\Sigma(\rho A u)_{\ell+1/2}}{\Sigma(\rho A)_{\ell-1/2}} . \tag{9.6}$$

Here, the summation is taken over all surface elements of a surface. This option is suitable when an outlet is very finely divided, as shown in Fig. 43.

9.2.2 Temperature Boundary Conditions

The five temperature-boundary-condition options available in COMMIX-1C are briefly described here and summarized in Table 21.

- *Constant Temperature*

  This option is for a constant surface temperature. The temperature associated with each surface element, as shown in Fig. 44, is set initially and remains unchanged throughout the calculation. While the temperature remains fixed, the surface element heat flux is calculated with the relation

$$\dot{q} = UA(T_w - T_f) . \tag{9.7}$$

  Here

$$U = \frac{1}{\frac{1}{h} + \frac{\Delta L}{2\lambda_w}} , \tag{9.8}$$

  where h is the heat transfer coefficient, λ is the conductivity of the wall material, and ΔL is the wall thickness. The subscripts w and f refer to the surface element and boundary fluid cell, respectively. For calculation of the overall heat transfer coefficient U, we must provide wall thickness, suitable correlation for h, and material properties for λ.

  If the wall is very thin, as shown in Fig. 45, we need not specify wall thickness and material properties. The overall heat transfer U is then equal to h.

  If a constant temperature is associated with, say an inlet surface as shown in Fig. 46, we need not specify even the heat transfer correlation. The surface heat flux is then calculated from the Fourier relation

$$\dot{q} = \frac{\lambda_{eff} A(T_w - T_f)}{\frac{\Delta x_f}{2}} , \tag{9.9}$$

  Here, λ_{eff} is the effective thermal conductivity of the fluid in the adjacent internal cell, Δx_f is the distance between the surface and the boundary cell center, and the subscripts w and f stand for wall (surface element) and adjacent internal cell, respectively.

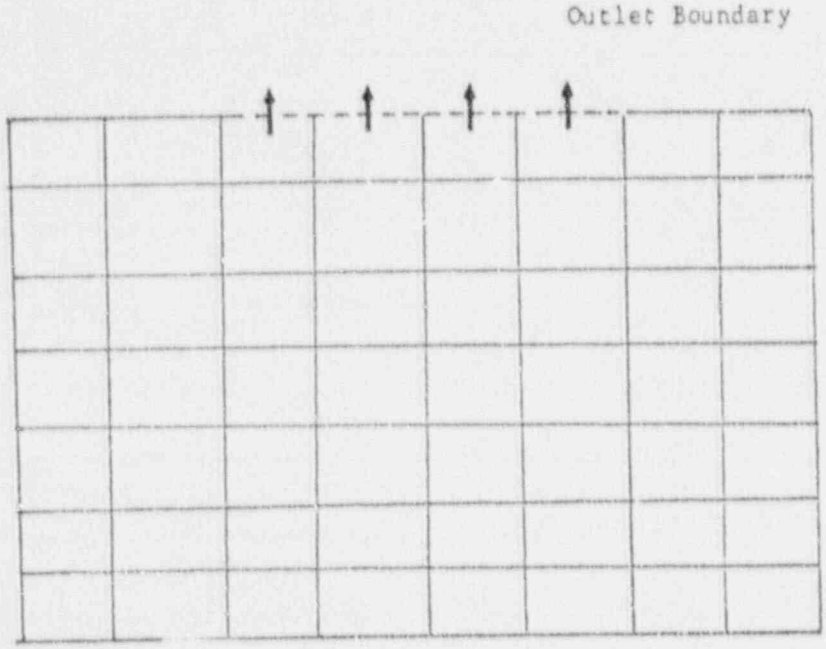

Fig. 43. Model suitable for uniform velocity outlet option

Table 21. Suitable temperature boundary options

Boundary/Option	Option No.	Remarks
Solid Surface		
Constant temperature	1	T_w = constant
Transient temperature	2	T_w = f(t)
Constant heat flux	3	q_w = constant
Transient heat flux	4	q_w = f(t)
Adiabatic	5	q_w = 0
Inlet		
Constant temperature	1	T_w = constant
Transient temperature	2	T_w = f(t)
Outlet		
Adiabatic	5	q_w = 0
Symmetry		
Adiabatic	5	q_w = 0

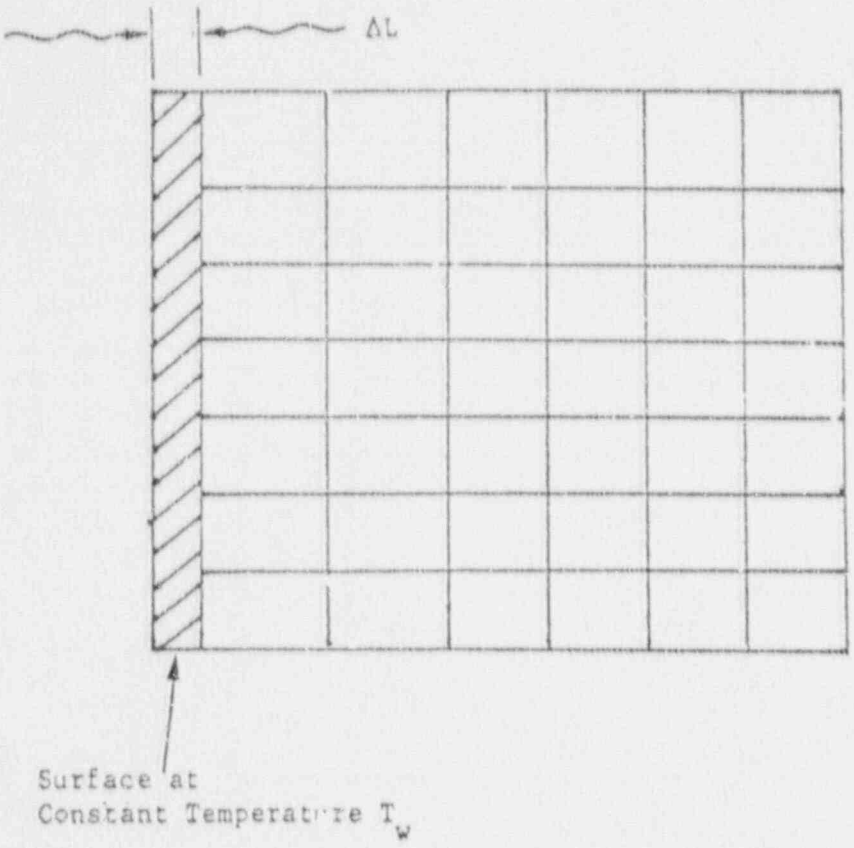

Fig. 44. Constant-temperature boundary

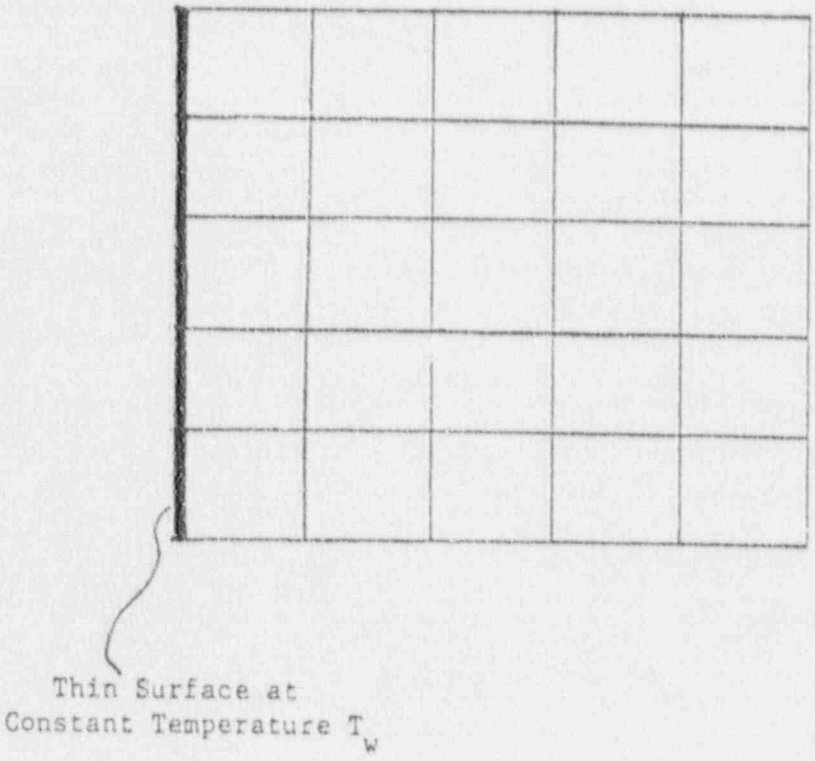

Fig. 45. Thin-wall constant-temperature boundary

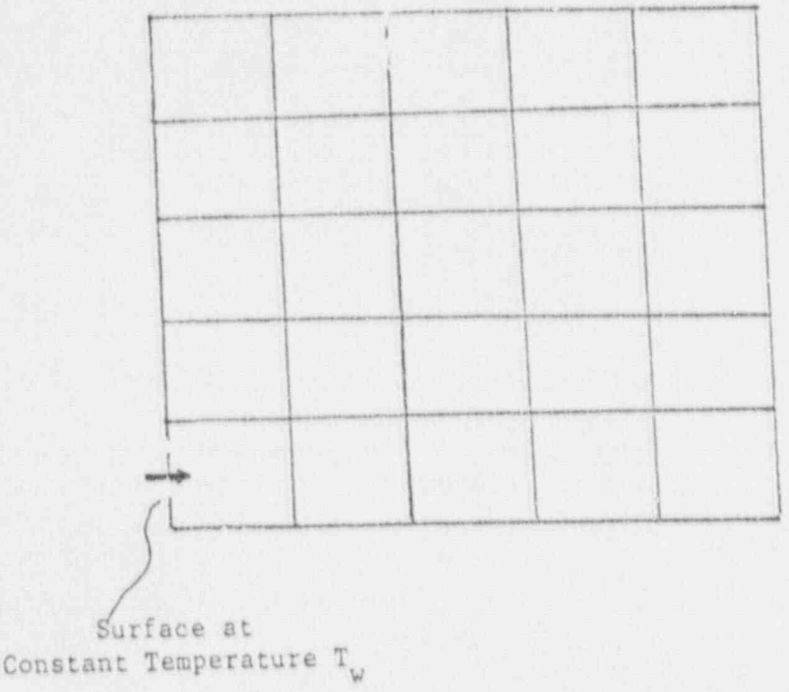

Fig. 46. Nonconvective constant-temperature boundary

- *Transient Temperature*

This option is for a surface whose temperature varies with time, e.g.,

$$T_w = T_0 f(t) \tag{9.10}$$

where

T_w = surface temperature at time t,

T_0 = surface temperature at time = 0,

and

f(t) = transient function .

We calculate the surface-element heat flux with the same procedure described for the constant-temperature-boundary option.

- *Constant Heat Flux*

When we have a surface with constant heat flux, we use this option. The heat flux associated with each surface element is set initially and remains unchanged throughout the calculation. Although the surface heat flux remains fixed, we now calculate the temperature using Eq. 9.9 based on the effective thermal conductivity of the adjacent internal cell.

- *Transient Heat Flux*

  This option is useful when we have surface heat flux varying with time, e.g.,

  $$\dot{q} = \dot{q}_0 \, f(t), \tag{9.11}$$

  where

  $\dot{q}$: surface heat flux at time t,

  $\dot{q}_0$: surface heat flux at time t = 0,

  and

  f(t) : transient function number nf.

  Once the surface heat flux is known for a given time t, the surface temperature can be calculated from Eq. 9.9.

- *Adiabatic Surface*

  The adiabatic boundary condition implies that surface heat flux $\dot{q} = 0$. In this option, the normal heat flux for all surface elements of a surface are initialized to zero and remain zero during calculation. The surface-element temperature is set equal to the temperature of the neighboring internal cell.

9.2.3 Pressure Boundary Conditions

Currently, two types of pressure-boundary-condition options are provided in COMMIX-1C:

- Constant pressure, and
- Transient pressure.

The pressure boundary is applied to cells adjacent to the surface. The option is usually used in conjunction with the continuative mass flow boundary condition.

If an inlet surface has a specified velocity boundary condition, we do not require a pressure boundary option because surface pressure does not enter into any calculation.

It is important to note here that the pressure boundary condition in COMMIX-1C refers to the pressure of the boundary adjacent fluid cells. It is therefore recommended to model the geometry so that the pressure boundary is applied to

- A surface with one surface element, or
- A surface that is normal to the direction of gravity and has parallel flow,

as shown in Fig. 47.

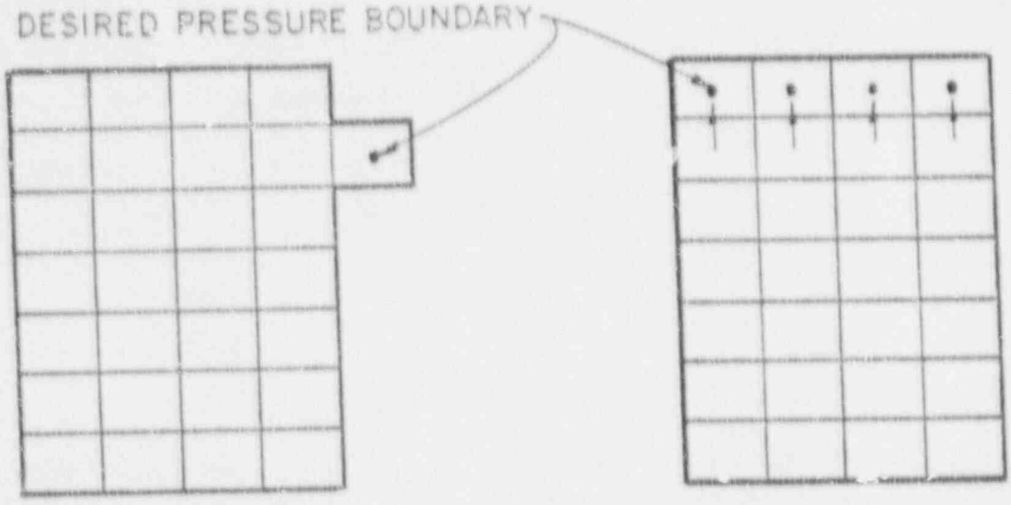

Fig. 47. Recommended surface arrangements for pressure boundary condition

When we specify a constant pressure boundary option, the pressures of all internal cells adjacent to a surface are set to a prescribed value. These values then remain unchanged during the calculation.

For a transient pressure over a surface, the pressures of all internal cells adjacent to that surface are calculated from

$$P_m = P_{m0}\, f(t) . \qquad (9.12)$$

Here,

P_m = pressure of the adjacent cell m and time t,

P_{m0} = pressure of adjacent cell m at time = 0,

and

$f(t)$ = transient function.

Volume II explains how to implement these options in the input.

9.3 Additional Options

The boundary conditions described in Sec. 9.2 are generally for uniform conditions at boundary surfaces. If the distribution of a parameter is not uniform for a given boundary surface, this parameter can be specified by using the boundary surface element initialization procedure in COMMIX-1C. For example, if the inlet velocity is not uniform, the velocity can be specified individually for each surface element at this inlet plane by using the variable velb. Similarly, if the heat flux on a given surface is not uniform, the heat flux can be specified individually for each surface element by using the variable qbn. Other variables such as mass flow rate, enthalpy, temperature, density, turbulence kinetic energy, and dissipation rate of turbulence kinetic energy are included in the boundary surface element

initialization procedure which overrides those described in Sec. 9.2. Quite frequently, a combination of these two procedures is used for a given simulation in order to achieve better accuracy in specifying the boundary conditions. The boundary-surface-element initialization procedure provides greater flexibility not only in specifying nonuniform boundary conditions, but also in specifying other uniform boundary conditions not described in Sec. 9.2. For example, if the user wishes to specify uniform mass flow at the inlet, Table 20 does not provide this option. However, the user can specify uniform mass flow at the inlet plane by using the boundary surface element initialization procedure. A detailed description of this procedure is given in Volume II of this report.

10 Solution Procedures

10.1 Introduction

COMMIX performs thermal-hydraulic calculations by marching in time. The values of the dependent variables at a given time-step, say n, are known and the values of the dependent variables at time step n+1 are calculated. By repeating this procedure, we determine thermal-hydraulic conditions for the desired time span. The overall flow chart of the program is shown in Fig. 48.

For steady-state calculation, the same procedure is followed. We start with an initial guess and continue the marching-in-time process until the values of all dependent variables are lower than some specified values. The time-step size for the implicit steady-state calculation can be many times as large as the Courant time-step criterion.

In COMMIX-1C, we have provided two options for the time-step size:

- The user-desired time-step size (details of this input are given in the Input Description in Volume II), and
- The automatic time-step option.

In the automatic time-step option, the time-step size is evaluated on the basis of the Courant condition:

$$\Delta t = C_1 \Delta t_C \,, \tag{10.1}$$

where C_1 is the user-prescribed coefficient and Δt_C is the time-step size evaluated from the Courant condition. The Courant time-step size is defined as the minimum time required for fluid to be convected through a cell. In COMMIX, each computational cell is examined with respect to all three component directions to calculate the Courant time-step size.

In COMMIX-1C, we have two distinct solution sequences: the fully implicit and the semi-implicit. Both are combined into one formulation through an implicit parameter α. The solution procedure option becomes semi-implicit when $\alpha = 0$ and fully implicit when $\alpha = 1$. Therefore, in principle, we can say that the formulation covers a full range from semi-

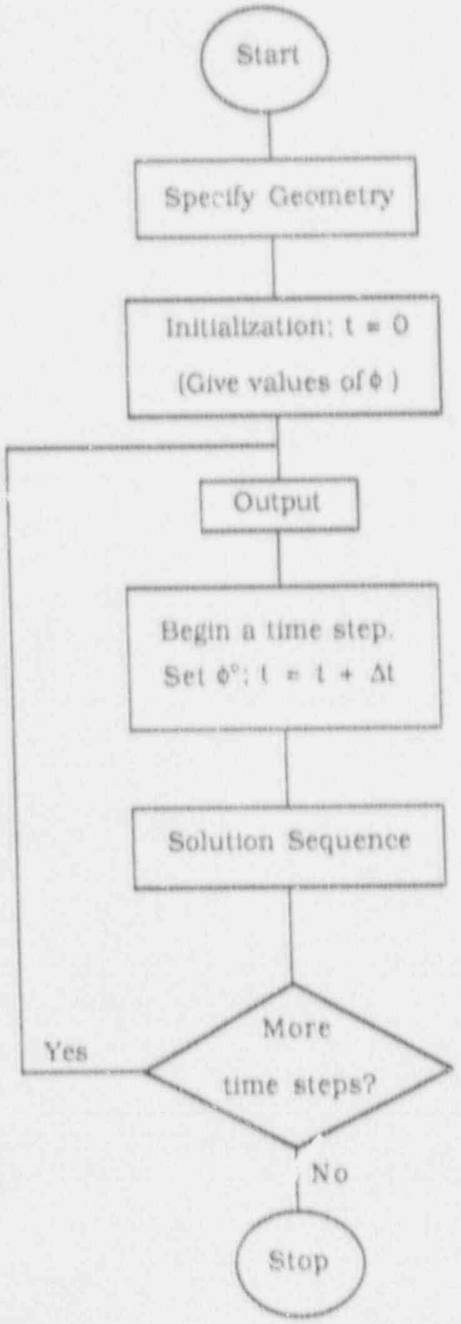

Fig. 48. COMMIX-1C flow chart

implicit ($\alpha = 0$) to fully implicit ($\alpha = 1$). But because we have not performed enough testing at this time, we do not recommend any value of α other than 1. The semi-implicit and the fully implicit schemes are described below in Secs. 10.2 and 10.3, respectively.

In COMMIX-1C, three matrix solvers are provided to solve the discretized equations; they are the successive overrelaxation (SOR) method, the Yale Sparse Matrix Package (YSMP), and the preconditioned Conjugate Gradient (PCG) method. All are incorporated in COMMIX-1C in a modular fashion so that the user has the flexibility of choosing any one of

the solvers for the pressure equation because the resulting matrix is symmetric. Either SOR or YSMP can be selected for the scalar transport equations. The three matrix solvers are described in Sec. 10.4. Iteration criteria for pressure equation and scalar transport equations are described in Sec. 10.5.

10.2 Fully Implicit (SIMPLEST-ANL) Solution Sequence ($\alpha = 1$)

The fully implicit solution sequence, named SIMPLEST-ANL, is based on a modification to the SIMPLE/SIMPLER procedures developed at the Imperial College in England. SIMPLEST/ANL requires less computer storage than SIMPLER and still has comparable or better computing efficiency. Because this procedure relieves many of the time-step size limitations and permits use of larger time-step sizes, it is most suitable for steady-state and transient calculations.

The procedure is called fully implicit because the new-time values of all variables are assumed to prevail during the time step. We therefore need an iterative procedure. Each outer* iteration loop yields a better estimate of the advanced-time values of all variables. When the change in all variable values becomes small from one outer iteration to the next, the iterative process is considered converged and the last outer iterate values are used for the advanced time-variable values. The solution sequence for the fully implicit formulation is a seven-step iterative process, as shown in Table 22.

10.3 Semi-Implicit Solution Sequence ($\alpha = 0$)

The semi-implicit solution sequence ($\alpha = 0$) used in the original version of COMMIX-1 is based on a modification of the ICE procedure developed at Los Alamos National Laboratory. The solution sequence is called semi-implicit because the old time values of some variables and parameters are assumed to prevail throughout the time-step period.

Because of the semi-implicit nature of the formulation, we are required to limit the size of the time step to obtain a stable solution. The time-step size must satisfy the Courant condition and must be less than the time-step sizes associated with all explicitly formulated terms. Thus,

$$\Delta t < \Delta t_{Courant} \sim \left(\frac{\Delta x_i}{u_i}\right)_{min}, \tag{10.2}$$

$$\Delta t < \Delta t_{vis} \sim C\left(\frac{\rho \Delta x_i^2}{\mu}\right)_{min}, \tag{10.3}$$

$$\Delta t < \Delta t_{cond} \sim C\left(\rho \frac{\Delta x_i^2}{\Gamma_h}\right)_{min}, \tag{10.4}$$

---

*Here, *outer iteration loop* is used to distinguish it from the inner iterative loops used for the solution of a specific variable equation, e.g., the iterative loop (successive overrelaxation procedure or the preconditioned conjugate gradient method) used for the solution of pressure equations is considered as an inner iterative loop.

Table 22. Fully implicit (SIMPLEST-ANL) solution sequence (α = 1)

1. *Calculate* velocity-pressure relation coefficients from the previous iterate values of u, v, and w:

   $\hat{\phi}, \hat{d}^{\phi} ; (\phi = u, v, w)$.

2. *Calculate* pressure equation coefficients using $\hat{\phi}, \hat{d}^{\phi}$:

   a_0^p, a_l^p, b_0^p.

3. *Solve* pressure equation for new-time, new-iterate pressure δP:

   $a_0^p \delta P_0 = \sum a_l^p \delta P_l + b_0^p$.

4. *Calculate* new-time, new iterate velocities u, v, w from velocity-pressure relations:

   $\phi = \hat{\phi} - \hat{d}^{\phi} \Delta \delta P ; (\phi = u, v, w)$

5. *Calculate* energy equation coefficients using new-time, new-iterate velocities:

   a_0^h, a_l^h, b_0^h.

6. *Solve* energy equation for new-time enthalpy h:

   $a_0^h h_0 = \sum a_l^h h_l + b_0^h$.

7. *Check* for convergence of u, v, w, h; if not converged, return to Step 1.

etc. Here, subscripts "Courant," "vis," and "cond" refer to time scales associated with Courant condition, viscous diffusion, and thermal diffusion, respectively, and subscript i refers to the three coordinate directions. The coefficient C has a value between 1/6 and 1/2. In most cases, the Courant limitation is the determining factor; Δt_{vis} and Δt_{cond} are usually much larger. The viscous-diffusion and thermal-diffusion time scales may require consideration only in the case of highly turbulent flow.

Although the semi-implicit scheme has time-step limitations, the solution of the equations requires less computer running time per time step. For fast transients, therefore, where the interest is in obtaining information at small time intervals, the semi-implicit sequence may be useful.

Details of the semi-implicit solution sequence are shown in Table 23.

10.4 Matrix Solvers

Of the three matrix solvers available in COMMIX-1C, SOR and PCG are iterative solvers, while YSMP is a direct solver and therefore requires no iteration. It should be noted that

Table 23. Semi-implicit (modified ICE) solution sequence ($\alpha = 0$)

1. *Calculate* momentum coefficients using old-time step values of u, v, and w:

   $\dot{\phi}, d^{\phi} ; (\phi = u, v, w)$.

2. *Calculate* pressure equation coefficients using $\dot{\phi}, d^{\phi}$:

   a_0^p, a_ℓ^p, b_0^p.

3. *Solve* pressure equation for new-time pressure δP^{n+1}:

   $a_0^p \delta P_0 - \sum a_\ell^p \delta P_\ell - b_0^p = 0$.

4. *Calculate* new-time velocities using

   $\phi = \dot{\phi} - d^{\phi} \Delta \delta P ; (\phi = u, v, w)$

   and new-time values of pressure.

5. *Calculate* energy equation coefficient using new-time values of velocities:

   a_0^h, a_ℓ^h, b_0^h.

6. *Calculate* new-time enthalpy h^{n+1}:

   $h_0 = \sum a_\ell^h h_\ell^h + b_0^h / a_0^h$.

both solution procedures, fully implicit and semi-implicit, require the solving of several sets of algebraic equations. These equations are solved by one or a combination of the three matrix solvers described in this section.

10.4.1 Successive Overrelaxation Iterative Solution

The successive overrelaxation (SOR) iteration scheme uses one pass through the computational cell domain. As each cell is visited, the residual of the ϕ-equation to be solved is computed, using the most recent values of the surrounding ϕ's. In this way, an updated value of ϕ is used if the neighboring cell has been visited earlier in the pass, and a previous iterate value of ϕ is used if the neighboring cell is to be visited later. Immediately after the residual of the ϕ equation for a cell under consideration is computed, the ϕ is adjusted in that cell before the computation proceeds to the next cell in the pass.

After all cells have been visited, the convergence is checked and if it has been achieved, the iterative process terminates; if convergence has not been achieved, another single-pass iteration is performed.

The SOR scheme requires the relaxation parameter ω to be between 0 and 2. Generally, convergence can be achieved in fewer iterations than for the Jacobi scheme.

Because ω can have values greater than 1.0, it is termed overrelaxation. The optimum value of the relaxation parameter is generally geometry- and problem-dependent; usually, it is between 1.4 and 1.8.

10.4.2 Yale Sparse Matrix Package

The YSMP is a collection of routines for solving the n x n system of linear algebraic equations[82] when the coefficient matrix is large and sparse. The package uses direct methods based on Gaussian elimination without pivoting. The coefficient matrix can be symmetric or nonsymmetric. The routines of YSMP decompose the coefficient matrix into triangular factors and then successively solve the triangular systems. Since the coefficient matrix is sparse, most entries of the coefficient matrix and the triangular factors are zero, and the routines take advantage of this by forming the decomposition and solving the triangular systems without storing or operating on zero entries. The advantage of YSMP is that it is a direct solver and no iteration is involved. It can solve symmetric and nonsymmetric matrices. However, as the number of computation cells is increased, both the storage and the work increase rapidly and other methods (SOR and PCG) become more economical and efficient.

10.4.3 Preconditioned Conjugate Gradient Method

The PCG is an iterative procedure that computes a sequence of approximate solutions to a system of linear algebraic equations. A number of preconditioned conjugate-gradient-like methods have been reported in the literature.[83] The conjugate gradient method employed in COMMIX-1C is an iterative procedure for solving symmetric, positive-definite systems; it requires no estimates of scalar parameters and is relatively inexpensive per step. These properties make the conjugate gradient method more robust, easier to implement, and more rapidly convergent than other iterative methods for solving symmetric, positive-definite problems. The convergence of the conjugate gradient method can be improved by preconditioning techniques.[83] Consider a linear system of the form

$$Mx = b, \tag{10.5}$$

where M is the coefficient matrix, and x, b are column vectors whose components are x_i, b_i ($i = 1, 2, \cdots, n$). Roughly speaking, preconditioning consists of solving a problem

$$Q^{-1} Mx = Q^{-1} b, \tag{10.6}$$

where Q is an approximation of M so that Eq. 10.6 is in some sense easier to solve than Eq. 10.5. The preconditioning technique employed in COMMIX-1C is the incomplete factorization of M. More detailed descriptions of the conjugate gradient methods and the preconditioning techniques can be found in Ref. 83.

10.4.4 Discussion

As described previously, the user has the flexibility of choosing any one or a combination of the three matrix solvers to solve the pressure equations and the scalar

Table 24. Properties of the three matrix solvers in COMMIX-1C

Matrix Solver	Coefficient Matrix	Scheme	Suitable for Pressure Eqs.	Suitable for Transport Eqs.
SOR	Symmetric/Nonsymmetric	Iterative	Yes	Yes
YSMP	Symmetric/Nonsymmetric	Direct	Yes	Yes
PCG	Symmetric	Iterative	Yes	No

transport (energy, turbulence kinetic energy, etc.) equations. Table 24 summarizes the properties of these matrix solvers and the type of equations each solver is suitable for. The pressure equations in COMMIX-1C are made symmetric and therefore can be solved by all three matrix solvers. The transport equations are nonsymmetric and therefore not suitable for PCG, but can be solved by either the SOR or the YSMP. Practically speaking, YSMP is more efficient for relatively small numbers of computational cells; it becomes less efficient when the number of computational cells is greater than 1000. When the number of computational cells exceeds 2000, PCG and SOR are more efficient and economical than YSMP. As a rough guide, YSMP should be used for all equations if the number of computational cells is less than 1000. If the number of computational cells is greater than 2000, PCG should be used to solve the pressure equations and SOR should be used to solve the scalar transport equations.

10.5 Iteration Criteria

In COMMIX-1C, there are two numerical schemes (fully implicit and semi-implicit) and three matrix solvers (SOR, YSMP, and PCG). The user can choose any combination of numerical scheme and the matrix solver for a given problem. If the fully implicit scheme ($\alpha = 1$) is selected, iteration criteria are required for the dependent variables to determine if further iteration is needed before advancing to the next time step. This is what we referred to as the outer iteration loop.

The seventh step (Table 22) in the fully implicit scheme is to check for convergence. Here, the changes from one iteration to the next, in all ϕ's, are checked against the convergence criteria. The iteration criteria are satisfied when

$$\frac{|\phi^{new} - \phi^{old}|_{max}}{\phi^{old}} < \varepsilon_3 ,$$

$$\frac{|U^{new} - U^{old}|_{max}}{V_{max}} < \varepsilon_3 ,$$

$$\frac{|V^{new} - V^{old}|_{max}}{V_{max}} < \varepsilon_3 , \text{ and}$$

$$\frac{|w^{new} - w^{old}|_{max}}{V_{max}} < \varepsilon_3 \qquad (10.7)$$

simultaneously. Here, V_{max} is the maximum velocity magnitude, ε_3 is a user input convergence parameter, and the superscripts "new" and "old" refer to current and previous iterate values. If any one of these convergence criteria is not met, the sequence is repeated from Step 1. The solution proceeds through the sequence until it converges or the specified maximum number of iterations have been performed. Here, ϕ again represents the general scalar transport variable (such as enthalpy, turbulence kinetic energy, etc.). It should be noted that iteration criteria are not needed for the semi-implicit scheme ($\alpha = 0$) because no iteration is involved during the solution sequence (Table 23).

Iteration criteria are also needed for the inner iteration loop if an iterative matrix solver is selected. The inner iteration loop solves the individual pressure and scalar transport equations within a given time step. If either SOR or PCG solver is selected, we will need a mass convergence criterion for the pressure equation and some other criteria for the scalar transport equations.

In theory, the pressure equation (Eq. 5.7) is considered solved when mass residue δ is equal to 0 for all cells. Because Eq. 5.7 is solved iteratively, this will, in general, never be true. Instead, a nonzero mass residual δ is computed for every cell and a maximum is determined as $|\delta|_{max}$. The iterative process continues until either a maximum specified number of iterations has been performed or the maximum mass residual falls below the convergence criterion.

$$|\delta|_{max} < \text{convergence criterion.} \qquad (10.8)$$

The mass convergence criterion is calculated using the relation

$$\text{Convergence criterion} = \varepsilon_1 * \left[\left(\frac{\rho \gamma_i u_i}{\gamma_v \Delta x_i}\right)_{max}\right] + \varepsilon_2 , \qquad (10.9)$$

where ε_1 and ε_2 are the input convergence constants, and subscript i stands for three coordinates.

The convergence criteria for the scalar transport equations in the inner iteration loop within a given time step are defined as

$$\frac{h_{ijk}^{m+1} - h_{ijk}^{m}}{h_{max}^{m} - h_{min}^{m}} \le \varepsilon_5 ,$$

$$\frac{k_{ijk}^{m+1} - k_{ijk}^{m}}{k_{max}^{m} - k_{min}^{m}} \le \varepsilon_6 ,$$

and

$$\frac{\varepsilon_{ijk}^{m+1} - \varepsilon_{ijk}^{m}}{\varepsilon_{max}^{m} - \varepsilon_{min}^{m}} \le \varepsilon_6 , \qquad (10.10)$$

Table 25. Convergence criteria for iterative scheme (fully implicit) and iterative matrix solvers (SOR and PCG) used in COMMIX-1C

Convergence Parameter	Default Value	Iteration Loop	Description
ε_1	10^{-4}	Inner	Mass convergence for pressure equations
ε_2	10^{-6}	Inner	Mass convergence for pressure equations
ε_3	5×10^{-5}	Outer	All transport variables
ε_5	10^{-5}	Inner	Enthalpy
ε_6	10^{-5}	Inner	Turbulence parameters k and ε

where the superscripts m and m+1 represent the previous and the current iterative values, respectively, the subscripts max and min represent the maximum and minimum values of the variable in the entire computational domain, and the subscript ijk indicates that the change in value of the variable from one iteration to the next is evaluated at the same location. The convergence criteria expressed by Eq. 10.10 means that if the change in value of a variable from one iteration to the next at any location divided by the maximum variation of that variable in the computational domain is equal to or smaller than some prespecified number ε, the solution is considered converged and no more iteration is required. Again, these criteria apply only to iterative matrix solvers such as SOR and PCG. If the direct solver YSMP is selected, these iteration criteria are not needed.

Table 25 summarizes the convergence criteria for the iterative scheme (fully implicit) and the iterative matrix solvers (SOR and PCG) and provides the default values of convergence parameters employed in COMMIX-1C.

11 Summary and Discussion

11.1 Major Features of COMMIX-1C

All important features of COMMIX-1C are briefly mentioned or described in detail in the text. Several features are unique and distinct from other computer codes. These features significantly expand the capabilities and increase the flexibility of COMMIX-1C. Five of these features are discussed here:

- Porous-medium formulation.
- Geometry modeling.

- Turbulence modeling.
- Flow-modulated skew-upwind discretization.
- Three matrix solvers.

11.1.1 Porous-Medium Formulation

In COMMIX, we use four parameters (volume porosity, directional surface porosity, distributed resistance, and distributed heat source or sink) to model a flow domain with solid objects. The inclusion of the parameter for directional surface porosity is relatively new. This inclusion has greatly facilitated the modeling of flow and heat transfer in an anisotropic medium and has improved the resolution and accuracy of numerical modeling.

The porous-medium formulation has been rigorously derived from the governing partial differential conservation equation. The derivations use the local-volume-averaging procedure. The resulting equations are more general. If we set directional surface porosity equal to the volume porosity in the formulation, the equations simplify to those for the conventional porous-medium formulation. Furthermore, if we set volume porosities and directional surface porosities to unity, and distributed resistances and heat sources to zero, then the new porous-medium formulation simplifies to that of the continuum formulation. We can therefore say that the continuum formulation is a subset of the conventional porous-medium formulation, which is a further subset of the present porous-medium formulation.

It is worth stressing here that the porous-medium formulation has provided a wide range of applicability to the COMMIX code and can be used to treat irregular geometries that are often encountered in most engineering applications. We can now analyze

- A single-component system, such as a
  - fuel assembly
  - reactor plenum,
  - piping system,
  - etc.,

as well as

- A multicomponent system, such as a
  - vessel,
  - downcomer and lower plenum,
  - cold leg, high-pressure injection system, downcomer,
  - etc.

in sufficient detail.

11.1.2 Geometry Modeling

Unique features related to geometry modeling are:

- *Identification of a computational cell by a cell number instead of its (i,j,k) location*: All "do loops" are performed with the cell number as an index

instead of with the conventional directional indices i,j,k. Consequently, the storage requirement depends on the total number of computational cells and not on the dimension of IMAX*JMAX*KMAX. This is illustrated through a simple example in Fig. 49.

- *Use of surface arrays to store boundary values at the boundary surface*: We do not use fictitious boundary cells to store boundary values.

- *Extra surface to model irregular geometry*: An irregular surface is defined as a surface that is at an angle to a grid plane. An irregular surface is an additional surface to the six normal surfaces (parallel to grid planes) of a computational cell. We also account for heat transfer in the energy equation and shear stress in the momentum equation from this seventh irregular surface, in addition to those from the six normal surfaces. This treatment of an irregular surface as an additional surface facilitates proper modeling of a complex irregular geometry.

11.1.3 Turbulence Modeling

Almost all flows in an engineering system are turbulent. For a computer code to realistically simulate a flow process, the code must account for the effects of turbulence. COMMIX-1C accounts for the effects of turbulence through

- Distributed resistance modeling and

- Turbulence modeling.

For many geometries and flow conditions, the experimentally verified resistance correlations, which include the effects of turbulence, are available in the literature, e.g., flow in a tube, flow normal to a rod bundle, flow through an orifice, etc. For such regions of a system, we employ appropriate correlations through distributed resistance modeling and can provide a realistic account of turbulence.

For geometries where correlations are not available, we have provided the following options in COMMIX-1C:

- Constant turbulent diffusivity model and

- k-ε two-equation turbulence model.

With the k-ε two-equation turbulence model and the distributed resistance model, one can perform a very realistic simulation of turbulence flow in any flow geometry system.

11.1.4 Options for Reducing Numerical Diffusion

In the finite-difference formulation, the even derivative terms of the truncation error have a general tendency to reduce the gradients, producing what is known as numerical diffusion. For high Peclet number flows and for flow parallel to grid lines, numerical diffusion is generally small. However, for multidimensional flow oblique to grid lines, the effects due to numerical diffusion can be significant.

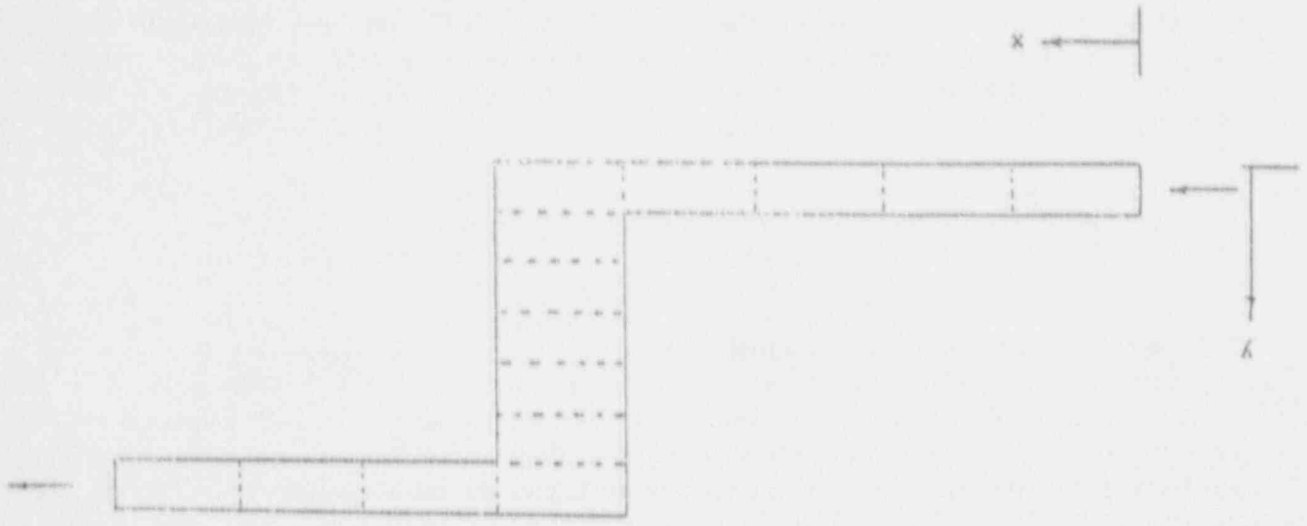

IMAX = 8
JMAX = 7
Total number of cells = 14
Conventional storage requirements = 8 x 7 = 56
Storage Requirement in COMMIX-1C = 14

Fig. 49. Grid arrangement in two-dimensional piping system, illustrating storage requirements in COMMIX-1C

To provide a more realistic and accurate solution, we have implemented an additional option, the flow-modulated skew-upwind discretization (FMSUD) scheme in COMMIX-1C. The FMSUD scheme has been demonstrated to reduce numerical diffusion when the velocity is oblique to grid lines and it does not produce physically unrealistic overshoots and undershoots.

11.1.5 Matrix Solvers

In COMMIX-1C, we have three matrix solvers:

- Successive overrelaxation (SOR) method,
- Yale Sparse Matrix Package (YSMP), and
- Preconditioned conjugate gradient (PCG) method

These matrix solvers are used to solve the individual discretized equations (pressure and scalar transport equations) in the inner iteration loop.

The SOR and YSMP solvers are suitable for both symmetric and nonsymmetric matrices, while the PCG method is limited to symmetric matrices only. Thus, the SOR and YSMP are applicable to both the pressure and the scalar transport equations, while the PCG

method is limited to the pressure equation only. Both the SOR and the PCG methods are iterative, while the YSMP is a direct solver and no iteration is involved. In general, if the number of computational cells is less than 1,000, YSMP should be used. On the other hand, if the number of computational cells is greater than 2,000, the SOR or PCG method should be selected.

The three matrix solvers significantly increase the flexibility and efficiency of COMMIX-1C for the numerical computation of a wide class of engineering problems.

11.2 Code Application and Validation

The COMMIX series of codes has been tested and applied to a variety of problems. Detailed descriptions and numerical results of problems that we have analyzed are provided in published ANL technical reports and in papers in technical journals.[4-39] We have also compared numerical results with available experimental measurements. Major applications in the nuclear power area include analyses and simulations of fuel assemblies, reactor upper plenum, reactor downcomer and lower plenum, cold-leg high-temperature injection system and downcomer, and reactor vessel. Applications of COMMIX-1C are mainly in the area of natural circulation in pressurized water reactor.[40,41] A number of simulations were performed to investigate the natural circulation phenomena during a postulated transient of both the Zion (four-loop) plant and the Surry (three-loop) plant. The numerical results are in general agreement with experimental observations.[40,41]

Validation of the k-ε two-equation turbulence model in COMMIX-1C were carried out by comparing the calculated results with experimental data on three relatively simple geometrical systems, i.e., (1) fully developed pipe flow, (2) two-dimensional single sudden expansion, and (3) axisymmetric buoyant jet. The results indicate that COMMIX-1C is capable of predicting these simple turbulent flows in general agreement with experimental data.[73]

It should be noted that validation and assessment is an integral part of the code development process. More validation and assessment will be added to the present collection of problems as time goes on. User feedback is welcome and will enhance the code development process.

11.3 Future Developments

Numerical simulation programming is a very active and developing field. New physical models and better solution procedures are expected to emerge. COMMIX will, therefore, continue to evolve. Listed below are possible developments that, if incorporated, will further augment the capabilities of COMMIX.

11.3.1 Single-Phase Development

New single-phase capabilities that are desirable for future implementation are:

- *Extension of the Flow-Modulated Skew-Upwind Discretization Scheme to Include the Momentum and Turbulence Equations*: As described previously, a flow-modulated skew-upwind discretization scheme (FMSUD) is implemented in COMMIX-1C in the energy equation. The numerical results indicate that this new scheme is able to reduce numerical diffusion without causing physically unrealistic overshoots/undershoots. There is a need to extend the FMSUD scheme to the momentum and turbulence equations to further reduce numerical diffusion when the flow is inclined to the grid lines.

- *Multispecies Transport*: During the later stage of a postulated reactor accident, hydrogen may be present simultaneously with steam in the reactor vessel. To predict this phenomenon accurately, a multispecies transport model is required. This will involve adding one or more transport equations in COMMIX-1C.

- *Anisotropic Turbulence Model for Natural Circulation*: The k-ε two-equation turbulence model in COMMIX-1C is valid only for isotropic turbulence. Natural circulation, which occurs in a reactor system under postulated accident conditions, is not isotropic. To improve the accuracy of COMMIX calculations, an anisotropic turbulence model (such as the Reynolds stress or the algebraic stress model) needs to be developed and implemented in COMMIX.

- *Treatment of Irregular Geometry*: Modeling of systems with irregular geometry is always a challenging problem. Improvement over the current treatment of irregular geometry in COMMIX can be made by using the boundary-fitted coordinate system or some kind of hybrid system combining finite-element and finite-volume approaches.

- *Automatic Time-Step Selection Logic and Implementation into COMMIX-1C*: Another important addition is the development of an automatic time-step selection logic and implementation into the COMMIX-1C code. The automatic time-step selection logic will provide a maximum time-step size to shorten the computer running time. At present, the user must specify the time-step size, which is not known a priori.

- *Implicit Treatment of Gravity Term in the z-momentum Equation*: When buoyancy is important, such as natural circulation in a postulated accident in a pressurized water reactor (PWR), it may be helpful to treat the density implicitly in the z-momentum equation. This is accomplished by integrating the gravity term over the momentum control volume in the following manner:

$$\int \rho g_z \, dxdydz = \bar{\rho} \bar{V}_0 g_z, \tag{11.1}$$

where $\bar{V}_0$ is the characteristic volume of the staggered mesh defined by Eq. 4.47, and $\bar{\rho}$ is an average density given by

$$\bar{\rho} = \frac{\Delta z_0 \rho_0 + \Delta z_6 \rho_6}{\Delta z_0 + \Delta z_6}. \tag{11.2}$$

To express $\bar{\rho}$ implicitly in the z-momentum equation, we assume

$$\bar{p} = \bar{p}^n + \frac{\partial \bar{p}}{\partial W_0}\left(W_0 - W_0^n\right), \tag{11.3}$$

where the superscript n refers to the old time value and n+1 refers to the new time value, which is omitted for convenience (as we have done throughtout this report). The term containing the new time value W_0 in Eq. 4.54 can be absorbed in the left side of the general finite-volume equation, Eq. 4.38. We must still evaluate $(\partial \bar{p}/\partial W)$, which is given by

$$\frac{\partial \bar{p}}{\partial W_0} = \frac{\Delta z_0}{\Delta z_0 + \Delta z_\theta}\left(\frac{\partial \rho_0}{\partial W_0}\right) + \frac{\Delta z_\theta}{\Delta z_0 + \Delta z_\theta}\left(\frac{\partial \rho_\theta}{\partial W_0}\right), \tag{11.4}$$

in view of Eq. 4.53. $(\partial \bar{p}_0/\partial W_0)$ and $(\partial \bar{p}_\theta/\partial W_0)$ can be expressed approximately by

$$\frac{\partial \rho_0}{\partial W_0} = \left(\frac{\partial \rho}{\partial h}\right)_0 \left(\frac{\partial h_0}{\partial W_0}\right), \tag{11.5}$$

$$\frac{\partial \rho_\theta}{\partial W_0} = \left(\frac{\partial \rho}{\partial h}\right)_\theta \left(\frac{\partial h_\theta}{\partial W_0}\right). \tag{11.6}$$

At present, both $(\partial h_0/\partial W_0)$ and $(\partial h_\theta/\partial W_0)$ are evaluated as follows:

$$W_0 \geq 0 \quad \frac{\partial h_0}{\partial W_0} = 0; \quad \frac{\partial h_\theta}{\partial W_0} = \frac{-A_0\rho_0}{\left(a_0^h\right)_\theta}(h_\theta - h_0), \tag{11.7}$$

$$W_0 < 0 \quad \frac{\partial h_0}{\partial W_0} = -\frac{A_0\rho_\theta}{\left(a_0^h\right)_0}(h_\theta - h_0); \quad \frac{\partial h_\theta}{\partial W_0} = 0. \tag{11.8}$$

Based on the numerical results obtained thus far with the implicit treatment as proposed here, it appears that convergence rate for the analyses of natural circulation has been improved in some cases. Additional work in this area is needed to ensure further improvement of convergence rate for all buoyancy-driven flows.

- *Free-Surface Boundary Condition*: Currently, COMMIX-1C does not have a free-surface boundary condition option. With implementation of this additional capability, one could apply the COMMIX computer code to the analysis of free-surface problems, e.g., pool-type reactors.

- *Transient Three-Dimensional Heat Conduction Equation for Solid Structures*: At present in COMMIX-1C, we solve the one-dimensional transient heat conduction equation to account for thermal inertia of submerged solid structures. We therefore assume that heat conduction in an axial direction is negligible. In most analyses, this is a valid assumption. But to extend the range of applicability, one must implement an option that will permit use of a three-dimensional heat conduction equation for structures where axial heat conduction is not negligible.

- *Vectorizing for Supercomputers*: Recently there has been a significant development in the area of vectorizing and parallel processing. These developments have increased the speed of computing by several orders of magnitude. Vectorizing COMMIX for adaptation to recent supercomputers will enhance the speed of COMMIX simulations.

- *Input/Output Processing*: COMMIX is a very large computer code with a wide range of generalities and applicabilities. Consequently, input preparation and output processing often become very tedious. Further developments and efforts are needed to make COMMIX a more user-friendly computer program.

11.3.2 Two-Phase and Multiphase Development

Concurrent with the development of the COMMIX-1C code, efforts have been made to develop a two-phase or multiphase code, using a two-fluid or multifluid model to analyze two-phase or multiphase flows. In developing the two-phase or multiphase fluid model, we will place emphasis on

- Developing a stable solution algorithm for the whole range of applications.

- Developing an efficient numerical scheme and taking full advantage of current computer architecture.

- Minimizing the requirements of computer storage.

- Validating physical models with appropriate experimental data.

Acknowledgments

The authors want to thank Drs. Y. Chen, J. Han, R. Meyers, R. Wood, and F. Altawila of the Office of Nuclear Regulatory Research, U.S. Nuclear Regulatory Commission, for supporting this work (A22559). Stimulating discussions with Dr. M. Bottoni on the Flow Modulated Skew-Upwind Discretization Scheme is also acknowledged.

References

1. W. T. Sha, H. M. Domanus, R. C. Schmitt, J. J. Oras, and E. I. H. Lin, *COMMIX-1: A Three-Dimensional Transient Single-Phase Component Computer Program for Thermal-Hydraulic Analysis*, NUREG/CR-0785, Argonne National Laboratory Report ANL-77-96 (Sept. 1978).

2. H. M. Domanus, R. C. Schmitt, W. T. Sha, and V. L. Shah, *COMMIX-1A: A Three-Dimensional Transient Single-Phase Computer Program for Thermal Hydraulic Analysis of Single and Multicomponent Systems: Vol. I User's Manual, and Vol. II Assessment and Verification*, NUREG/CR-2896, Argonne National Laboratory Report ANL-82-25 (Dec. 1983).

3. Analytical Thermal Hydraulic Research Program, *COMMIX-1B: A Three-Dimensional Transient Single-Phase Computer Program for Thermal Hydraulic Analysis of Single and Multicomponent Systems: Vol. I Equations and Numerics, Vol. II User's Manual*, NUREG/CR-4348, Argonne National Laboratory Report ANL-85-42 (Sept. 1985).

4. W. T. Sha, H. M. Domanus, R. C. Schmitt, and K. Chen, *Three-Dimensional Numerical Simulation of LMFBR Outlet Plenum Mixing*, Trans. Am. Nucl. Soc., **26**, pp. 434-435 (June 1977).

5. H. M. Domanus, R. C. Schmitt, and W. T. Sha, *Numerical Results Obtained from the Three-Dimensional Transient Single-Phase Version of the COMMIX Computer Code*, NUREG-0355, Argonne National Laboratory Report ANL-CT-78-3 (Oct. 1977).

6. H. M. Domanus, R. C. Schmitt, and W. T. Sha, *Three-Dimensional Numerical Simulation of a 19-Pin LMFBR Fuel Assembly in a Hexagonal Duct*, Trans. Am. Nucl. Soc. **28**, pp. 540-543 (June 1978).

7. H. M. Domanus and W. T. Sha, *Numerical Results for a Hexagonal Fuel Assembly with a Planar Blockage using the COMMIX-1A Computer Code*, NUREG/CR-0483, Argonne National Laboratory Report ANL-CT-79-8 (Sept. 1978).

8. H. M. Domanus and W. T. Sha, *Three-Dimensional Numerical Simulation of Flow Blockage in a 129-Pin LMFBR Fuel Assembly*, Trans. Am. Nucl. Soc. **30**, pp. 534-535 (Nov. 1978).

9. W. T. Sha, H. M. Domanus, and R. C. Schmitt, *Some Numerical Results Obtained from the Single-Phase Version of the COMMIX Code*, Proc. IAEA Specialists' Meeting on Thermodynamics of FBR Fuel Assemblies under Nominal and Non-Nominal Operating Conditions, Karlsruhe, West Germany (Feb. 2-7, 1979).

10. H. M. Domanus, M. J. Chen, and W. T. Sha, *Analysis of a Loss-of-Piping Integrity Transient in an LMFBR Fuel Assembly*, Trans. Am. Nucl. Soc. **32**, pp. 827-829 (June 1979).

11. H. M. Domanus, M. J. Chen, and W. T. Sha, *Pretest Prediction of the W-1 SLSF Experiment using the COMMIX-1A Computer Code*, NUREG/CR-0816, Argonne National Laboratory Report ANL-CT-79-33 (May 1979).

12. H. M. Domanus, M. J. Chen, and W. T. Sha, *Simulation of a 7-Pin Bundle During a Flow-Rundown Transient*, Trans. Am. Nucl. Soc. **33**, pp. 630-532 (Nov. 1979).

13. W. T. Sha, H. M. Domanus, R. C. Schmitt, J. J. Oras, and E. I. H. Lin, *A New Approach for Rod-Bundle Thermal-Hydraulic Analyses*, Proc. of International Meeting on Nuclear Power Reactor Safety, Brussels, October 16-19, 1978; Nuclear Technology, **46**, pp. 268-280 (Dec. 1979).

14. H. M. Domanus, M. J. Chen, and W. T. Sha, *Computational Results for a 7-Pin Hexagonal Fuel Assembly during a Flow Rundown Transient using the COMMIX-1A Computer Code*, NUREG/CR-1285, Argonne National Laboratory Report ANL-CT-80-10 (Jan. 1980).

15. H. M. Domanus, M. J. Chen, T. M. Kuzay, and W. T. Sha. *Numerical Simulation of the 6MW P2 Transient Free Convection Test using the COMMIX-1A Computer Code*, Proc. of the Specialists' Meeting on Decay Heat Removal and Natural Convection in FBRs (Feb. 1980).

16. M. J. Chen, H. M. Domanus, and W. T. Sha, *Simulation of a Thermohydraulic Transient in a Pipe Using the COMMIX-1A Computer Code*, NUREG/CR-1323, Argonne National Laboratory Report ANL-CT-80-15 (Feb. 1980).

17. H. M. Domanus and W. T. Sha, *Simulation of the CRBR Upper Plenum under Thermal Stratification Conditions*, Trans. Am. Nucl. Soc **34**, pp. 884-887 (June 1980).

18. M. J. Chen, H. M. Domanus, and W. T. Sha, *Numerical Thermal Hydraulic Simulation of an LMFBR Pipe during a Flow Coastdown*, Trans. Am. Nucl. Soc **35**, pp. 673-674 (Nov. 1980).

19. H. M. Domanus, V. L. Shah, and W. T. Sha, *Applications of the COMMIX Code using the Porous Medium Formulation*, Nucl. Engr. & Des. (Special Issue on LMFBR Single-Phase Rod Bundle Thermal Hydraulics) (Dec. 1980).

20. H. P. Fohs, R. W. Lyczkowski, and W. T. Sha, *A Three-Dimensional Simulation of Diversion Cross-Flow between Two Parallel Channels Connected by a Narrow Lateral Slot using the COMMIX-1A Computer Program*, Argonne National Laboratory Report ANL-CT-81-34 (Oct. 1981).

21. H. M. Domanus and W. T. Sha, *Numerical Simulation of Combined Natural and Forced Convection during Thermal Hydraulic Transients*, Proc. of 74th Annual Meeting of AIChE (Nov. 1981).

22. R. W. Lyczkowski, H. M. Domanus, R. C. Schmitt, W. T. Sha, J. H. Kim, and K. H. Sun, *Prediction of Thermal Stratification in the Cold Leg of a PWR during a LOCA*, Trans. Am. Nucl. Soc. **39**, pp. 1057-1058 (Nov. 1981).

23. R. W. Lyczkowski, W. L. Baumann, H. M. Domanus, W. T. Sha, and J. H. Kim, *Analysis of B&W/EPRI Thermal Mixing Experiments for OCONEE1 PWR using COMMIX-1A*, Trans. Am. Nucl. Soc. **39**, pp. 1062-1063 (Nov. 1981).

24. S. P. Vanka, H. M. Domanus, and W. T. Sha, *COMMIX-1A Three-Dimensional In-Vessel Simulation of the FFTF Thermal Hydraulics*, NUREG/CR-2535, Argonne National Laboratory Report ANL-CT-82-1 (Jan. 1981).

25. S. P. Vanka, H. M. Domanus, and W. T. Sha, *COMMIX-1A Three-Dimensional In-Vessel Simulation of the FFTF Transient Thermal Hydraulics*, NUREG/CR-2772, Argonne National Laboratory Report ANL-CT-82-14 (July 1982).

26. R. W. Lyczkowski, J. R. Hull, C. C. Miao, H. M. Domanus, R. C. Schmitt, and W. T. Sha, *Three-Dimensional Modeling of Thermal and Fluid Mixing in PWR's during High Pressure Coolant Injection*, Trans. Am. Nucl. Soc. **41**, pp. 261-263 (June 1982).

27. S. P. Vanka, H. M. Domanus, and W. T. Sha, *Steady State Simulation of the FFTF In-Vessel Thermal Hydraulics*, Trans. Am. Nucl. Soc. **41**, pp. 703-706 (June 1982).

28. W. T. Sha, A. Amorosi, S. S. Borys, P. R. Huebotter, J. R. Hull, and R. M. Singer, *Three-Dimensional Analysis of LMFBR Decay Heat Removal System*, Proc. International Topical Meeting on LMFBR Safety and Related Design and Operational Aspects, Lyon-Ecully, France (July 1982).

29. W. L. Baumann, H. M. Domanus, M. Mohr, W. T. Sha, R. C. Schmitt, and J. E. Sullivan, *In-Vessel Thermal Hydraulic Analysis*, Proc. IAHR Specialists Meeting on Liquid Metal Thermal Hydraulics in Plena and Pipes, Sunnyvale, CA (Jan. 1983).

30. W. L. Baumann, H. M. Domanus, and W. T. Sha, *EBR-II In-Vessel Thermal-Hydraulic Transient Simulation using COMMIX-1A Computer Code*, Trans. Am. Nucl. Soc. **43**, pp. 499-501 (Nov. 1982).

31. W. T. Sha, W. L. Baumann, H. M. Domanus, R. C. Schmitt, and J. E. Sullivan, *In-Vessel Thermal Hydraulic Analysis*, Proc. of IAHR Specialists Mtg. on Liquid Metal Thermal Hydraulics in Plena and Pipes, Sunnyvale, CA (Jan. 1983).

32. W. T. Sha, *A Unified Approach for Thermal Hydraulic Numerical Simulation*, Proc. of ASME International Meeting on Modeling and Simulation, Bermuda (Mar. 1983).

33. B. C-J. Chen, B. K. Cha, C. C. Miao, W. T. Sha, J. H. Kim, and B. K. H. Sun, *COMMIX-1A Analysis of Fluid and Thermal Mixing in a Model Cold Leg and Downcomer of a PWR*, Canadian Nuclear Society Numerical Methods in Nuclear Engineering Conf., Montreal (Sept. 6-9, 1983).

34. F. F. Chen, H. M. Domanus, and W. T. Sha, *Turbulence Modeling of Thermal and Fluid Mixing in PWRs during High Pressure Coolant Injection using COMMIX-1B*, Canadian Nuclear Society Numerical Methods in Nuclear Engineering Conf., Montreal (Sept. 6-9, 1983).

35. R. W. Lyczkowski, C. C. Miao, J. R. Hull, H. M. Domanus, R. C. Schmitt, and W. T. Sha, *Three-Dimensional Analysis of Thermal and Fluid Mixing for Creare Scaled Experiments and Generic Full-Scale PWR's*, EPRI Interim Report RP-1749-2 (Sept. 1983).

36. F. F. Chen, H. M. Domanus, W. T. Sha, and V. L. Shah, *Turbulence Modeling in the COMMIX Computer Code*, Argonne National Laboratory Report ANL-83-65 (March 1984).

37. C. C. Miao, R. W. Lyczkowski, G. K. Leaf, F. F. Chen, B. K. Cha, B. C-J. Chen, H. M. Domanus, W. T. Sha, and V. L. Shah, *A Volume-Weighted Skew-Upwind Difference Scheme in COMMIX*, NUREG/CR-35605, EPRI NP-3547, Argonne National Laboratory Report ANL-83-66 (March 1984).

38. R. W. Lyczkowski, C. C. Miao, H. M. Domanus, J. R. Hull, W. T. Sha, and R. C. Schmitt, *Three-Dimensional Analysis of Thermal and Fluid Mixing in Cold Leg and Downcomer of PWR Geometries*, EPRI NP-3321 (Dec. 1983).

39. W. T. Sha and V. L. Shah, *Natural Convection Phenomena in a Prototypic PWR during a Postulated Degraded Core Accident*, NP-6324-D, Electric Power Research Institute, Nuclear Power Division, Palo Alto, CA (1989).

40. H. M. Domanus and W. T. Sha, *Analysis of Natural Convection Phenomena in a 3-Loop PWR during a TMLB' Transient Using the COMMIX Code*, NUREG/CR-5070, Argonne National Laboratory Report ANL-87-54 (Jan. 1988).

41. Y. S. Cha, H. M. Domanus, K. V. Liu, R. C. Schmitt, W. T. Sha, and V. L. Shah, *Numerical Simulation of Natural Circulation Phenomena in a PWR During TMLB' Transients Prior to Core Damage*, NUREG/CR-5274, Argonne National Laboratory Report ANL-88-47 (May 1989).

42. W. T. Sha, H. M. Domanus, R. C. Schmitt, J. J. Oras, and E. I. H. Lin, *A New Approach for Rod-Bundle Thermal-Hydraulic Analysis*, Proc. International Meeting on Nuclear Power Reactor Safety, Brussels, Belgium (Oct. 1978), Nuclear Technology, 46, pp. 268-290 (Dec. 1979).

43. W. T. Sha and B. T. Chao, *Conservation Equations for Finite Control Volume Containing Single-Phase Fluid with Fixed, Dispersed, and Heat Generating (or Absorbing) Solids*, NUREG/CR-0945, Argonne National Laboratory Report ANL-CT-79-42 (July 1979).

44. W. T. Sha and J. C. Slattery, *Local Volume-Time Averaged Equations of Motion for Dispersed, Turbulent, Multiphase Flows*, NUREG/CR-1491, Argonne National Laboratory Report ANL-80-51 (Nov. 1980).

45. W. T. Sha and B. T. Chao, *Local Volume-Averaged Transport Equations for Single-Phase Flow in Regions Containing Fixed, Dispersed, Heat-Generating (or Absorbing) Solids*, NUREG/CR-1969, Argonne National Laboratory Report ANL-80-124 (April 1981).

46. W. T. Sha, *A New Porous Media Approach for Thermal Hydraulic Analysis*, Trans. Am. Nucl. Soc. **39**, pp. 510-512 (Nov. 1981).

47. W. T. Sha, B. T. Chao, and S. L. Soo, *Local Volume-Averaged Transport Equations for Multiphase Flow in Regions Containing Distributed Solid Structures*, NUREG/CR-2354, Argonne National Laboratory Report ANL-81-69 (Dec. 1981).

48. W. T. Sha, B. T. Chao, and S. L. Soo, *Time Averaging of Local Volume-Averaged Conservation Equations of Multiphase Flow*, NUREG/CR-3434, Argonne National Laboratory Report ANL-83-49 (July 1983).

49. W. T. Sha, B. T. Chao, and S. L. Soo, *Time-Averaging of Local Volume-Averaged Conservation Equations of Multiphase Flow*, Proc. AIChE/ASME National Heat Transfer Conf., Seattle (July 25-29, 1983).

50. W. T. Sha, B. T. Chao, and S. L. Soo, *Porous Media Formulation for Multiphase Flow with Heat Transfer*, Nuclear Engineering and Design (Special Issue on LMFBR Two-Phase Rod Bundle Thermal Hydraulics), **82**, pp. 93-106 (Oct. 1984).

51. W. T. Sha, B. T. Chao, and S. L. Soo, *Time- and Volume-Averaged Conservation Equations for Multiphase Flow, Part One: System without Internal Solid Structures*, NUREG/CR-3989, Argonne National Laboratory Report ANL-84-66 (Dec. 1984).

52. F. H. Harlow and A. A. Amsden, *A Numerical Fluid Dynamics Calculation Method for All Flow Speeds*, J. Comp. Phys. **8**, p. 197, (1971).

53. F. H. Harlow and A. A. Amsden, *Numerical Calculation of Multiphase Fluid Flow*, J. Comp. Phys. **17**, pp. 19–52 (1975).

54. F. H. Harlow and A. A. Amsden, *Flow of Interpenetrating Material Phases*, J. Comp. Phys. **18**, pp. 440–464 (1975).

55. S. V. Patankar, *Numerical Heat Transfer and Fluid Flow*, Numerical Heat Transfer, Vol. 2, McGraw-Hill, New York (1979).

56. A. Padilla, Jr. and D. S. Rowe, *A Donor Flow Formulation for Momentum Flux Differencing*, Trans. Am. Nucl. Soc. **46**, pp. 851–852 (1984).

57. L. Prandtl, *Berich uber Untersuchungen zer ansgebil-derter Turbulenz*, ZAMM, **5**, pp. 136–139 (1925).

58. L. Prandtl, *Nach. Akad. Wiss. Goett. Math-Phys. Kl.* (1945), translated as Jet Propul. Laboratory Publication 13 (1952).

59. F. H. Harlow and P. I. Nakayama, *Transport of Turbulence Energy Decay*, Los Alamos Scientific Laboratory Report LA-3854/UC-34 Physics/TID-4500 (1968).

60. W. P. Jones and B. E. Launder, *The Prediction of Laminarization with a 2-equation Model of Turbulence*, Int. J. Heat Mass Trans. **15**, pp. 301–313 (1982).

61. P. Y. Chou, *On Velocity Correlation and Solution of the Equations of Turbulent Fluctuations*, Q. J. Mech. App. Math. **3**, pp. 38–54 (1945).

62. K. Hanjalic and B. E. Launder, *A Reynolds-Stress Model of Turbulence and its Application to Asymmetric Shear Flows*, J. Fluid Mech. **52**, pp. 609–638 (1972).

63. B. E. Launder, G. J. Reese, and W. Rodi, *Progress in the Development of a Reynolds-Stress Turbulent Closure*, J. Fluid Mech. **68**, pp. 537–566 (1975).

64. J. Rotta, *Statistische Theorie Nichthomogener Turbulenz*, Zeitsch. für Physik **129**, p. 547 (1951).

65. W. T. Sha and B. E. Launder, *A General Model for Turbulent Momentum and Heat Transport in Liquid Metals*, Argonne National Laboratory Report ANL-77-78 (1979).

66. R. Nijsing and W. Eifler, *Temperature Fields in Liquid Metal Cooled Assemblies*, Prog. Heat Mass Transfer **7**, p. 115 (1973).

67. B. E. Launder and D. B. Spalding, *Lectures in Mathematical Models of Turbulence*, Academic Press (1972).

68. V. S. Arpaci and P. S. Larsen, *Convective Heat Transfer*, Prentice-Hall, Englewood Cliffs, NJ (1974).

69. B. J. Daley and F. H. Harlow, *Transport Equation in Turbulence*, Physics of Fluids **13**, pp. 2634–2649 (1970).

70. J. J. Lumley and B. J. Khajeh-Nouri, *Computational Modeling of Turbulent Transport*, Adv. Geophysics **18A**, pp. 169–192 (1974).

71. B. E. Launder, A. Morse, W. Rodi, and D. B. Spalding, *The Prediction of Free Shear Flows—A Comparison of the Performance of Six Turbulent Models*, Proc. of NASA Conference on Free Shear Flows, Langbery (1972).

72. M. Ciofalo and M. W. Collins, *k-ε Predictions of Heat Transfer in Turbulent Recirculation Flows Using an Improved Wall Treatment*, Numerical Heat Transfer, Part B, **15**, pp. 21–49 (1989).

73. Y. S. Cha, H. M. Domanus, and W. T. Sha, *Validation and Assessment of the k-ε Two-Equation Turbulence Model in the COMMIX Code*, Argonne National Laboratory Report ANL/ATHRP-42 (Feb. 1990).

74. The 1980–1981 AFOSR-HTTM-Stanford Conference on Complex Turbulent Flows, S. J. Kline, B. J. Cantwell, and G. M. Lilley, eds, published by Thermosciences Division, Mechanical Engineering Dept., Stanford University, Stanford, CA (1982).

75. J. N. Lillington, *A Vector Upstream Differencing Scheme for Problems in Fluid Flow Involving Significant Source Terms in Steady-State Linear Systems*, Int. J. for Numer. Methods Fluids **1**, pp. 3–16 (1981).

76. G. D. Raithby, *Skew Upstream Differencing Schemes for Problems Involving Fluid Flow*, Comp. Methods Appl. Mech. Eng. **9**, pp. 153–164 (1976).

77. S. V. Patankar, *Numerical Heat Transfer and Fluid Flow*, Hemisphere Publishing Corp. (1980).

78. M. A. Leschziner, *Practical Evaluation of Three Finite Difference Schemes for the Computation of Steady-State Recirculatory Flows*, Comp. Methods Appl. Mech. Eng. **23**, pp. 293–312 (1980).

79. Y. A. Hassan, J. G. Rice, and J. H. Kim, *A Stable Mass Flow Weighted Two-Dimensional Skew-Upwind Scheme*, Numer. Heat Transfer **6**, p. 395–408 (1983).

80. Y. A. Hassan, *Implementation of a Mass-Flow-Weighted Skew-Upwind Differencing Scheme in COMMIX-1A*, EPRI NP-3518, Prepared by Babcock and Wilcox Co., Lynchburg, VA (1984).

81. W. T. Sha and V. L. Shah, *Some Resistance Correlations for COMMIX Users*, Argonne National Laboratory Report ATHRP-13 (1983).

82. S. C. Eisenstat, M. C. Gursky, M. H. Schultz, and A. H. Sherman, *Yale Sparse Matrix Package, II. The Nonsymmetric Codes*, Research Report #114, Dept of Computer Science, Yale University (1977).

83. H. C. Elman, *Iterative Methods for Large, Sparse, Nonsymmetric Systems of Linear Equations*, Ph.D. Dissertation, Yale University (May 1982).

Distribution for NUREG/CR- 5649 Vol. I (ANL-90/33 Vol. I)

Internal:

M. Bottoni
Y. S. Cha
T. H. Chien
H. M. Domanus
E. M. Gelbard
G. K. Leaf
C. A. Malefyt
R. C. Schmitt
W. T. Sha (21)
C. E. Till
R. A. Valentin
R. W. Weeks
ANL Patent Dept.
ANL Contract File
TIS Files (3)

External:

NRC, Washington, for distribution per R7 (250)
ANL Libraries (2)
Manager, Chicago Operations Office, DOE
Materials and Components Technology Division Review Committee:
P. Alexander, The Foxboro Co., Foxboro, MA 02035-2099
M. S. Dresselhaus, Massachusetts Institute of Technology, Cambridge, MA 02139
S. J. Green, Electric Power Research Institute, Palo Alto, CA 94303
R. A. Greenkorn, Purdue University, West Lafayette, IN 47907
L. J. Jardine, Lawrence Livermore National Laboratory, Livermore, CA 94550
C.-Y. Li, Cornell University, Ithaca, NY 14853
R. E. Scholl, Counter Quake Corporation, Redwood City, CA 94061
P. G. Shewmon, The Ohio State University, Columbus, OH 43210
R. E. Smith, Electric Power Research Institute, Charlotte, NC 28221

NRC FORM 335 (2-89) NRCM 1102, 3201, 3202

U.S. NUCLEAR REGULATORY COMMISSION

BIBLIOGRAPHIC DATA SHEET

(See instructions on the reverse)

1. REPORT NUMBER *(Assigned by NRC. Add Vol., Supp., Rev., and Addendum Numbers, if any.)*

NUREG/CR-5649
ANL-90/33
Vol. 1

2. TITLE AND SUBTITLE

COMMIX-1C: A Three-Dimensional Transient Single-Phase Computer Program for Thermal-Hydraulic Analysis of Single- and Multicomponent Engineering Systems

Equations and Numerics

3. DATE REPORT PUBLISHED

MONTH	YEAR
November	1990

4. FIN OR GRANT NUMBER

A22550

5. AUTHOR(S)

H. M. Domanus, Y. S. Cha, T. H. Chien, R. C. Schmitt, and W. T. Sha

6. TYPE OF REPORT

Technical

7. PERIOD COVERED *(Inclusive Dates)*

09/01/85 - 09/30/90

8. PERFORMING ORGANIZATION - NAME AND ADDRESS *(If NRC, provide Division, Office or Region, U.S. Nuclear Regulatory Commission, and mailing address; if contractor, provide name and mailing address.)*

Argonne National Laboratory
9700 South Cass Avenue
Argonne, IL 60439

9. SPONSORING ORGANIZATION - NAME AND ADDRESS *(If NRC, type "Same as above"; if contractor, provide NRC Division, Office or Region, U.S. Nuclear Regulatory Commission, and mailing address.)*

Division of Systems Research
Office of Nuclear Regulatory Research
U. S. Nuclear Regulatory Commission
Washington, DC 20555

10. SUPPLEMENTARY NOTES

11. ABSTRACT (200 words or less)

The COMMIX-1C computer program, an extended version of previous single-phase COMMIX codes, is designed to analyze steady-state/transient, single-phase three-dimensional fluid flow with heat transfer in reactor components and multicomponent systems. The concepts of volume porosity, directional surface porosity, distributed resistance, and distributed heat source or sink is used to model a flow domain with stationary structures. The new porous-medium formulation permits a simulation of either a single component or a multicomponent engineering system. The conservation equations of mass, momentum, and energy based on the new porous-medium formulation are solved as a boundary-value problem in space and an initial-value problem in time.

Volume I of this report, entitled *Equations and Numerics*, describes in detail the basic equations, formulations, solution procedures, flow-modulated skew-upwind discretization scheme, models to describe the auxiliary phenomena, etc. Volume II, entitled *User's Guide and Manual*, contains the flow charts, available options, input instructions, sample problems, etc.

12. KEY WORDS/DESCRIPTORS *(List words or phrases that will assist researchers in locating this report.)*

Thermal Hydraulics
Numerical Analysis
Finite-Volume Procedures
Computer Codes

13. AVAILABILITY STATEMENT

Unlimited

14. SECURITY CLASSIFICATION

(This Page)

Unclassified

(This Report)

Unclassified

15. NUMBER OF PAGES

16. PRICE

NRC FORM 335 (2-89)

THIS DOCUMENT WAS PRINTED USING RECYCLED PAPER.

UNITED STATES
NUCLEAR REGULATORY COMMISSION
WASHINGTON, D.C. 20555

OFFICIAL BUSINESS
PENALTY FOR PRIVATE USE, $300

SPECIAL FOURTH-CLASS RATE
POSTAGE & FEES PAID
USNRC
PERMIT No. G-67

A20555139531 1 1AN1R7
US NRC-OADM
DIV FOIA & PUBLICATIONS SVCS
TPS POR-NUREG
P-223
WASHINGTON DC 20555